

PhD 15940

THE THERMODYNAMICS OF DISPLACIVE PHASE TRANSITIONS
IN FRAMEWORK SILICATES

Simon Anthony Turner Redfern

Gonville & Caius College

Cambridge



A dissertation submitted for the degree of Doctor of Philosophy
at the University of Cambridge.

August 1989

"It is the glory of God to conceal things;
the glory of men is to search them out."

Proverbs 25:2

I declare that the work embodied in this dissertation is my own and includes nothing which is the outcome of work done in collaboration. Reference is made throughout the text to the sources and extent to which I have availed myself of the work of others.

No part of this dissertation has been submitted for a degree, or other qualification, at any other University.

S.A.T. Redfern

S.A.T. Redfern

ABSTRACT

The critical behaviour of displacive phase transitions in framework silicates is studied within the framework of Landau's model for free energy. In particular, the concept of spontaneous strain is employed as a measure of the degree of order in framework silicates undergoing such phase transitions. The ferroelastic phase transition in the framework binary oxide As_2O_5 is taken as a model to demonstrate the applicability of Landau theory to such problems. Spontaneous strain is measured by high-temperature lattice parameters obtained from high-resolution X-ray powder diffraction. It is found that Landau theory works particularly well for the description of displacive transitions in framework structures, due to the long length scale of correlated ordering.

The relationship of spontaneous strains to other ordering processes is considered for the Ca-rich plagioclases and anorthite, where the displacive $\text{I}\bar{1}\text{-P}\bar{1}$ transition couples with Al/Si ordering and degree of albite in solid solution. The behaviour of the order parameter (and spontaneous strain) for the $\text{I}\bar{1}\text{-P}\bar{1}$ transition is found to change from classical second-order through tricritical to first-order as coefficients in the Landau expansion vary according to structural state.

The Landau model is further applied to the non-equilibrium time-dependent behaviour at the hexagonal-orthorhombic transition in annealed cordierite samples. Here coupling between strain and Al/Si order is studied by synchrotron X-ray powder diffraction and infrared spectroscopy and found to be very non-linear and quite different to that observed in plagioclases. The influence of potassium incorporated within the cordierite structure is considered in terms of a defect stress field.

Finally, a similar study is made of the orientational ordering transition in the calcite structure, to investigate the applicability of these ideas to non-framework non-silicates. Direct calorimetric measurements, coupled with the information obtained from diffraction studies of calcite and the analogous transition in NaNO_3 , enable the prediction of the excess entropy, enthalpy and volume for calcite at all temperatures below the $\text{R}\bar{3}\text{m-R}\bar{3}\text{c}$ transition. This is shown to account for the previously-reported curving of the calcite/aragonite phase boundary.

The concept of spontaneous strain combined with the Landau model is thus successfully applied to a number of rock-forming mineral systems and seen to shed new light on the thermodynamic properties of such minerals.

ACKNOWLEDGEMENTS

I would particularly like to thank my supervisors: Dr. Ekhard Salje and Dr. Michael Carpenter, who introduced me to the study of phase transitions in minerals, for their advice and encouragement whilst I carried out the work described in this thesis. I am grateful for the stimulating environment created by all the members of the mineral physics group at Cambridge; it is difficult to name one without naming all, and I thank each who has given their time to guide me on my way. Mention must be made of Dr. Bernd Güttler who gave me an introduction to the Bruker FTIR spectrometer, as well as Dr. Bernd Wruck and Dr. Wolfgang Schmahl who helped in various discussions. The technical assistance of Ann Graeme-Barber has been invaluable, and assistance from Brian Cullum and Tony Abraham has also been most welcome.

I am grateful to Prof. W. Prandl of the Institut für Kristallographie at Tübingen University for allowing me access to the low-temperature Guinier apparatus. Prof. A. Navrotsky welcomed me to Princeton University and kindly provided facilities for the high-temperature calorimetric study of calcite. Dr. R. Cernick of SERC Daresbury Laboratories and Prof. R. Catlow of the University of Keele enabled the synchrotron X-ray study of cordierite to be carried out.

This work would have been impossible without the receipt of a research studentship from the Natural Environment Research Council, who have also partially funded conference expenses. Gonville and Caius College also provided generous support for conference travel. Work at Princeton was funded by the Harkness Scholarship fund.

ACKNOWLEDGEMENTS

I would particularly like to thank my supervisors: Dr. Ekhard Salje and Dr. Michael Carpenter, who introduced me to the study of phase transitions in minerals, for their advice and encouragement whilst I carried out the work described in this thesis. I am grateful for the stimulating environment created by all the members of the mineral physics group at Cambridge; it is difficult to name one without naming all, and I thank each who has given their time to guide me on my way. Mention must be made of Dr. Bernd Güttler who gave me an introduction to the Bruker FTIR spectrometer, as well as Dr. Bernd Wruck and Dr. Wolfgang Schmahl who helped in various discussions. The technical assistance of Ann Graeme-Barber has been invaluable, and assistance from Brian Cullum and Tony Abraham has also been most welcome.

I am grateful to Prof. W. Prandl of the Institut für Kristallographie at Tübingen University for allowing me access to the low-temperature Guinier apparatus. Prof. A. Navrotsky welcomed me to Princeton University and kindly provided facilities for the high-temperature calorimetric study of calcite. Dr. R. Cernick of SERC Daresbury Laboratories and Prof. R. Catlow of the University of Keele enabled the synchrotron X-ray study of cordierite to be carried out.

This work would have been impossible without the receipt of a research studentship from the Natural Environment Research Council, who have also partially funded conference expenses. Gonville and Caius College also provided generous support for conference travel. Work at Princeton was funded by the Harkness Scholarship fund.

TABLE OF CONTENTS

	Page
Title Page	i
Epigraph	ii
Declaration	iii
Abstract	iv
Acknowledgements	v
Table of Contents	vi to ix
CHAPTER 1 GENERAL ASPECTS OF PHASE TRANSITIONS IN MINERALS	1
1.1 Introduction	1
1.1.1 Atomistic Processes and Polymorphism	1
1.1.2 Coupled Processes: An Example	3
1.1.2 The Need for a Theory	5
1.2 The Essential Features of Landau Theory	7
1.2.1 Symmetry Breaking and Q	7
1.2.2 The Landau Potential $G(Q, T, p, \dots)$	10
1.2.3 Continuous Second-Order Transitions	11
1.2.4 Discontinuous First-Order Transitions	15
1.2.5 Tricritical Behaviour	19
1.3 Ferroelastic Phase Transitions	22
1.3.1 Ferroic Distortive Transitions	23
1.3.2 Physical Characteristics of Ferroelastic Phases	24
1.3.3 Strain and Order-Parameter Coupling	28
CHAPTER 2 FERROELASTIC BEHAVIOUR IN ARSENIC PENTOXIDE	32
2.1 Introduction	32
2.1.1 Structure, Symmetry and Previous Investigation	32
2.1.2 Spontaneous Strain and the Twin Law	37

2.2	Experimental Details	40
2.2.1	Lattice Parameter Measurements	40
2.2.2	Line Profiles	44
2.3	Critical Behaviour in Arsenic Pentoxide	44
2.3.1	Order Parameter Behaviour from Strain	44
2.3.2	Critical Linewidth and Susceptibility	47
2.3.3	Coupling Between Acoustic and Optic Modes	50
2.3.4	Implications for the Grüneisen Relation	53
2.4	Summary, Conclusions, and Consequences	54
CHAPTER 3 CO-ELASTIC BEHAVIOUR AT THE $I\bar{1}$ - $P\bar{1}$ TRANSITION IN ANORTHITE		56
3.1	Introduction	56
3.1.1	The $C\bar{1}$ - $I\bar{1}$ Al/Si Ordering Transition	58
3.1.2	The $I\bar{1}$ - $P\bar{1}$ Transition in Pure Ordered Anorthite	61
3.2	Experimental	67
3.2.1	High-Resolution Powder X-ray Diffraction	67
3.2.2	Lattice Parameters and Thermal Expansion	68
3.3	The Spontaneous Strain of the Phase Transition $I\bar{1}$ - $P\bar{1}$	71
3.4	Thermodynamic Calculations and Discussion	75
3.4.1	The Landau Free-Energy Expansion	75
3.4.2	Strain Behaviour and Transition Character	76
3.4.3	Strain Energy of the Transition	81
CHAPTER 4 CHANGING TRANSITION CHARACTER IN Ca-RICH PLAGIOCLASE		83
4.1	Introduction	
4.2	Strain Behaviour in Monte Somma Anorthite	85
4.2.1	Measurement of Lattice Parameters	85
4.2.2	Spontaneous Strain and the Order Parameter in $P\bar{1}$ Anorthite	88

4.2.3	Comparison with Val Pasmada and Saturation	92
4.2.4	Magnitude of Coupling to other Transitions	94
4.3	The $I\bar{1}-P\bar{1}$ Transition at High-Pressure	96
4.4	Conclusions: the P-T-X Phase Diagram	103
CHAPTER 5 HEXAGONAL-ORTHORHOMBIC TRANSITION IN Mg-CORDIERITE		106
5.1	Mg-Cordierite: a Kinetic Problem	106
5.1.1	Cordierite Structure and Stability	106
5.1.2	Landau Theory of Cordierite	109
5.1.3	The Measurement of Q_{od} and Q	111
5.2	Experimental Investigation of Mg-Cordierite	112
5.2.1	Synchrotron X-ray Powder Diffraction: Pure Mg-Cordierite	112
5.2.2	Results from Diffractometry	114
5.3	Coupling Between Q and Al/Si Ordering	118
5.4	The Influence of Potassium	122
5.4.1	X-ray Diffraction Experiments	123
5.4.2	Hard-mode Infrared Measurements	125
5.4.3	Strain Behaviour from Diffractometry	126
5.4.4	Results from Hard-mode Infrared Spectroscopy	129
5.4.5	Potassium as a Defect Stress Field	132
5.5	Synopsis and Conclusions	135
CHAPTER 6 CO-ELASTICITY AND ORIENTATIONAL DISORDER IN THE CALCITE STRUCTURE		137
6.1	Introduction	137
6.1.1	Orientalional Order/Disorder in Sodium Nitrate	138
6.1.2	Orientalional Order/Disorder in Calcite	140
6.2	Strain in Sodium Nitrate at Low Temperature	143
6.2.1	Materials and Methods	144

6.2.2	Lattice Parameter Results	146
6.2.3	Symmetry and Spontaneous Strain	147
6.2.4	Order Parameter Coupling	150
6.2.5	Scalar Strain and Strain Energy	152
6.3	Orientational Ordering and the Calcite/Aragonite Equilibrium	153
6.3.1	Comparison with Sodium Nitrate	153
6.3.2	Measurement of Enthalpy	155
6.3.3	Results from Calorimetry	158
6.3.4	Landau Theory of Calcite	159
6.3.5	Implications on the Calcite/Aragonite Phase Equilibrium Boundary	162
6.3.6	Consequences of Order-Parameter Saturation	166
6.4	Summary	167
CHAPTER 7 GENERAL OVERVIEW AND CONCLUSIONS		169
APPENDIX 1 HIGH-TEMPERATURE GUINIER X-RAY POWDER DIFFRACTION		174
A1.1	The Huber Guinier System	174
A1.1.1	Instrumental Configuration	175
A1.1.2	Sample Preparation and Mount	175
A1.1.3	Modification of Oscillation Mechanism	176
A1.2	Furnace and Temperature Calibration	176
APPENDIX 2 PROGRAMS FOR SPONTANEOUS STRAIN CALCULATION		179
A2.1	'STRAINS'	179
A2.2	'DIAGNL'	180
REFERENCES CITED		183

CHAPTER 1

GENERAL ASPECTS OF PHASE TRANSITIONS IN MINERALS

1.1 Introduction

In starting this account of features of displacive phase transitions in minerals we shall first point to the general significance of such transitions in mineral systems, and the philosophy behind the study of phase transitions.

1.1.1 Atomistic Processes and Polymorphism The crystal structures of minerals are usually relatively complex and capable of a variety of changes as extensive thermodynamic variables such as temperature and pressure alter, and these changes may lead to changes in symmetry of the crystal structure. Common examples of processes of change in minerals include ordering and disordering of cations, distortions of the framework of the crystal lattice, atomic displacements, ordering of the spins of magnetic species of atom or of electric dipoles, as well as ordering of molecular groups within the crystal. This wide range of crystalline behaviour creates potential mechanisms for many possible phase transitions of diverse nature between polymorphs of natural Earth-materials. In addition a single mineral may experience many phase transitions due to separate processes at different temperatures and pressures. Since the processes all occur within one crystal it is easy to see that although separate, they may influence one another, and the consequent phase transitions may couple to one another through the influence they have on the crystal structure. Although not directly distortive in character, any of the processes listed above may lead to distortions in the crystal lattice. It is the study, the

description, and the implications of coupling between distortions of the crystal lattice and processes such as aluminium-silicon ordering in minerals which form the theme of this thesis.

Why study these phase transitions? An underlying principle fundamental to the study of phase transitions in minerals is that the investigation of the properties of a system undergoing change enhances the understanding of that same system when it is static. Historically, mineralogy has involved the characterisation and description of phases, and concentrated on aspects such as the systematics of differences between polymorphs. This descriptive approach has, however, recently been developed and extended to the deeper consideration of the processes of change, in particular to the temperature dependent behaviour of the physical properties of minerals in the vicinity of polymorphic phase transitions and the motivating thermodynamic driving force for such transitions.

The microstructures of minerals which have undergone phase transitions are often a direct result of those transitions; this may shed light on aspects such as the thermal history of the rock of origin, if the phase transitions themselves are understood. Features such as transformation twins, anti-phase domains and modulated structures resulting from phase transitions can act as geobarometers and geothermometers: they are well known for their usefulness as petrogenetic indicators (McConnell, 1975).

Physical properties at and near phase transitions are observed to undergo large changes, sometimes in a catastrophic manner. For example, in quartz the thermal expansion coefficient twenty degrees below the high-low phase transition is over twenty times that just above the transition (Salje et al., 1989). Such

anomalous behaviour may be revealed in a number of properties: heat capacity, elastic constants, birefringence, lattice parameters, dielectric constants, lattice mode frequencies and so on. These properties may, in turn, be used to probe the transition behaviour. A phase transition may also alter the properties of a mineral a long way away from the transition (in terms of temperature, say) compared to those expected in the absence of a transition. We see that rather than being just isolated anomalies, phase transitions can have a significant impact on mineral behaviour over very wide temperature intervals.

1.1.2 Coupled Processes: An Example An example of a system in which several processes taking place in the lattice give rise to complex coupled phase transitions (which in turn lead to a variety of microstructures and anomalies in physical and thermodynamic properties) is that of the alkali feldspars. Within these minerals there is the possibility of ordering of aluminium and silicon, collapse of the tetrahedral feldspar framework, as well as segregation of sodium and potassium into two phases at compositions intermediate between the end members Na-feldspar and K-feldspar. Recent work on this system is reviewed by Carpenter (1988) who outlines the effects of coupling between all these processes. In albite, for example, the Al/Si disordered $C2/m$ form would transform to $C\bar{1}$ symmetry continuously at 1251 K due to a displacive collapse of the tetrahedral framework, but in the absence of this displacive transition $C2/m$ albite would in any case transform to $C\bar{1}$ symmetry discontinuously at 833 K by ordering of Al and Si (Salje et al., 1985a). In equilibrium the temperature of the displacive transition at high temperature is modified, by coupling to the process of Al/Si

ordering, to 1290 K where the C2/m monoclinic albite transforms continuously to triclinic $C\bar{1}$ high albite. Upon further cooling the Al/Si ordering becomes more important (as the crystal approaches 833 K) and at around 950 K there is a crossover between a regime where the framework collapse is the dominant process and the regime where aluminium and silicon ordering is important. This is the crossover between Al/Si disordered "high albite" and Al/Si ordered "low albite" which occurs within the $C\bar{1}$ structure without a change in symmetry of the lattice, so it is not a true phase transition. The physical and thermodynamic properties of albite, however, depend significantly upon the coupling between these two processes, in effect between two phase transitions which would occur independently (in the absence of coupling) in one mineral.

The thermodynamic importance of the crossover is demonstrated by Salje et al. (1985a) who calculate the

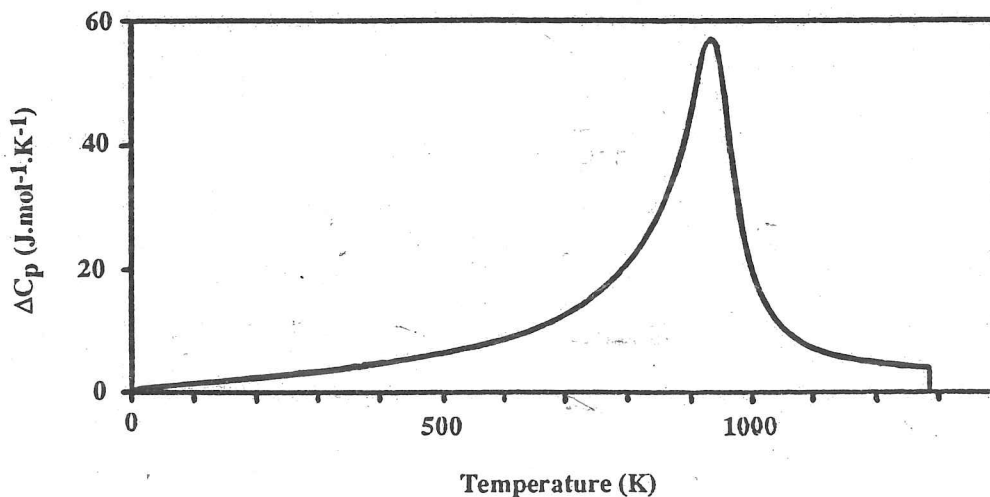


Figure 1.1 Excess heat capacity in albite (after Salje et al., 1985a). The small step at 1290 K results from the monalbite-high albite framework collapse, the large excess around 950 K is due to the coupling between the framework distortion and Al/Si ordering.

temperature dependence of the heat capacity C_p of albite in thermodynamic equilibrium and find that the excess specific heat anomaly at the $C2/m-C\bar{1}$ displacive transition is far less than that at the high-low crossover temperature (Figure 1.1). The understanding of the equilibrium state of albite at any temperature depends upon the understanding of the interplay between the phase transitions which occur in the structure. In general the widely occurring process of ordering of aluminium and silicon within the structure of framework silicates is very important energetically, in the case of albite this process can be probed experimentally by the measurement of distortion of the crystal structure since this is the coupled process. Al/Si cation distributions are difficult to determine directly by experiment (methods such as neutron diffraction structure analysis or the interpretation of complex NMR signals may be employed) whereas the distortion of the crystal lattice gives an indirect method which is simply determined from the experimental observation of the lattice parameters. Once the coupling between phase transitions in albite was understood so also were the thermodynamic properties (free energy, enthalpy, entropy, heat capacity), the temperature evolution of the crystal structure (tetrahedral site occupancies, lattice parameters), and the phase diagram.

1.1.3 The Need for a Theory The unravelling of the subsolidus behaviour of albite is one of the first examples of a new approach to the study of phase transitions in minerals, which will be developed here. The success in the quantitative understanding of the coupled phase transitions of albite lies in the theoretical approach adopted by Salje et al. (1985a). The

satisfactory prediction of the features of a phase transition depends upon the accurate modelling of the form of the Gibbs free energy of the crystal and from this the determination of the derivatives of free energy. Significant steps forward have been made recently by the application of Landau theory (Landau, 1937; Landau and Lifshitz, 1954) to the problems of mineral behaviour. The Landau model expands the free energy of the crystal in terms of the degree of long-range correlated order, Q , of the crystal structure. This allows a link to be made between the behaviour of experimentally measurable physical properties and the thermodynamic properties of mineral phases, enabling the prediction of phase equilibria. Conversely once the free energy has been formulated other unmeasured physical properties may be predicted, these predictions can then be used to further test and tune the model for free energy.

In this thesis we shall test the range of applicability of the Landau model starting with simple model systems such as the binary oxide As_2O_5 and then moving on to the more complicated problem of coupled phase transitions in complex framework silicates, such as the plagioclase feldspars, and to other coupled processes in minerals, such as translation-rotation coupling in the rhombohedral carbonates. Before the discussion of these particular problems, however, we shall outline those essential features of Landau's theory of phase transitions which are necessary for its application to mineralogy, since at present no text bridges the gap between an elementary and rather naïve treatment of the theory (e.g. Rao and Rao, 1978) and the more advanced physics monographs on the subject (e.g. Bruce and Cowley, 1981).

satisfactory prediction of the features of a phase transition depends upon the accurate modelling of the form of the Gibbs free energy of the crystal and from this the determination of the derivatives of free energy. Significant steps forward have been made recently by the application of Landau theory (Landau, 1937; Landau and Lifshitz, 1954) to the problems of mineral behaviour. The Landau model expands the free energy of the crystal in terms of the degree of long-range correlated order, Q , of the crystal structure. This allows a link to be made between the behaviour of experimentally measurable physical properties and the thermodynamic properties of mineral phases, enabling the prediction of phase equilibria. Conversely once the free energy has been formulated other unmeasured physical properties may be predicted, these predictions can then be used to further test and tune the model for free energy.

In this thesis we shall test the range of applicability of the Landau model starting with simple model systems such as the binary oxide As_2O_5 and then moving on to the more complicated problem of coupled phase transitions in complex framework silicates, such as the plagioclase feldspars, and to other coupled processes in minerals, such as translation-rotation coupling in the rhombohedral carbonates. Before the discussion of these particular problems, however, we shall outline those essential features of Landau's theory of phase transitions which are necessary for its application to mineralogy, since at present no text bridges the gap between an elementary and rather naïve treatment of the theory (e.g. Rao and Rao, 1978) and the more advanced physics monographs on the subject (e.g. Bruce and Cowley, 1981).

1.2 The Essential Features of Landau Theory

In presenting a brief description of Landau theory we must cut some corners and what follows can be thought of as a pragmatist's version of the theory rather than a thorough and rigorous justification of the useful results.

1.2.1 Symmetry Breaking and Q Landau's description of phase transitions uses the concept of the order parameter (Q) to relate the changing symmetry of the crystal to its Gibbs free energy (we shall only consider the cases where pressure or temperature are the extensive variables, when the Landau potential is equivalent to the free energy). The order parameter characterizes the extent of deviation of the low-symmetry, low-temperature form of the crystal from the high-temperature phase (we shall assume that on going from high to low temperature the symmetry of the crystal decreases; this need not be so, NaOH (Yoshimitsu, 1986) shows for example an interesting exception, but is true for almost all phase transitions). Physically, the order parameter may be related to the degree of distortion of the unit cell from the high-temperature cell, or the degree of Al/Si order on specific crystallographic sites, or the displacement of an atom in the crystal from its position in the high-temperature space group, or the resultant magnetic moment of a ferromagnetic domain which becomes paramagnetic at high temperatures. In fact the physical meaning of the order parameter depends upon the specific material and the phase transition which is taking place; relating the order parameter to the crystal structure is often actually the question of interest in the study of a specific phase transition. So the order parameter vanishes to zero in the high-temperature space group of the crystal and increases below the transition,

the increase may be continuous or discontinuous and in this way the temperature evolution of the order parameter reflects the thermodynamic character of the phase transition. The order parameter is dimensionless and is defined as unity at absolute zero.

Landau theory describes those phase transitions where the space group of the low-symmetry form is a subgroup of the space group of the high-symmetry form of the crystal. This means it refers only to topotactic phase transitions where the underlying crystal lattices of the two polymorphs are topologically similar; Landau theory does not apply to reconstructive nucleation and growth transformations. The fact that the underlying translational symmetry of the high and low temperature forms are related gives rise to the mathematical definition of the order parameter, which is outlined below.

The group theoretical foundations of Landau theory are detailed in the books of Kociński (1983) and Tolédano and Tolédano (1987). They rest on the consideration of the basis functions related to the irreducible representations of the space groups of the high- and low-symmetry forms of the crystal. The basis functions are simply those functions which, when superposed, describe the periodic structure (the density function $\rho(\mathbf{x})$, which defines the atomic co-ordinates and structure) of the crystal. Groups of basis functions transform into one another under the action of the symmetry operators of the space group of the crystal, and these groups of functions form classes described by the irreducible representations of the space group. When the crystal undergoes a phase transition from a high-symmetry space group G_0 to a low-symmetry space group G_1 (where G_1 is a subgroup

of G_0) some symmetry elements are lost and this change results in a change in transformation behaviour of the basis functions, in other words it leads to changes in $\rho(\mathbf{x})$. That irreducible representation in G_0 which is not the identity representation of G_0 but which is invariant under the operations of the symmetry elements present in G_1 (i.e. becomes the identity representation in G_1) is called the active representation, and it is this active representation which relates to the features of the crystal which change critically at the phase transition. The basis functions in the class of the active representation, the active basis functions, describe the part of the density function which changes through the phase transition, $\delta\rho(\mathbf{x})$, so that the overall density function in G_1 is given by:

$$\rho_1(\mathbf{x}) = \rho_0(\mathbf{x}) + \delta\rho(\mathbf{x}) \quad \{1.1\}.$$

The coefficients of the active basis functions must be zero in G_0 giving $\delta\rho(\mathbf{x}) = 0$ in G_0 . Below the phase transition $\delta\rho(\mathbf{x}) \neq 0$ and the coefficients of the active basis functions similarly become non-zero. These coefficients are temperature- and pressure-dependent and are in fact the order parameters for the phase transition. In other words, the order parameter (Q) can be thought of as a measure of the amount of the eigenfunction of the active representation present in the low-temperature subgroup, G_1 .

Knowledge of the active representation at a particular phase transition is useful since it defines the symmetry and dimension of the order parameter. In addition it enables the identification and prediction of the physical properties which will behave like the order parameter; the frequency of

vibrational modes with the symmetry of the active representation should, for example, show temperature and pressure dependence coupled to that of the order parameter.

An example of the determination of the active representation and active basis function of the point group 422 on transformation to point group 222 is given in section 2.1.2 in the discussion of the displacive phase transition in As_2O_5 .

1.2.2 The Landau Potential $G(Q, T, p, \dots)$ The assumption that Landau (1937) made when he linked the symmetry aspects of a phase transition to the thermodynamic description of a phase transition was that the thermodynamic potential of the crystal can be expressed as a polynomial expansion of the order parameter. This potential, the Landau potential, is a function of Q , and other extensive variables such as T , p , and ^{composition, X} . The minimum of the Landau potential ($G(Q, T, p, X, \dots)$) determines the equilibrium state of the crystal (in terms of, say, Q) and the Landau potential can be thought of as a free energy.

The form of the polynomial expansion of the Landau potential can be determined by considering the symmetry properties of the order parameters and their coupling to other physical properties (again, the form of the coupling is symmetry determined). These points will be clarified in the discussion below of a Landau potential derived from a simple one-dimensional order parameter, and in the discussion of more complicated real systems described in this thesis. We take as a starting point, however, a general power series expansion of a scalar order parameter, Q , initially including all terms (and ignoring symmetry constraints):

$$G(Q, T, p, X, \dots) = G_0 + \alpha Q + \frac{1}{2}A Q^2 + \frac{1}{3}b Q^3 + \frac{1}{4}B Q^4 + \dots \quad \{1.2\}.$$

Here G_0 is the Gibbs free energy of the high temperature phase; α , A , b , and B are coefficients which may or may not be dependent on material properties of the crystal or extensive variables. We shall now go on to consider how such an expansion leads to a form of free energy which describes continuous phase transitions.

1.2.3 Continuous Second-Order Transitions At a continuous phase transition Q changes continuously from zero in the high-symmetry phase to unity in the low-symmetry phase at absolute zero. The Landau potential should describe this equilibrium behaviour of Q , which is determined by minimization of the series expansion.

Taking equation 1.2 as our starting point we see straight away that some modifications must be made. If the expansion is to yield a minimum with respect to Q then $dG/dQ = 0$ and thus $\alpha = 0$. Now we consider the second-order term in the expansion:

$$G = G_0 + \frac{1}{2}AQ^2 + \dots \quad \{1.3\}.$$

If the free energy is to be a minimum for $Q = 0$ in the high-symmetry form and for $Q \neq 0$ in the low-symmetry form then (taking the higher-order terms in the expansion into account) the coefficient of Q^2 , A , must be positive above the phase transition and negative below it. This is achieved if A is temperature dependent, and the expansion for free energy is modified to:

$$G = G_0 + \frac{1}{2}a(T-T_c)Q^2 + \frac{1}{3}bQ^3 + \frac{1}{4}BQ^4 + \dots \quad \{1.4\},$$

where T_c is the temperature at which the phase transition takes place, the critical temperature. Now, however, at T_c the condition $dG/dQ = 0$ is met not only at $Q = 0$ but also at $Q = -b/B$. This contradicts our starting premise: that Q changes continuously from zero to one, and for this reason the third-order

coefficient $b = 0$, similarly all other odd-order coefficients are zero. Finally we see that the inclusion of the potential G_0 plays no part in the description of the phase transition and may be omitted. Thus, we arrive at the Landau potential to describe the excess free energy at a continuous second-order phase transition:

$$G = \frac{1}{2}a(T-T_c)Q^2 + \frac{1}{4}BQ^4 + \frac{1}{6}cQ^6 + \dots \quad \{1.5\}.$$

The expansion is obviously infinite and there is no proof of its convergence, however it is normally limited to only two or three terms since it is found that this adequately describes the excess free energy for the purpose of comparison with experiment. That the Landau expansion often works well, even using only two or three terms, is rather surprising. Landau formulated his expansion in the belief that it would only be valid for small Q , but in fact the Landau expansion can be useful for the description of phases even when Q increases to near unity (see the case of NaNO_3 , chapter 6). Landau theory actually fails not when Q is large, but when Q is small and dynamical fluctuations of the order parameter become larger than the mean amplitude of Q itself (i.e. in the Ginzburg interval: Als-Nielsen and Birgeneau, 1977; Ginzburg, 1960; Ginzburg et al., 1987). We shall discuss some of the factors which influence the breakdown of Landau theory in more detail in chapter 2.

Excess quantities arising below T_c other than the free energy may be derived from equation 1.5. For stability of the low-temperature phase a and B must be positive, the temperature dependent form of the Landau potential is shown in Figure 1.2. Now the equilibrium behaviour of the order parameter as a

function of temperature can easily be determined by solution of:

$$\begin{aligned} \frac{dG}{dQ} &= 0 \\ &= a(T-T_c)Q + BQ^3 \quad \left(\text{and } \frac{d^2G}{dQ^2} = a^{-1} > 0\right) \end{aligned} \quad \{1.6\}$$

$$\Rightarrow \begin{aligned} Q &= 0 & T > T_c \\ Q &= \pm \sqrt{a/B} \cdot (T_c - T)^{\frac{1}{2}} & T \leq T_c \end{aligned} \quad \{1.7\}$$

and since $Q=1$ at $T=0$

$$T_c = \frac{B}{a} \quad \{1.8\}$$

It will be seen that many quantities dependent on the phase transition behave as $(T_c - T)^\lambda$ where λ is a critical exponent. Each quantity is assigned a particular critical exponent, the critical exponent for Q is usually termed β so we have the result that for a second-order phase transition $\beta = \frac{1}{2}$. The equilibrium behaviour of Q is shown in Figure 1.3.

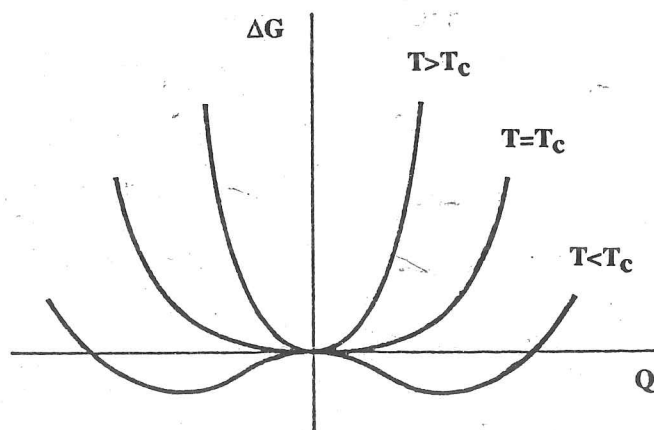


Figure 1.2 Temperature dependence of the Landau potential at a continuous second-order phase transition.

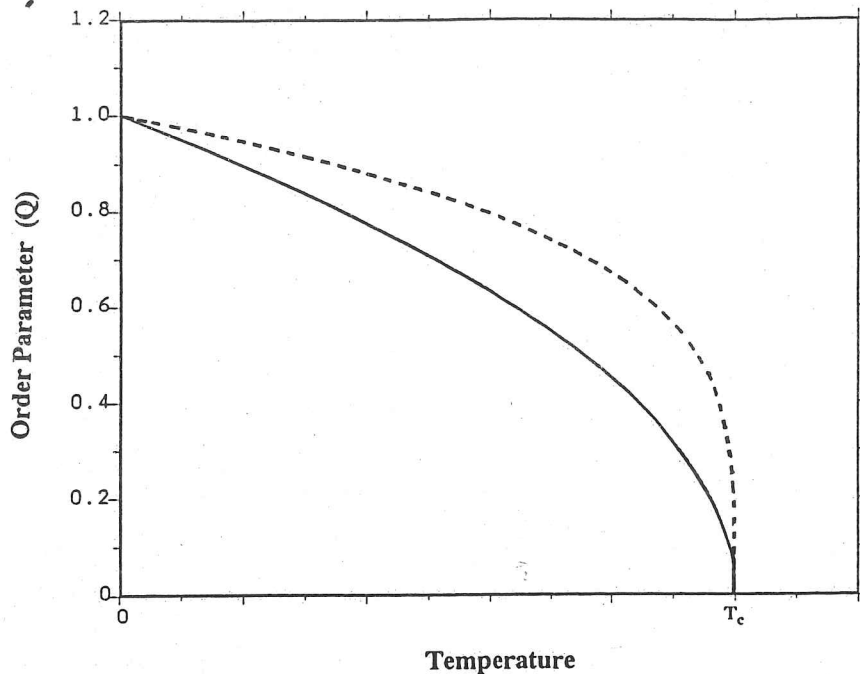


Figure 1.3 Temperature dependence of the order parameter (Q) below a second-order (solid line) and tricritical (dashed line) phase transition at T_c .

Substituting the result of equation 1.7 back into the Landau expansion (up to fourth order) we obtain a simple temperature dependence for the excess free energy:

$$G = - \frac{a^2}{4B}(T-T_c)^2 \quad \{1.9\}.$$

Other excess thermodynamic properties are derived from the Landau potential. The excess entropy due to the phase transition is given by:

$$S = - \frac{dG}{dT} = \frac{a^2}{2B}(T-T_c) = - \frac{1}{2}aQ^2 \quad \left. \begin{array}{l} T \leq T_c \\ \\ = 0 \quad \quad \quad T > T_c \end{array} \right\} \quad \{1.10\}$$

and the excess heat capacity is obtained from:

$$C_p = - T \frac{d^2G}{dT^2} = \frac{a^2}{2B}T \quad \left. \begin{array}{l} T \leq T_c \\ \\ = 0 \quad \quad \quad T > T_c \end{array} \right\} \quad \{1.11\}.$$

The advantage of such a simple form for free energy as equation 1.5 is seen here. All thermodynamic quantities relating

to a second-order phase transition can be determined once a and B are known. Thus a single experiment which measures the transition temperature, T_c , and a thermodynamic quantity at one other temperature leads to a full description of the energetics of the mineral over a wide temperature interval.

1.2.4 Discontinuous First-Order Transitions Although Landau first intended his theory for the description of continuous phase transitions it also works for first-order phase transitions which are nearly continuous. In particular the same supergroup-subgroup relation must exist between the two phases. We will see that equation 1.4 can lead to a discontinuous phase transition (where there is a jump in Q at T_c) in two ways. Firstly if b in 1.4 is zero a first-order transition occurs if a is positive and B is negative, and secondly if the symmetry of the order parameter allows a third-order term in the expansion 1.4 this leads to first-order behaviour. We shall take each of these in turn.

a) **B negative.** The first description of a discontinuous phase transition is based upon a Landau expansion of the excess free energy in even powers of Q , as given by equation 1.5. If a is positive and B negative then we must also include the sixth-order term for stability of the low-temperature phase, and c must be positive. The temperature dependent form of the Landau potential is shown by Figure 1.4. Minimization of 1.5 gives:

$$\frac{dG}{dQ} = a(T-T_c)Q + BQ^3 + cQ^5 = 0 \quad \{1.12\}$$

$$\Rightarrow Q^2 = \frac{-B \pm (B^2 - 4ac(T-T_c))^{\frac{1}{2}}}{2c} \quad \{1.13\}$$

(ignoring the trivial solution $Q = 0$).

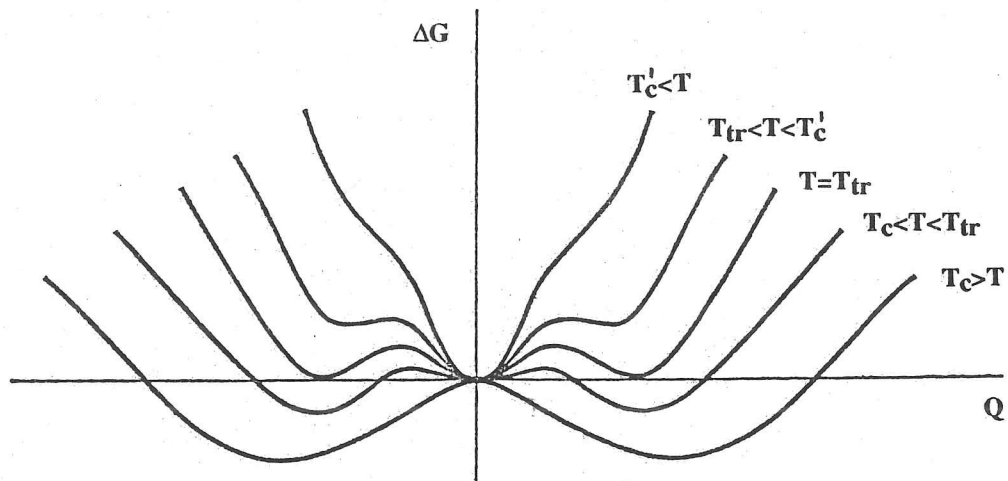


Figure 1.4 Temperature dependence of the Landau potential for a first-order phase transition with $B < 0$.

Notice that in a first-order phase transition the form of Q cannot be easily expressed by a simple critical exponent, and in this case $\beta \neq \frac{1}{2}$. The stability of the phase depends only on Q sitting in a local minimum of the potential, and from Figure 1.4 it is clear that on cooling the high-symmetry form will remain stable until $T < T_c$, and on heating the low-symmetry form remains stable until $T > T_c'$. By considering the second derivative of 1.5 we find

$$T_c' = T_c + \frac{B^2}{4ac} \quad \{1.14\}$$

and the interval T_c to T_c' corresponds to the hysteresis loop characteristic of first-order phase transitions. Between T_c and T_c' the low- and high-temperature phases can exist metastably either side of the true thermodynamic transition temperature. At the transition temperature, T_{tr} , the potential of both high- and

low-symmetry phases are equal, and this temperature is found to be:

$$T_{tr} = T_c + (3/16) \frac{B^2}{ac} \quad \{1.15\}.$$

At T_{tr} the order parameter jumps from zero in the high-symmetry form to Q_0 in the low-symmetry form:

$$Q_0 = \pm \left[-\frac{4a(T_{tr} - T_c)}{B} \right]^{\frac{1}{2}} \quad \{1.16\}$$

and the size of this jump is an indication of how first-order the phase transition is. The more negative B is, the greater the difference between T_{tr} and T_c and the larger the first-order step at T_{tr} , Q_0 . The equilibrium behaviour of Q is shown in Figure 1.5. Other thermodynamic quantities may be derived from equation 1.5, the model predicts a latent heat proportional to Q_0^2 at T_{tr} and other discontinuities as expected at a first-order phase transition. The forms of entropy and enthalpy are listed by Carpenter (1988).

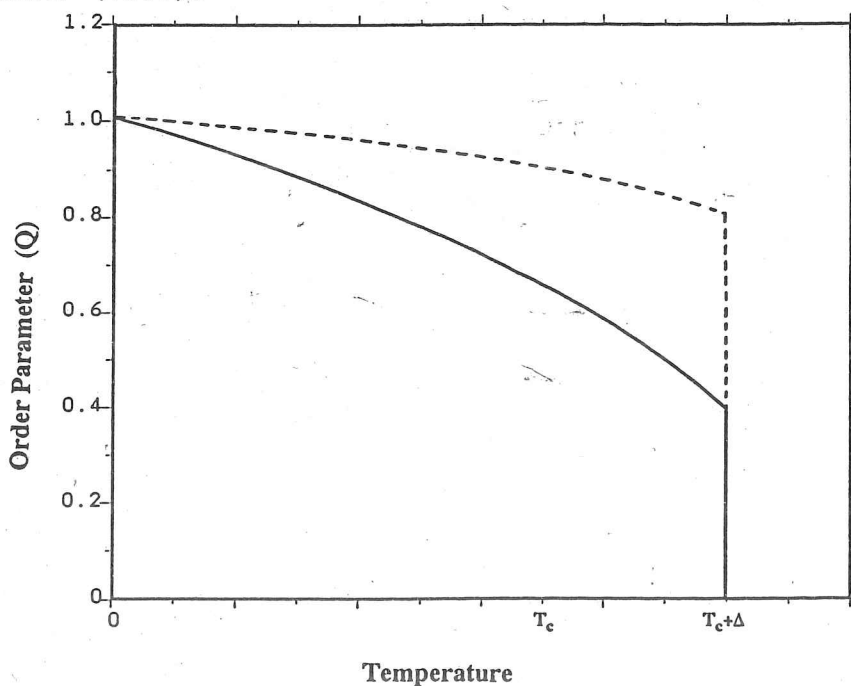


Figure 1.5 Temperature dependence of Q at a first-order transition. The solid line represents behaviour due to $B < 0$, the dashed line corresponds to a symmetry-driven first-order transition.

b) Third-order term present. A first-order phase transition also occurs when the symmetry of the order parameter leads to a cubic term in the Landau expansion {1.4}. The Landau potential now becomes asymmetric (Figure 1.6) but shares many of the features outlined in case (a) above. When a cubic term is present the condition for stability for Q is:

$$\frac{dG}{dQ} = a(T-T_c)Q + bQ^2 + BQ^3 = 0 \quad \{1.17\}$$

$$\Rightarrow Q = \frac{-b \pm (b^2 - 4aB(T-T_c))^{1/2}}{2B} \quad \{1.18\}$$

and again there is a region of metastable equilibrium for the low-symmetry and high-symmetry phases upon heating and cooling.

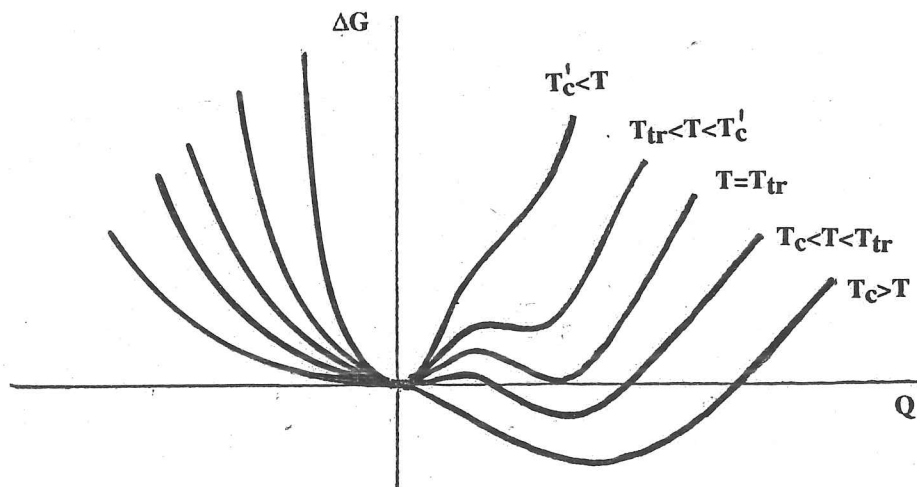


Figure 1.6 Temperature dependence of the Landau potential when there is a cubic term in the expansion.

The phase transition now occurs at a T_{tr} given by:

$$T_{tr} = T_c + (2/9) \frac{b^2}{aB} \quad \{1.19\}$$

where the order parameter steps to a value

$$Q_0 = - (2/3) \frac{b}{B} \quad \{1.20\}.$$

Whereas previously the magnitude of B determined how strongly first-order the phase transition is (when there is no cubic term in the expansion), now the first order character is regulated by the size of b , a measure of how much of the odd-order basis function pervades the structure. Comparison of equations 1.13 and 1.18 shows that although originating from the same basic theory, the two types of first-order phase transition described by Landau theory have quite different order parameter behaviour, and are distinct in a number of ways (the equilibrium behaviour of Q for both cases of first-order transition are compared in Figure 1.5). The first-order transition due to $B < 0$ arises simply from the dependence of the sign of that coefficient on p , T and material related properties, whereas the first-order transition due to $b \neq 0$ is a direct result symmetry aspects of the phase transition. The transition from hexagonal to orthorhombic cordierite is a mineralogical example of such symmetry-driven first-order behaviour (see McConnell (1985) and Salje (1987a) for discussions of the symmetry aspects of hexagonal-orthorhombic cordierite).

1.2.5 Tricritical Behaviour We have seen that equation 1.5 yields a continuous phase transition when $a > 0$, $B > 0$ and a discontinuous phase transition when $a > 0$, $B < 0$, $c > 0$. There is a special case when $B = 0$; the phase transition is then termed "tricritical". The tricritical phase transition, therefore, corresponds to the situation when the transition is on the boundary between first-order and second-order behaviour. It is

often thought of as the point on a line of phase transitions (in say pressure-temperature or temperature-composition space) which terminates the line of continuous phase transitions and heralds the switch to discontinuous behaviour. The term "tricritical" may be somewhat confusing since the transition remains one between two polymorphic phases, and a tricritical point should not be confused with a triple point. Rather, tricritical is a special form of a normal critical point (an ordinary second- or first-order phase transition); one that can be thought to result from the special values of three parameters applied to the crystal, for instance T , p and the field conjugate to Q (e.g. a magnetic field acting against Q when Q is the spontaneous magnetization below the Curie temperature at a ferromagnetic phase transition).

With $B = 0$ the expansion (equation 1.5) must be taken up to sixth-order with $c > 0$ for stability of the low temperature phase. So the Landau expansion for excess free energy is:

$$G = \frac{1}{2}a(T-T_c)Q^2 + \frac{1}{6}cQ^6 \quad \{1.21\}$$

which gives the solutions for the equilibrium order parameter behaviour in the usual manner:

$$\begin{array}{ll} Q = 0 & T > T_c \\ Q = \pm \left(\frac{a}{c} (T_c - T) \right)^{\frac{1}{4}} & T \leq T_c \end{array} \quad \{1.22\},$$

and

$$T_c = \frac{a}{c} \quad \{1.23\}.$$

The pathway of Q through the phase transition is continuous, as in the second-order phase transition (section 1.2.3), and the transition occurs at T_c . Now, however, Q depends on the fourth

root of the temperature below T_c in contrast to the result of equation 1.7. In other words, the critical exponent β changes from $\beta = \frac{1}{2}$ when $B > 0$ at a second-order transition to $\beta = \frac{1}{4}$ at a tricritical phase transition (when $B = 0$). The behaviour of Q at a tricritical phase transition is shown in Figure 1.3 where it is compared with that at a second-order transition.

The excess heat capacity at the tricritical transition may easily be derived since the entropy still behaves as $-\frac{1}{2}aQ^2$ (as in equation 1.8) and hence

$$C_p = T \frac{dS}{dT} = \frac{a}{4} \sqrt{a/c} \cdot T \cdot (T_c - T)^{-\frac{1}{2}} \quad T \leq T_c \quad \{1.24\}$$

which is quite distinct from the form given by equation 1.9. The critical exponent describing the temperature dependent form of C_p is usually given the symbol α with C_p proportional to $(T_c - T)^{-\alpha}$. Hence, we see that for a tricritical phase transition $\alpha = \frac{1}{2}$ whereas for a second-order phase transition $\alpha = 0$. The form of the heat capacity described by equation 1.24 diverges (without a latent heat) at T_c and is similar to the form often described as a lambda anomaly. In this way the heat capacity as well as the order parameter reflects the 'boundary' nature of the tricritical transition, displaying aspects on the verge of first-order but in fact remaining continuous. In real crystals defects and imperfections cause a 'smearing-out' of C_p near T_c and interpretation of C_p data can be rather more difficult than simple Landau theory suggests (Aleksandrov and Flerov, 1979).

Tricritical phase transitions may at first appear rather an oddity and the result of exceptional circumstance since they depend upon the fourth-order term in the Landau expansion being zero. In actual fact tricritical transitions are rather more

common than this reasoning suggests and have been observed in a number of systems, examples include anorthite (chapter 3; Redfern and Salje, 1987), calcite (Dove and Powell, 1989), lead phosphate-arsenate (Bismayer and Salje, 1981), and ND_4Cl (Yelon et al., 1974). This is because the coefficient of the fourth-order term, like the other coefficients in the Landau expansion, is not necessarily a simple constant, but may itself be a function of coupling between processes in the crystal, in particular coupling between lattice strains and Q . For this reason we will outline some aspects of phase transitions where the strain and the order parameter are coupled, or indeed identical.

1.3 Ferroelastic Phase Transitions The major benefit of Landau's theory of phase transitions is that a single simple concept can be applied to a wide variety of seemingly unrelated transformation processes. So far we have not considered in detail the real systems which Landau theory describes, and have not dwelt upon the specific physical meaning of the order parameter in terms of macroscopic measurable quantities. It is possible, however, to categorize transitions in crystals according to the physical process of change (rather than the temperature dependence of that change, as the categories second-order, first-order and tricritical apply) in other words in terms of the property which directly reflects Q . Some of the first real systems in which Landau theory was tested involved ferroelectric and ferromagnetic phase transitions, where a spontaneous magnetization or polarization below T_c corresponds to the order parameter. In these cases it is easy to see that the

symmetry relations between the paramagnetic (or paraelectric) phase and the ferromagnetic (or ferroelectric) phase are restricted to certain space groups in which a magnetic moment (or electric dipole) may arise from zero. It is also conceptually easy to see how the Landau potential may be linked to the potential of a dipole ordering in a double-well potential in the mean field of a lattice, and so the theory was readily applied to these systems. Another class of phase transitions (forming the theme of this thesis) more widespread and of greater general importance in rock-forming minerals, however, is that encompassing distortive transformations of the crystallographic unit-cell. How does Landau theory relate to these?

1.3.1 Ferroic Distortive Transitions Phase transitions which involve a change in point group of the crystal are termed ferroic transitions. Ferromagnetic and ferroelectric crystals are the examples of ferroic phases mentioned above, are there equivalent ferroic phases linked to distortive phase transitions?

The physical property representing the main peculiarity of a distortive phase transition is the strain of the low-symmetry unit-cell with respect to the high-symmetry unit-cell. This is a second-rank tensor property of the low-symmetry crystal and is analogous to the tensor properties magnetization and polarization which spontaneously arise at ferromagnetic and ferroelectric transitions. Since this strain (which is additional to linear effects such as normal thermal expansion) arises spontaneously below the transition it is called the spontaneous strain and this type of ferroic distortive transition is usually termed "potentially ferroelastic". The spontaneous strain below a ferroelastic phase transition is the macroscopic order parameter,

the idea of strain as order parameter for a distortive transition was discussed by Boccara (1968) and earlier by Idenbom (1960). The spontaneous strain must always be taken with respect to the high-symmetry or para-phase, and unlike polarization or magnetization the para-phase symmetry must be defined if the strain is to be measured.

The first systematic analysis of possible symmetry allowed ferroelastic crystallographic space groups was made by Aizu (1969) who went on to formulate the spontaneous strain expected in these ferroic groups with respect to possible paraphase symmetries (Aizu, 1970). A ferroelastic phase transition induces a modification of the crystallographic unit cell, and for a pure proper ferroelastic this limits the possible supergroup-subgroup relations. Transitions must be between groups in different crystal systems (where the trigonal and hexagonal system are counted as one, having the same unit cell). The strain at a particular ferroelastic phase transition itself has a defined symmetry, which reflects the symmetry of the order parameter. Using this relation Tolédano and Tolédano (1980) list the form of the Landau free energy for each of the possible ferroelastic phase transitions. The general principles of ferroelastic phase transitions are discussed by Tolédano (1979) and reviewed at greater length by Wadhawan (1982).

1.3.2 Physical Characteristics of Ferroelastic Phases When strain behaves like the order parameter at a distortive phase transition the low symmetry phase may exhibit a number of features characteristic of such a transition. The strain corresponds to changes in unit cell shape (and hence anomalous thermal expansion measurable by lattice parameters), is

accompanied by excess birefringence through the elasto-optic effect as well as changes in the polarizability tensor (measurable by Raman spectroscopy), and may induce the formation of twin domains. In addition certain of the elastic constants at a ferroelastic phase transition should change critically, this can be thought of as the trigger mechanism for the transition since it causes structural instability of either the high- or low-temperature phase with respect to certain applied forces. This feature can be detected by Brillouin scattering or measurement of full phonon dispersion curves by inelastic neutron scattering experiments.

The relationship between twin domains and ferroelasticity in minerals was discussed in a general fashion by Newnham (1974) when he reviewed several types of ferroic twinning. Again, symmetry is the determining factor for a number of features of twinning. The symmetry constraints on orientation of domain walls in ferroelastics, derived by Sapriel (1975), follow the same principles as for ferroelectric domains (Fousek and Janovec, 1969). The origin of ferroelastic twin boundaries has been considered in the framework of Landau theory by Barsch and Krumhansl (1984). They find that domain walls can be described mathematically by solitons (mobile solitary waves) in the crystal lattice at temperatures near T_c . The shapes of domains and interactions of domain walls have also been considered theoretically (Salje et al. 1985b) and are easily observable by transmission electron microscopy: examples recently studied include ferroelastic twins in leucite (Palmer et al., 1988) as well as in high- T_c superconducting materials (Kawamata et al., 1988; Schmid et al., 1988). Ferroelastic twins are thought to

have an important influence on the superconducting properties of these materials through their control of correlation lengths (Smith and Wohleben, 1988). More important mineralogically, the presence of ferroelastic twin domains is one of the most easily identifiable features of a low-temperature ferroelastic phase and these domains may be used to characterize a sample in terms of its transition behaviour (which can be useful petrogenetically if the equilibrium thermodynamics of the material are known).

Lattice parameters reflect directly the behaviour of the spontaneous strain, and in turn the order parameter. In the next chapter we will see how the lattice parameters of As_2O_5 may be used to determine the temperature evolution of Q at a ferroelastic phase transition. Powder X-ray diffraction at high temperatures is an essential tool for the characterization of such transitions. Figure 1.7, for example, demonstrates the sensitivity of this technique to the cubic-tetragonal transition in leucite where diffraction maxima of $\{h00\}$ type planes in the cubic phase split into $\{h00\}$ and $\{00h\}$ maxima in the tetragonal phase. The experimental details of this technique will be discussed later.

Changes in birefringence at ferroelastic phase transitions present the opportunity for one of the most sensitive and accurate measurements of spontaneous strain and Q . This technique is reviewed by Glazer (1988) and the important result for proper ferroelastic phase transitions is that the morphic birefringence (the excess birefringence, which vanishes in the high-temperature phase) is directly proportional to the order parameter as long as the indicatrix axes are not rotated by the transition. Complications can arise, however, if the low-

temperature phase is optically active, or the transition is not pure ferroelastic, and care must be taken in establishing the relation between the measured birefringence and the order parameter.

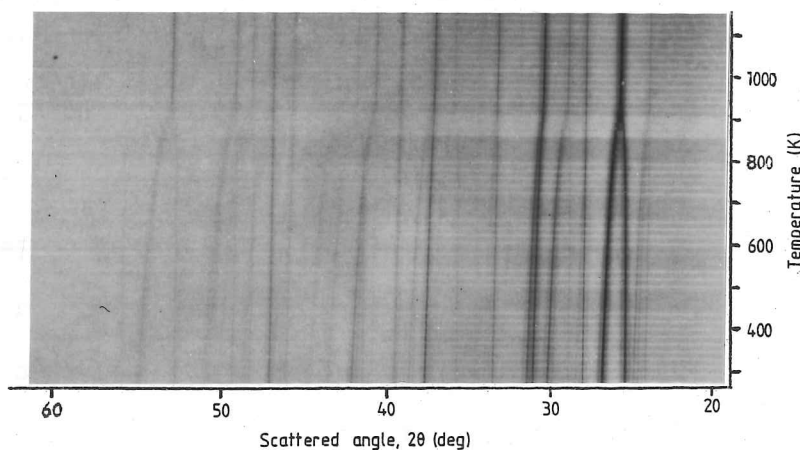


Figure 1.7 Continuous movement high-temperature Guinier diffraction pattern of leucite ($\text{KA}_2\text{Si}_2\text{O}_6$) powder, together with Si internal standard. The cubic-tetragonal transition at around 660°C leads to the large spontaneous strain indicated by the significant peak splitting in the low-temperature tetragonal phase.

The magnitude of the spontaneous strain, determined directly from lattice parameters, is typically found to vary from around 5×10^{-3} in anorthite at room temperature (Redfern and Salje, 1987) to around 55×10^{-3} in sodium nitrate at room temperature (Reeder et al., 1988). This leads to an excess elastic energy contribution in the low-temperature phase given by $\sum C_{ij} \epsilon_i \epsilon_j$ where C_{ij} are the elastic constants and ϵ_i are the spontaneous strain components. Using typical values of these constants the elastic strain due to a ferroelastic transition can correspond to an excess energy of around 2 kJ.mol^{-1} (as found in NaNO_3 at room

temperature; Reeder et al., 1988). Although the elastic energy contribution may in other cases be much smaller (only a small fraction of the total excess internal energy below a transition) its importance remains undiminished: the overall influence of spontaneous strain is most obviously seen when its rôle in coupling order parameters is considered.

1.3.3 Strain and Order-Parameter Coupling So far we have discussed only those phase transitions which are pure ferroelastic, in other words which have as their only order parameter the spontaneous strain and which involve a change in crystal system. The interesting aspect of lattice distortion in many mineral systems, however, is the interaction of strains with other processes (for example Al/Si order).

Suppose a crystal undergoes two symmetry-breaking transitions each described by a separate order parameter (Q_1 and Q_2), then the Landau expansion for the crystal must incorporate both order parameters. It is possible that, if the active representations of Q_1 and Q_2 are identical, they will couple directly (i.e. have a direct influence on one another) as has been discussed by Oleksy and Przystawa (1983). Other types of coupling, for instance direct biquadratic (via a $Q_1^2 \cdot Q_2^2$ term in the Landau expansion; Imry, 1975) may still be allowed even if the two active representations are different. Even if allowed by symmetry, however, direct coupling between ordering processes may be inapplicable if Q_1 and Q_2 have totally unrelated physical origins. On the other hand, if both of these processes induces a strain (either directly by collapse of the structure due to an elastic instability, or indirectly through the effect the ordering process has as the lattice relaxes in response to it)

then the two order parameters may now influence one another through the strain as has been pointed out by Salje and Devarajan (1986). This form of indirect coupling between Q_1 and Q_2 is especially relevant in minerals since most silicate frameworks show quite large lattice strains in response to cation ordering as well as displacive transitions. Gufan and Larin (1980) discussed the influence of order parameter coupling on the topology of the phase diagram, demonstrating that significant changes can be expected if the coupling is sufficiently strong. Coupling cannot, therefore, be ignored since it can affect the relative stability of phases and can change the character of Q_1 or Q_2 from continuous to discontinuous or vice versa.

In describing a system with two order parameters and coupling between each order parameter and the form of strain-coupling must be determined. Strain could couple to Q , to Q^2 , Q^3 and so on. Usually only the lowest order coupling is considered since this generally describes the system sufficiently accurately. Coupling between strain, ϵ , and the order parameters is symmetry determined and introduces terms like $dQ\epsilon$ or $eQ^2\epsilon$ into the Landau expansion, where d and e are coupling constants representing the strength of the coupling. In order to minimize the free energy with respect to strain we must also incorporate the elastic energy, represented below by $f\epsilon^2$. Thus we arrive at a Landau expansion to describe a crystal undergoing two ordering processes (1 and 2) coupled to one another via bilinear and biquadratic coupling to a common strain (ϵ):

$$\begin{aligned}
 G(Q_1, Q_2) = & \frac{1}{2}A_1 Q_1^2 + \frac{1}{4}B_1 Q_1^4 + \frac{1}{6}C_1 Q_1^6 \\
 & + \frac{1}{2}A_2 Q_2^2 + \frac{1}{4}B_2 Q_2^4 + \frac{1}{6}C_2 Q_2^6 \\
 & + d_1 Q_1 \epsilon + d_2 Q_2 \epsilon + e_1 Q_1^2 \epsilon + e_2 Q_2^2 \epsilon + f\epsilon^2 \quad \{1.25\}
 \end{aligned}$$

where A, B, c are Landau coefficients, d and e are strain coupling terms, and f corresponds to ^{an} elastic constant. In addition there may be direct coupling terms in the expansion, of the form gQ_1Q_2 or $hQ_1^2Q_2^2$ where g and h are coupling constants, if such coupling is symmetry allowed.

The implications of strain-induced order parameter coupling for plagioclase feldspar will be dealt with in the course of this thesis. For the moment therefore we will not go on to derive the results for Q_1 and Q_2 from equation 1.25 (further discussion is given by Salje and Devarajan, 1986), but rather present it as an example of how the Landau potential may be formulated for a case more complicated than those given in section 1.2.

An interesting aspect of strain-order parameter coupling is that if such coupling exists a strain will arise below T_c for Q analogous to the spontaneous strain at a ferroelastic phase transition, even if the symmetry of the phase transition does not correspond to one of Aizu's (1970) classes of pure ferroelastic transitions. Since the strain couples to the order parameter it may conveniently be taken as an experimental measure of the order parameter, although it may not be the order parameter itself.

There are two classes of elastic transition in which the spontaneous strain is not the order parameter, but where the strain may still arise below T_c . The first is termed improper ferroelastic, at these phase transitions the symmetry change must induce a spontaneous strain, but that strain does not fully account for the order parameter. Any phase transition between crystal classes which also changes the size of the unit cell (i.e. due to a critical point on the Brillouin zone boundary) may

be improper-ferroelastic, these are sometimes referred to as antiferrodistortive transitions. For most improper ferroelastic transitions the spontaneous strain couples to Q^2 (Janovec et al., 1975; Tolédano and Tolédano, 1980), although higher-order coupling is sometimes possible. The second class of phase transition in which strain coupling causes a spontaneous strain at a non-ferroelastic transition is known variously as co-elastic or pyroelastic. At a co-elastic transition there is no change in crystal system, so the high-temperature phase is not a true paraphase for the low-temperature phase. The transition is due to some non-elastic phenomenon, but the relaxation of the lattice in response to this ordering process induces a strain. In some cases the spontaneous strain at a co-elastic transition can nonetheless be very large (e.g. CaCO_3 ; see Dove and Powell, 1989) and the elastic energy associated with the strain can be a significant part of the excess energy below T_c . Since strain coupling is such a prevalent feature of phase transitions in minerals we shall investigate its effect on some specific examples. The $I\bar{1}-P\bar{1}$ transition in anorthite and the $R\bar{3}c-R\bar{3}m$ transition in CaCO_3 and NaNO_3 show co-elastic behaviour which will be discussed in the course of this thesis. Before tackling the relatively complex issue of coupled order parameter behaviour in minerals we shall first expand on the concepts laid out in section 1.2 and 1.3.1. In particular, chapter 2 will investigate the applicability of Landau theory to the description of ferroelastic phase transitions in framework structures, using the example of As_2O_5 as a simple 'model' compound.

CHAPTER 2

FERROELASTIC BEHAVIOUR IN ARSENIC PENTOXIDE

2.1 Introduction

Arsenic pentoxide is a simple binary oxide with a framework crystal structure. In this chapter, arsenic pentoxide is used as a 'model compound' to test the applicability of Landau theory at ferroelastic transitions in such structures. Before presenting the results of this investigation we shall briefly outline the salient features of this material, in particular those relating to the ferroelastic phase transition it displays.

2.1.1 Structure, Symmetry and Previous Investigation The stable oxide of arsenic at room temperature and pressure is As_2O_3 , but using high oxygen pressures this can be oxidised to As_2O_6 which, when subsequently sublimed, yields an interesting oxide, As_2O_5 (Jansen, 1978). The structure of arsenic pentoxide, As_2O_5 , can be described in terms of chains of corner-linked AsO_6 octahedra running parallel to the z-axis, with the chains connected to one another by AsO_4 tetrahedra around a screw-tetrad in the high-temperature tetragonal phase (Figure 2.1). The high-temperature structure distorts at lower temperatures so that at room temperature the tetrad has been lost and the symmetry is reduced to orthorhombic. The room-temperature structure was first reported by Jansen (1978) by single-crystal X-ray structure determination and found to be space group $P2_12_12_1$ (or D_2^2 in Schönflies notation). The transformation to tetragonal symmetry occurs at $T_c = 578$ K (Jansen, 1979). The high-temperature space group was assumed to be $P4_12_12$ (D_4^2) on the basis of Jansen's comparison of high-temperature X-ray powder diffraction

intensities to a postulated high-temperature structure derived from an average of two orientations of the low-temperature twinned structure. No further study was carried out by Jansen to test this postulated para-phase symmetry, however, although Raman and morphic birefringence behaviour are consistent with a phase transition between these two space group symmetries (Bismayer et al., 1986; Salje et al., 1987). It appears that the transition involves distortion of the polyhedral framework by polyhedral tilts so that the polyhedra themselves remain relatively undistorted and may be regarded as rigid units. The maximum displacements of the arsenic atoms resulting from the transition are only around 5 pm (at room temperature relative to the high-temperature structure) with maximum displacements of about 20 pm

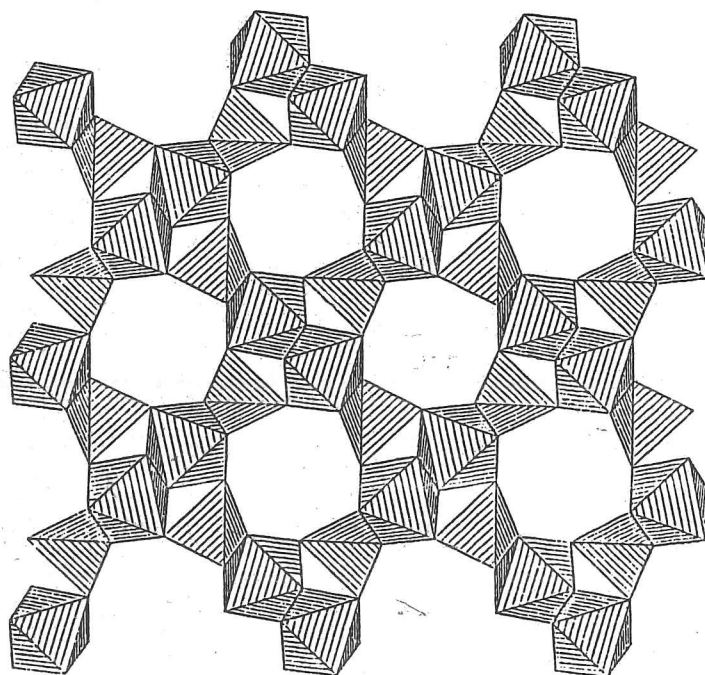


Figure 2.1 A projection down the z axis of the corner-linked polyhedral framework of As_2O_5 .

for the oxygen atoms. No other structural phase transitions of any variety are observed in arsenic pentoxide and so it seems reasonable that a single non-coupled order parameter be adopted to describe the tetragonal-orthorhombic transition.

The symmetry relation between high- and low-temperature structures indicates the low-temperature form is a possible pure-ferroelastic according to the nomenclature of Aizu (1970), in which case the order parameter should transform as the spontaneous strain. The first study of the order parameter behaviour as a function of temperature in As_2O_5 was carried out by Bismayer et al. (1986) using Raman spectroscopy. They described the driving free energy for the transition in terms of a Landau expansion of the order parameter, the elastic energy, and direct coupling between the order parameter and the spontaneous strain (they did not assume the strain was the order parameter itself). The thermodynamic potential thus described is:

$$G = \frac{1}{2}aQ^2 + \frac{1}{4}bQ^4 + \dots + \lambda Q \epsilon_s + \frac{1}{2} \sum_{ik} C_{ik} \epsilon_i \epsilon_k \quad \{2.1\}.$$

Here the single order parameter Q is linearly coupled to the strain via the constant λ . If the transition is indeed that of a pure proper ferroelastic then it can be described by the critical behaviour of the strain ϵ_s . In this case the free energy is minimised for any value of Q by applying the condition:

$$\left. \frac{dG}{dQ} \right|_Q = 0 \quad \{2.2\}$$

$$\Rightarrow Q = - \frac{\lambda}{a} \cdot \epsilon_s + \dots \quad \{2.3\}$$

Substituting equation 2.3 back into 2.1 we see that the elastic constants enter a general ϵ_s^2 term. Representing the sum of the

appropriate elastic constants by C the free energy can now be rewritten:

$$G = \frac{1}{2}(C+(\lambda^2/a))\epsilon_s^2 + \frac{1}{4}b(\lambda/a)^4 \epsilon_s^4 + \dots \quad \{2.4\}$$

which describes a pure ferroelastic system in which the structural instability arises from critical behaviour of the temperature dependent elastic constants, inducing a macroscopic lattice distortion ϵ_s . In this case Q is approximately proportional to the strain.

If, however, there is some other process in As_2O_5 driving the transition (Bismayer et al., 1986, postulated a driving sublattice distortion which they link to Q) then Q, the order parameter itself, is used for the description of the transition with the temperature dependence of the potential (2.1) arising from the prefactor a. This arises from the condition that the crystal is free of stress at any temperature:

$$\left. \frac{dG}{d\epsilon_s} \right|_{\epsilon_s} = 0 \quad \{2.5\}$$

In the description resulting from condition 2.5 the strain is again coupled to the order parameter and again we expect temperature dependent elastic constants.

The two approaches (application of condition 2.2 or condition 2.5) represent two seemingly indistinguishable driving mechanisms for the phase transition in arsenic pentoxide, we shall attempt to unravel them and discuss the implications of these two approaches towards the end of this chapter.

In either case symmetry allows coupling between Q and ϵ via λ . This coupling may itself give rise to the transformation if λ

is temperature dependent. Bismayer et al. (1986) point out that it is possible to distinguish between this third mechanism and the first two by considering the temperature dependence of the elastic constants. Furthermore their Raman observations reveal that softening of optic modes occurs without full recovery in the high-temperature phase. This may indicate that the structural phase transition shows aspects of relaxational or order-disorder behaviour in addition to the pure displacive behaviour expected at a proper ferroelastic phase transition. Their measurements showed that within experimental resolution the temperature dependence of Q , which they related to an unspecified sublattice distortion, follows that predicted by the Landau model (equation 2.1 with condition 2.5) for a second-order phase transition between T_c and room temperature.

The temperature evolution of the optical birefringence of As_2O_5 has also been studied within the scope of Landau theory which again was shown to apply between room temperature and $T_c - 5$ K, where $T_c = 578$ K (Salje et al., 1987). They found no evidence of crossover behaviour between order-disorder and displacive transition character.

Although the optic modes (and sublattice distortion) and the morphic birefringence have been studied in much detail, nothing is known about the basic ferroelastic parameter in As_2O_5 : the spontaneous strain. In this chapter we consider the temperature evolution of the spontaneous strain and the coupling between softening of elastic constants and softening of optic modes at the phase transition. The strain is measured by X-ray powder diffraction, which also yields information regarding the variation of correlation length through the transition.

2.1.2 Spontaneous Strain and the Twin Law Before describing the experimental results from the investigation of As_2O_5 we shall first outline the process by which the form of the spontaneous strain and order parameter symmetry at a phase transition between known symmetries may be predicted.

The transition from the high-temperature space group $P4_{1,2,1,2}$ to the low-symmetry subgroup $P2_{1,1,2,1}$ involves no loss of translational symmetry and must be due solely to the critical behaviour of phonons associated with the centre (Γ point) of the Brillouin zone. The representation tables of the high- and low-temperature point groups are given in Table 2.1. The active representation of the high-temperature symmetry is that which transforms to the identity under the operation of the low-temperature symmetry elements (diads parallel to x , y , and z). The characters transforming as the identity are shown circled in Table 2.1 and we see that the active representation of the order

High Temperature					Low Temperature					
422 D_4	E	$2C_4$ [001]	C_2 [001]	$2C_2'$ [100] [010]	$2C_2''$ [110]	222 D_2	E	C_2 [100]	C_2 [010]	C_2 [001]
A_1	1	1	1	1	1	A_1	1	1	1	1
A_2	1	1	1	-1	-1	A_1	1	1	1	1
B_1	1	-1	1	1	-1	B_1	1	-1	-1	1
B_2	1	-1	1	-1	1	B_2	1	-1	1	-1
E	2	0	-2	0	0	B_2	1	1	-1	-1

x^2+y^2, z^2
 z, R_z
 x^2-y^2
 xy
 $(x,y) (R_x, R_y) (xz,yz)$
 x^2, y^2, z^2
 z, R_z xy
 y, R_y xz
 x, R_x yz

Table 2.1 Representation tables for point groups 422 and 222 showing the correlation between symmetry operators and demonstrating that B_1 is the active representation for the phase transition.

parameter corresponds to B_1 in the supergroup $P4_12_12_1$. The spontaneous strain must also transform according to this active representation, in other words the symmetry adapted strain is proportional to x^2-y^2 (the basis function for this representation). Hence the form of the spontaneous strain is $\epsilon_s \propto (\epsilon_{11}-\epsilon_{22})$ or in Voigt notation $(\epsilon_1-\epsilon_2)$. Aizu (1970) lists the forms of the scalar spontaneous strain for all proper ferroelastic phases with appropriate constants of proportionality and according to his scheme the scalar spontaneous strain for orthorhombic As_2O_5 is given by:

$$\epsilon_s = \frac{|\epsilon_1 - \epsilon_2|}{\sqrt{2}} \quad \{2.6\}.$$

There are two orientational states of the ferroelastic $P2_12_12_1$ structure with respect to the high-symmetry para-elastic phase. These are denoted S and S' by Aizu and correspond to the two possible twin domains observed in As_2O_5 at room temperature, which must have equal and opposing strains.

Applying the approach of Salje et al. (1985b), it is now possible to determine the twin law for the ferroelastic domains in As_2O_5 . The spontaneous strains for the two adjacent domains are given by the second-rank tensors (Nye, 1957):

$$S = \begin{bmatrix} \epsilon_{11} & 0 & 0 \\ 0 & \epsilon_{22} & 0 \\ 0 & 0 & 0 \end{bmatrix} = (\epsilon_1 \ \epsilon_2 \ 0 \ 0 \ 0 \ 0) \quad \{2.7\}$$

$$S' = \begin{bmatrix} -\epsilon_{11} & 0 & 0 \\ 0 & -\epsilon_{22} & 0 \\ 0 & 0 & 0 \end{bmatrix} = (-\epsilon_1 \ -\epsilon_2 \ 0 \ 0 \ 0 \ 0) \quad \{2.8\}.$$

At the domain boundary all strain components must be equal. Adopting the arguments of Sapriel (1975), the domain wall is the plane defined by

$$(S_{ij} - S'_{ij})x_i x_j = 0 \quad \{2.9\}$$

which leads to the condition that $x=y$ or $x=-y$ at the domain boundary. The twin planes are therefore of the form $\{110\}$. According to David (1983), this implies that any soft acoustic modes associated with the transition propagate in the $\langle 110 \rangle$ directions. The rôle of acoustic softening will be more fully discussed in section 2.3. We would also expect the formation of needle domains and related twin interactions in As_2O_5 as has recently been described in the symmetrically similar tetragonal-orthorhombic ferroelastic transition in the 1-2-3 oxide high- T_c superconductors (Wadhawan, 1988).

The spontaneous strain is a measure of the distortion of the unit cell and may be calculated from the lattice parameters measured by X-ray powder diffraction (Figure 2.3). The strains ϵ_1 and ϵ_2 are given by

$$\epsilon_1 = \frac{a}{a_0} - 1 \quad \{2.10\}$$

$$\epsilon_2 = \frac{b}{b_0} - 1 \quad \{2.11\}$$

where the subscript 0 refers to those parameters expected by extrapolation from the high-symmetry para-phase to the ferroelastic phase. For the transition considered here $a_0=b_0=(a+b)/2$, hence, applying equation 2.6, ϵ_s is given by

$$\epsilon_s = \sqrt{2} \left| \frac{a-b}{a+b} \right| \quad \{2.12\}.$$

Thus, we see that the form of the spontaneous strain at a

ferroelastic transition is constrained by symmetry, and as we saw in chapter 1, this also constrains the expected form of the Landau potential. Having explored the implications of the symmetry of the transition, ϵ_s (and in turn Q) can now be determined experimentally from lattice parameter measurements through the transition.

2.2 Experimental Details

Arsenic pentoxide is extremely hygroscopic; the samples used for this study were grown in a dry atmosphere at the University of Hanover and generously provided by Dr M Jansen.

2.2.1 Lattice Parameter Measurements Lattice parameters were measured by X-ray powder diffraction using Guinier geometry. The Guinier camera has several advantages over standard Debye-Scherrer geometry. The principal advantage of the focussing geometry is high-resolution, allowing accurate lattice parameter determination. In addition, the intensity of the focussed beam enhances the observation of weak reflections. Film methods are also superior to standard counter detection if absolute intensity data are unimportant since film is a more efficient X-ray detector over usual exposure times.

As_2O_5 powder was loaded into 0.3mm diameter silica glass capillaries, and sealed under dry argon to prevent sublimation of the samples above around 100°C. Diffraction experiments were carried out using a Huber 632 heating Guinier powder camera configured to record transmission powder patterns. $CuK\alpha_1$ was selected from a bent quartz monochromator. A Huber 633 temperature controller allowed relative temperature stability better than 1 K, as measured by a chromel/alumel thermocouple

positioned within 1 mm of the sample. Exposures were made under isothermal conditions, the controller allowing automatic film movement and temperature variation between exposures. The absolute temperature scale was calculated and correction facilitated by measuring known transitions in the temperature range 370 K to 700 K. Care was taken to avoid errors arising from fluctuations in thermal gradient through the furnace by ensuring draught-free conditions in the vicinity of the apparatus and keeping the sample position within the furnace fixed. Further details of the temperature calibration of the high-temperature Guinier camera furnace are given in appendix 1. The film-lift device of the Huber high-temperature Guinier camera allows consecutive exposure of diffraction patterns at preset temperatures to be made on a single film. This allows a single

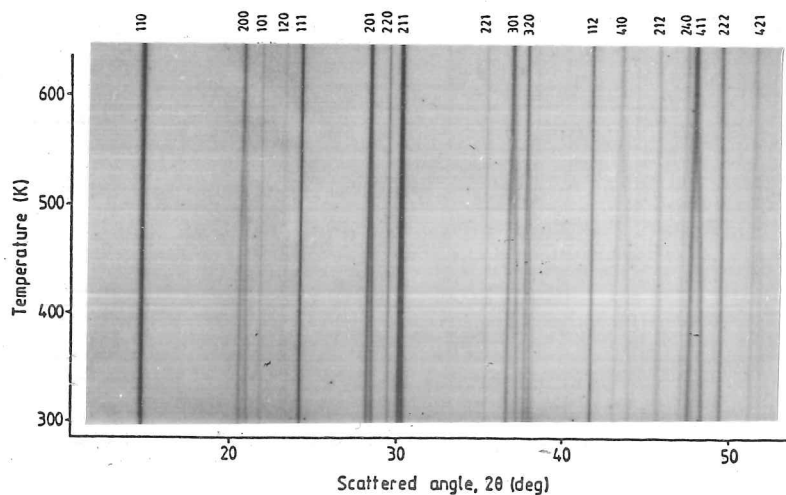


Figure 2.2 Continuous movement high-temperature Guinier diffraction pattern of As_2O_5 powder. Lines in the tetragonal phase are indexed, and splitting in the low-temperature orthorhombic phase corresponds to the onset of spontaneous strain.

shrinkage and zero correction to be made for exposures at several temperatures and eliminates cumulative errors arising from film shrinkage correction and zero-errors which would arise if each pattern was recorded on a separate film.

Figure 2.2 shows a photograph obtained from a continuous heating experiment, which is effectively a plot of line position with temperature. The large spontaneous strain is evident from the obvious peak splitting of pairs of reflections in the orthorhombic phase. Lines showing no peak splitting correspond to those with equal multiplicities in the orthorhombic and tetragonal phases.

Diffraction patterns taken between room temperature and 770 K were measured using an Enraf-Nonius Guinier film viewer. Rather similar to a standard microfilm reader, the film viewer enables the alignment of a cursor to each line; the line position may then be read off from a Vernier scale to within $0.01^\circ 2\theta$. The film cassette holder incorporates two radioactive marker lines which generate fine marks at accurately fixed positions at the top of each developed film against which measured line positions were corrected for film shrinkage. The zero- 2θ position was obtained by short exposure of the incident X-ray beam.

Cell parameters were calculated by least squares refinement of about twenty measured and corrected reflections at each temperature using the program "CELL" developed from a general least squares regression program. Typically lattice parameters were obtained with one standard deviation error of around 0.0014 \AA in a and b and 0.0007 \AA in c. The measured cell parameters of As_2O_5 are presented in Table 2.2. The temperature evolution of these lattice parameters is shown in Figure 2.3.

Arsenic Pentoxide

T(K)	a (Å)	b (Å)	c (Å)	volume	strain
293	8.45281	8.64919	4.62863	338.399	0.0162
308	8.45429	8.64675	4.62865	338.364	0.0159
323	8.45731	8.64390	4.62890	338.392	0.0154
338	8.45980	8.64220	4.62970	338.454	0.0151
353	8.46493	8.64262	4.63034	338.752	0.0147
368	8.46546	8.64037	4.63041	338.690	0.0145
383	8.47034	8.63989	4.63187	338.963	0.0140
398	8.47608	8.63577	4.63238	339.079	0.0132
413	8.47773	8.63277	4.63020	338.868	0.0128
413	8.47846	8.63161	4.62870	338.741	0.0127
430	8.48537	8.63127	4.62897	339.023	0.0121
440	8.48902	8.63049	4.63031	339.236	0.0117
450	8.49410	8.63153	4.63135	339.558	0.0113
460	8.49662	8.62897	4.63066	339.506	0.0109
476	8.50125	8.62512	4.63258	339.681	0.0102
491	8.50499	8.62140	4.63146	339.602	0.0096
506	8.50890	8.61455	4.63171	339.506	0.0087
522	8.51260	8.61119	4.63216	339.554	0.0081
537	8.51737	8.60739	4.63268	339.632	0.0074
552	8.52891	8.60079	4.63186	339.772	0.0059
567	8.53588	8.58785	4.63218	339.561	0.0043
582	8.5702		4.6318	340.204	
597	8.5693		4.6293	339.947	
597	8.5715		4.6329	340.382	
612	8.5674		4.6301	339.849	
612	8.5716		4.6335	340.436	
626	8.5713		4.6333	340.393	
626	8.5667		4.6299	339.787	
641	8.5693		4.6304	340.026	
655	8.5688		4.6303	339.977	
669	8.5714		4.6308	340.212	
684	8.5725		4.6318	340.382	
699	8.5733		4.6323	340.481	
713	8.5733		4.6332	340.548	
727	8.5740		4.6328	340.580	
742	8.5738		4.6333	340.591	
756	8.5735		4.6335	340.579	
771	8.5741		4.6333	340.616	

Table 2.2 High-temperature lattice parameters of As_2O_5 .

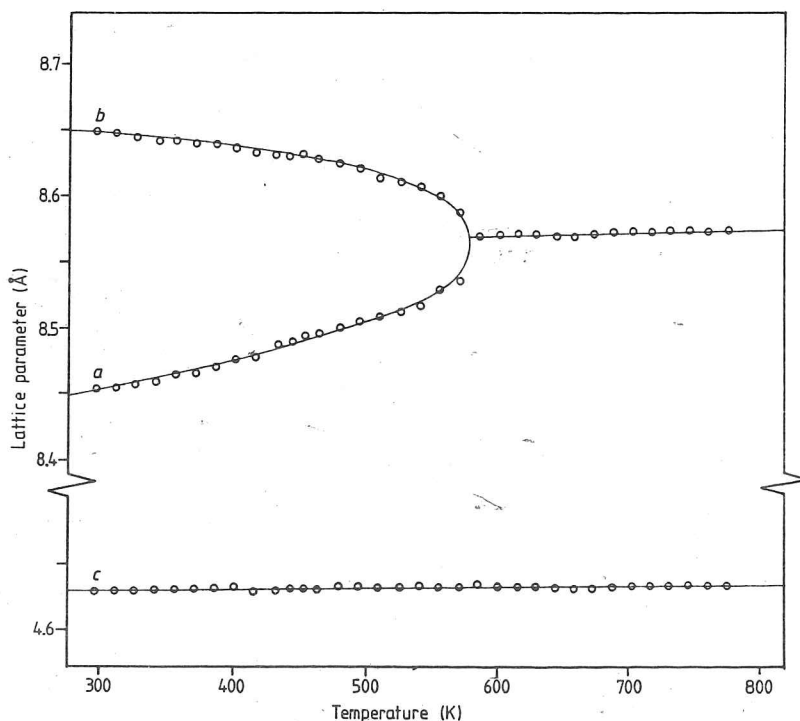


Figure 2.3 Temperature dependence of the lattice parameters of As_2O_5 .

2.2.2 Line Profiles The exposed films were scanned using a Joyce-Loebl microdensitometer to obtain line profiles of diffracted peaks. Five densitometer scans were superimposed for each exposure at each temperature to reduce the influence of statistical effects arising from film grain and average the noise. The resulting densitometer traces shown in Figure 2.4 demonstrate the splitting of the strong tetragonal 411 reflection into the orthorhombic 411 and 141 reflections through the transition, and show the behaviour of the 222 reflection, which is unaffected by the transition.

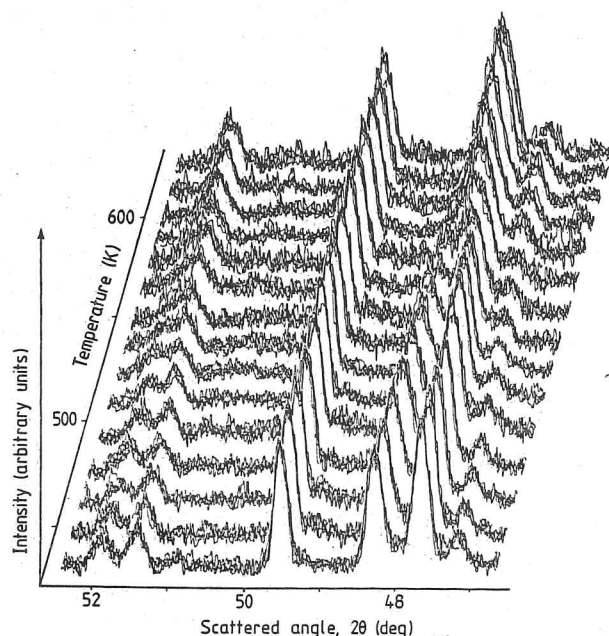


Figure 2.4 Densitometer traces of diffraction patterns of As_2O_5 through the tetragonal to orthorhombic transition. The 411 peak near $48^\circ 2\theta$ splits to 411 and 141 in the orthorhombic phase.

2.3 Critical Behaviour in Arsenic Pentoxide

2.3.1 Order Parameter Behaviour from Strain It is now

straightforward to derive the strain behaviour from the lattice parameters given in Table 2.2 by applying equation 2.12. The calculated scalar spontaneous strain, ϵ_s , is given in the last column of Table 2.2. The variation of the spontaneous strain,

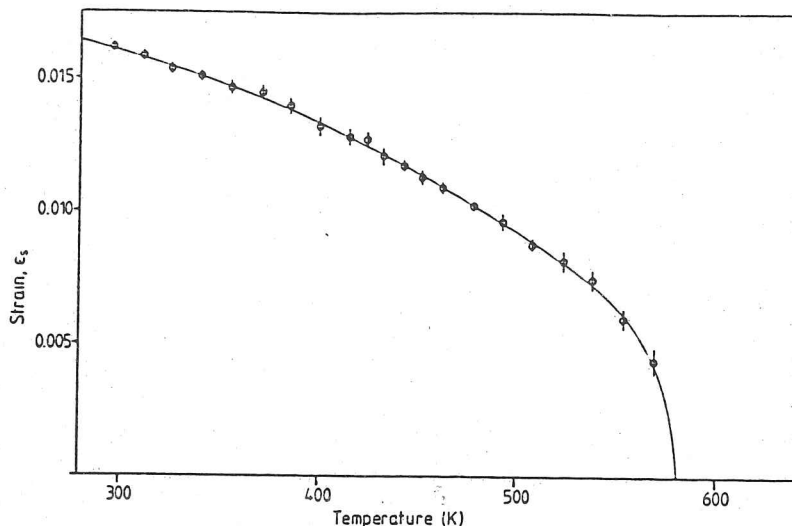


Figure 2.5 Temperature dependence of the scalar spontaneous strain in As_2O_5 . Error bars represent $\pm 2\sigma$. The solid line indicates the behaviour expected below a second-order phase transition, predicted from Landau theory.

ϵ_s , with temperature is shown in Figure 2.5. We noted in section 2.1.1 that the spontaneous strain is linearly coupled to the order parameter, hence the strain shown in Figure 2.5 may be directly correlated to Q . The full curve shows the strain predicted by a Landau potential with critical exponent $\beta = \frac{1}{2}$ (equation 1.7) and linear coupling between Q and ϵ_s . We see that the spontaneous strain follows second-order Landau behaviour within the limit of error. The coupling constant is easily determined, and we arrive at:

$$Q = \left| \frac{578-T}{578} \right|^{\frac{1}{2}} = (42.2 \pm 0.6) \cdot \epsilon_s \quad \{2.13\}.$$

The temperature dependence of the spontaneous strain in As_2O_5 is in agreement with that expected from Landau theory of the structural phase transition. The excellent agreement with theory may be related to the restricted directions of propagation of the critical acoustic phonons. The acoustic mode softening is

limited to waves in the $\langle 110 \rangle$ directions in the tetragonal phase at the Brillouin zone centre, as the elastic constants $C_{11} - C_{22}$ go to zero. The polarization vector associated with these transverse phonons is perpendicular to the wavevector and within the (001) plane. In these respects the phase transition in As_2O_5 is analogous to those found in TeO_2 (Peercy and Fritz, 1974) and DCN (Mackenzie and Pawley, 1979). This type of displacive phase transition has been considered theoretically by Folk et al. (1976) and Cowley (1976). Cowley (1976) points out that in such cases (which he denotes as type I) a continuous phase transition may be expected to occur. Deviations from Landau behaviour result from fluctuations in the order parameter near T_c . As fluctuations become more pronounced and comparable with the value of Q itself, and if they extend over distances corresponding to the correlation range ξ , then the Ginzburg criterion is no longer fulfilled and Landau theory breaks down. In the case of type I structural instabilities, however, fluctuations of the acoustic phonons are restricted to cones around the two perpendicular directions of wave propagation in k -space (Figure 2.6), and thus a Landau model can be expected to be obeyed even at temperatures close to T_c . In addition to the restricted directions of acoustic softening (and thus restricted directions in k -space of associated order parameter fluctuations), the framework structure of As_2O_5 allows correlated distortions over long distances in the structure, further reducing the volume of phase space in which fluctuations might occur. There is no experimental evidence for deviations from a Landau model due to either fluctuations or other coupling effects. In this respect As_2O_5 may be described as an ideal 'model' ferroelastic material.

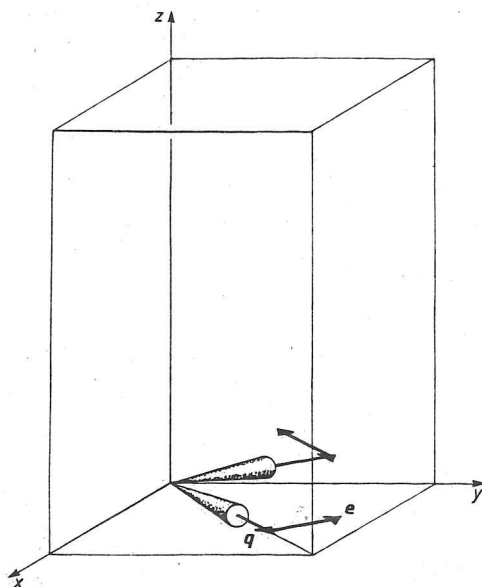


Figure 2.6 The wavevectors (\underline{q}) and polarisation vectors (\underline{e}) of the critical transverse acoustic mode in As_2O_5 . Cones indicate regions of critical fluctuations.

2.3.2 Critical Linewidth and Susceptibility In addition to the onset of spontaneous strain, the phase transition is also reflected by a singularity in the width of those powder diffraction lines which split in the orthorhombic phase. Figure 2.7 shows the temperature evolution of the line width Γ of such reflections, namely the orthorhombic 141 and 411 reflections, which merge to 411 in the tetragonal phase. Linewidths were measured directly from densitometer traces of the Guinier films. The observed increase in Γ does not occur for reflections whose Bragg angle does not depend on the order parameter, for example 222, as can be seen in Figure 2.4. Above T_c we observe significant but decreasing line broadening of the tetragonal 411 peak, corresponding to the increasing correlation length of fluctuations beyond that seen by X-rays. The linewidth of the

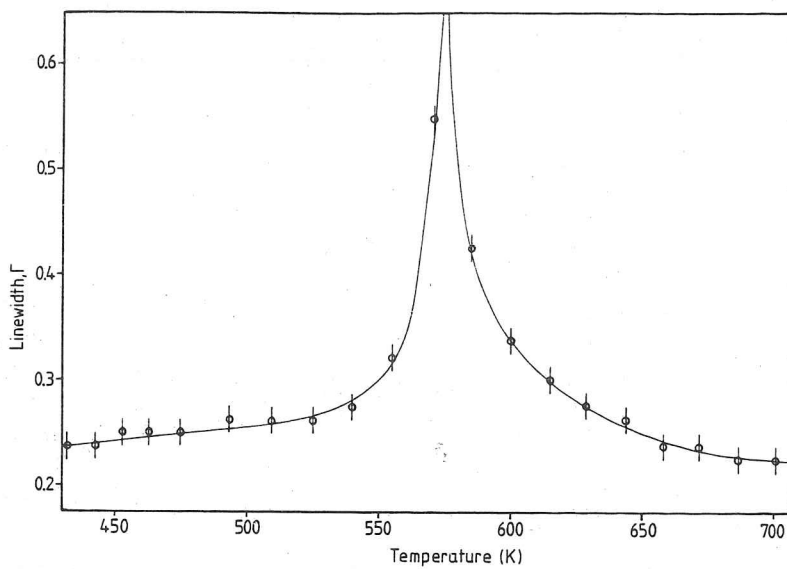


Figure 2.7 The absolute linewidth of the tetragonal 411 reflection ($^02\theta$) as a function of temperature in As_2O_5 .

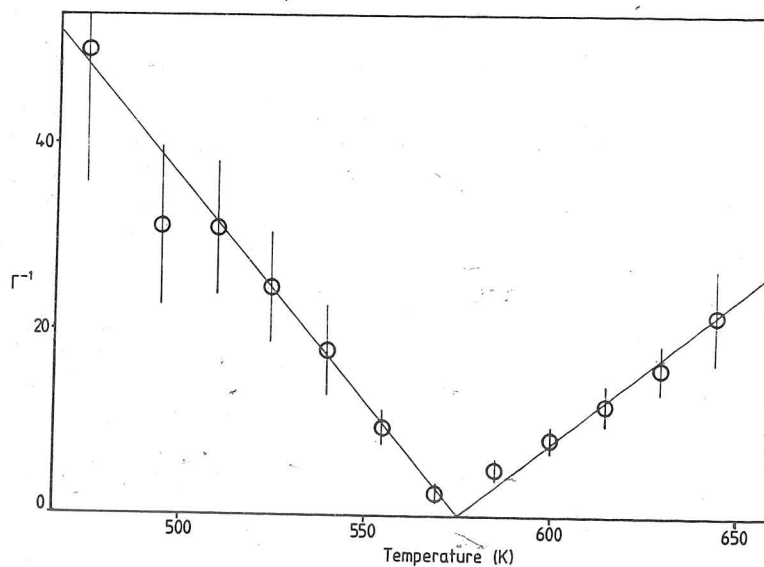


Figure 2.8 The reciprocal of the corrected linewidth of the tetragonal 411 and orthorhombic 141 and 411 reflections as a function of temperature in As_2O_5 .

411 peak falls to that of the original low temperature orthorhombic peaks. The possible order-disorder behaviour inferred from the non-recovery of the softened raman mode observed by Bismayer et al. (1986) should lead to broadening of lines in the tetragonal phase, which we do not observe. The broadening may be explained solely in terms of spatial fluctuations of the order parameter near T_c : the linewidth increases due to inhomogeneous variations of the spontaneous strain, and lines which are independent of the order parameter remain sharp. The physical origin of such spatial variation of the order parameter could be ascribed to the possible variation of twin domain size below T_c . It is anticipated that observations of the domain pattern of As_2O_5 would reveal an increasing number and decreasing size of twin domains as T_c is approached from below. The correlation length of the spatial fluctuations (which might be thought of in our model as twin walls) increases as T_c is approached from below, and becomes comparable and then greater than the correlation length of the X-rays. The linewidth, in this case, is therefore directly proportional to the susceptibility χ of the order parameter. Landau theory predicts that, at a second-order phase transition, the susceptibility shows the following temperature dependence;

$$\chi \propto |T - T_c|^{-\gamma} \quad \{2.14\}$$

and the slope of χ^{-1} against T below T_c is twice that above T_c . Data have been plotted in Figure 2.8 for χ^{-1} close to T_c and it can be seen that this relationship between the slopes above and below T_c is followed. This corresponds to the critical exponent $\gamma = 1$ as expected for a phase transition following

Landau theory. Hence the line broadening is entirely consistent with Landau theory, and results from the expected variation in correlation length of fluctuations of the order parameter near T_c .

Softening of the $\langle 110 \rangle$ transverse acoustic phonons at the zone centre might be expected to lead to dynamical broadening of the powder lines, but this diffuse scattering would affect all Bragg peaks and we have not been able to observe such an effect. Nevertheless such a phonon instability, resulting in softening of the mode near $q=0$ as T_c is approached, may be used to describe the driving order parameter. At the analagous transition in DCN (Mackenzie and Pawley, 1979), phonon dispersion curves have been measured by neutron scattering and are observed to soften. Similar acoustic softening has been observed in s-triazine (Dove et al. 1983), where the ferroelastic transition at 198 K is accompanied by significant changes in the dispersion curves above T_c .

2.3.3 Coupling Between Acoustic and Optic Modes Consideration of the symmetry change $P4_12_12 - P2_12_12_1$ indicates that Bragg reflections (00ℓ) , $\ell = 4n + 2$ are prohibited in the high symmetry phase but may appear in the low symmetry distorted structure as a result of conversion of the 4_1 axis to 2_1 . Schmahl and Redfern (1988) presented the results of X-ray critical scattering studies of the (006) reflection which further probed the nature of the phase transition and tested the validity of the proposed high-temperature space group.

The theory of X-ray scattering intensities of critical superlattice reflections at displacive phase transitions is well established and considered by Bruce and Cowley (1981). For soft

mode transitions the structure factor can be expanded in terms of the normal mode mean amplitudes $\langle Q_j \rangle$ which become non-zero below the transition temperature. In As_2O_5 , however, the phase transition is driven by acoustic mode softening along $\langle 110 \rangle$ for $|q|$ tending to the Brillouin zone centre. These acoustic phonons with vanishingly small wave vector correspond to a homogeneous deformation of the crystal and the phase factors, $\exp(-i\underline{S} \cdot \underline{r}_k)$, for waves scattered from atoms at \underline{r}_k to the reciprocal lattice point with scattering vector \underline{S} are invariant. Hence the pattern of systematic extinctions is not affected by the acoustic mode softening and critical superlattice reflections are not expected to arise, since in itself a $q=0$ (Γ -point) instability does not lead to broken translational symmetry.

The symmetry change in arsenic pentoxide however implies there is a change in the screw periodicity of the structure along the z -axis (due to the loss of the 4_1 axis) at the phase transition. Atoms within one unit cell are displaced 'out of phase' parallel to the z -axis in the low temperature structure, breaking the $\frac{1}{4}c$ periodicity and giving rise to reflections of the type (00ℓ) , $\ell = 4n + 2$, below T_c . Thus the cooperative $q=0$ atomic displacement pattern responsible for the temperature evolution of the (006) reflection is of optic character rather than acoustic. Jansen (1979) discussed the relationship between the high and low-temperature structures, and consideration of the differences between twin-related orthorhombic cells suggests the displacement pattern which is shown in stylized form in Figure 2.9. Octahedral tilts around axes within the $\{110\}$ planes lead to atomic displacements with a component parallel to z and we can see from Figure 2.9 that these are of optic character breaking

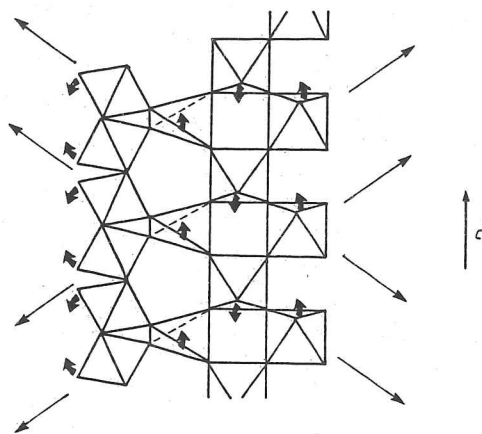


Figure 2.9 A schematic diagram showing the atomic displacements in the orthorhombic phase of As_2O_5 away from the positions in the tetragonal phase. Fine arrows indicate the projections of the polyhedral tilt axes which lie in the $\{110\}$ planes.

the 4_1 symmetry.

Schmahl and Redfern's (1988) measurements of the temperature dependence of the integrated intensity of the (006) reflection demonstrate that I_{006} behaves as Q^2 below T_c . This implies the amplitude of the atomic displacement pattern, $\langle Q_j \rangle$, is coupled linearly to the order parameter for the transition, and hence linearly to ϵ_s . The measurements of superlattice intensity are consistent with the strain data presented here, and furthermore, they confirm the postulated high-temperature space group symmetry ($4_1 2_1 2$).

The Raman-active optic phonons measured by Bismayer et al. (1986) soften appreciably as T_c is approached from below but do not recover above T_c and none is a true soft mode. The primary order parameter for the transition is, therefore, not an optic phonon. The atomic displacement pattern considered by Schmahl and Redfern (1988) results from a combination of the acoustic and

optic modes associated with the transition. Rae (1982) has described the proper ferroelastic transition in s-triazine similarly. The eigenvectors of the displacement pattern $\langle Q_{j0} \rangle$ do not, therefore, correspond to those of the soft acoustic mode or any optic mode, but to a combination of them all. Because of their low frequency the acoustic modes make only a small contribution to the free energy available to drive the transition, but the incomplete softening of the optic distortions coupling to them is more significant energetically. In this sense although the driving order parameter itself is the acoustic shear (the softening of $C_{11} - C_{12}$) the synergetic influence of the acoustic-optic coupling is most important.

2.3.4 Implications for the Grüneisen Relation The incompletely softened optic modes and the cooperative distortion $\langle Q_{j0} \rangle$ have the same irreducible representation as the spontaneous strain, and the lowest order coupling between the optic distortion and Q is linear. This linear coupling is responsible for the observation by Bismayer et al. (1986) that the low temperature excess frequency, $\Delta\omega^2$, is proportional to $|T_c - T|$. The softening of the hard-mode raman lines observed by Bismayer et al. (1986) thus arises from direct coupling between the acoustically driven spontaneous strain and the optic modes. The spontaneous strain behaves as the order parameter, and is proportional to the shift in the hard mode frequency ($\Delta\omega$):

$$\Delta\omega^2 \propto \epsilon_S^2 \propto Q^2 \propto (T_c - T)^{2\beta} \quad \beta = \frac{1}{2} \quad \{2.15\}$$

These dependences obviously violate the Grüneisen relation:

$$\frac{\Delta\omega}{\omega} = \gamma_i \frac{\Delta V}{V} \quad \{2.16\}$$

where V is the molar volume and ω is the hard-mode frequency. In the orthorhombic phase the cell volume is given by $a \times b \times c$, and the lattice parameters a and b can be expressed in terms of the extrapolated tetragonal parameters a_0 and b_0 ($a_0 = b_0$) as:

$$\left. \begin{aligned} a &= a_0 - \alpha(T_c - T)^{1/2} \\ b &= b_0 + \alpha(T_c - T)^{1/2} \end{aligned} \right\} \quad \{2.17\}$$

$$\Rightarrow V = c_0(a_0 b_0 - \alpha^2(T_c - T)) \quad \{2.18\}$$

$$\Rightarrow \Delta\omega \propto \Delta V \propto (T_c - T) \propto \epsilon_S^2 \quad \{2.19\}$$

which conflicts with the observed result: $\Delta\omega \propto \epsilon_S$. Hence the Grüneisen relation is not obeyed in the ferroelastic phase of As_2O_5 , where the dilation along b counteracts the contraction along a in the expression for volume.

2.4 Summary, Conclusions, and Consequences

It is apparent that the Landau model for free energy successfully predicts a number of features associated with the ferroelastic phase transition in As_2O_5 . In particular we have seen that the spontaneous strain in As_2O_5 behaves like the order parameter exactly according to the model for a second-order phase transition, even for quite large values of Q (when the power series expansion might be expected to become invalid) as well as very near T_c (where dynamical fluctuations of Q might be expected to become important). The strict adherence to Landau theory is attributed to the long length scale over which correlated ordering can operate in the framework structure. It seems that Landau theory is best applied to the description of ferroelastic and related phase transitions. This argument has a significant

bearing on the expected behaviour of framework silicates undergoing ferroelastic and co-elastic phase transitions. The success of Landau theory in the example of As_2O_5 in this way justifies the application of this same theory to the description of displacive phase transitions in minerals with framework structures.

Although the orthorhombic-tetragonal phase transition in As_2O_5 at first appears quite simple (with no evidence of a crossover or coupling to other phase transitions in the structure, and describable by a single component order parameter) we have seen that even in this 'model' case there are complicating subtleties that must be considered if the transition mechanism is to be fully understood. The rôle of coupling between the driving acoustic mode softening to optic mode softening appears very important energetically, but is not an essential feature of the Landau description. Thus we see that in a particular case (no matter how apparently straightforward) the full description of a phase transition may depend on the application of a variety of experimental methods. Nonetheless, in a ferroelastic or co-elastic phase transition the spontaneous strain is seen to provide a sensitive measure of the transition behaviour.

CHAPTER 3

CO-ELASTIC BEHAVIOUR AT THE $I\bar{1}-P\bar{1}$ TRANSITION IN ANORTHITE

3.1 Introduction

The behaviour and thermodynamic properties of feldspars are of fundamental importance to Earth scientists because together this mineral family comprises some 60% of the Earth's crust. The structure of feldspar was first solved by Taylor (1933) in Cambridge during his study of sanidine. It consists of a three-dimensional framework of AlO_4 and SiO_4 corner-linked tetrahedra, with larger cations (Ca in anorthite, Na in albite, and K in orthoclase) occupying cavities within this framework (Figure 3.1). The unparalleled complexity in the sub-solidus phase relations of feldspars is due to the interplay of the state of

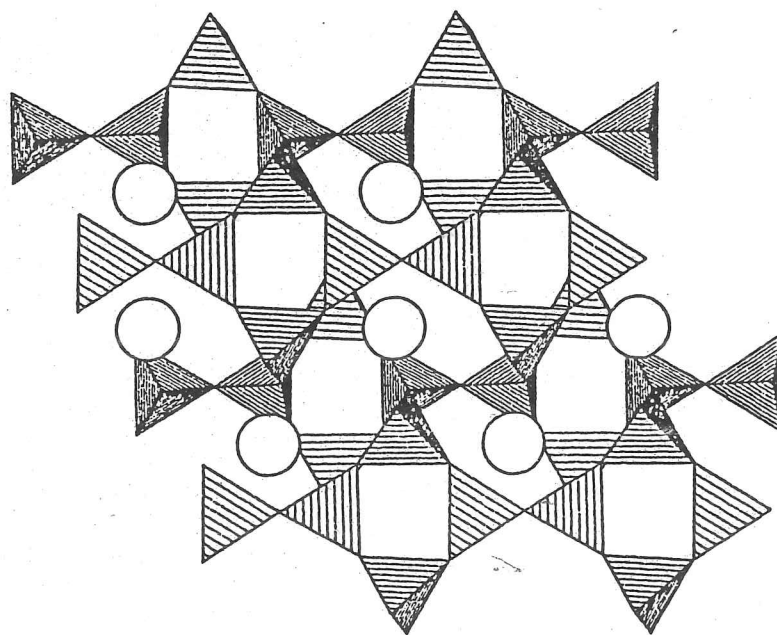


Figure 3.1 The crystal structure of feldspar projected almost parallel to the y -axis. Each aluminosilicate tetrahedron is corner-linked to four others. The large circles represent alkali-earth cations.

order of the Al and Si atoms with displacive transitions of the framework as a whole. The recent application of Landau theory to the feldspar system (Salje, 1985; Salje, 1987b; Carpenter, 1988) has allowed a start to be made at understanding this complex behaviour as a function of temperature and sample characteristics. In this chapter and chapter 4 the behaviour of Ca-rich plagioclases at the $I\bar{1}-P\bar{1}$ displacive phase transition will be investigated. The influence of the degree of Al/Si order (represented by Q_{od}), sample composition and homogeneity, and increased pressure as well as temperature will be discussed within the framework of Landau theory for the free energy.

The example of the displacive primitive to body-centred transition in anorthite ($CaAl_2Si_2O_8$) and calcium-rich plagioclases ($Ca_xNa_{1-x}Al_{1+x}Si_{3-x}O_8$) is interesting since it demonstrates the potential importance of strain-induced order parameter coupling in problems of mineral behaviour. We shall see that the phase transition is sensitive to both the chemistry and the thermal history of the particular plagioclase studied. It has already been observed that framework structures exhibiting ferroelastic phase transitions often follow Landau-type models fairly closely over large temperature intervals (e.g. As_2O_5 (see chapter 2 and Redfern and Salje, 1988), quartz (Salje et al., 1989), alkali-feldspars (Salje et al., 1985a), leucite (Palmer et al., 1989), cordierite (chapter 5 and Putnis et al., 1987)), and we shall see that the plagioclase feldspars provide another example where the Landau approach works well. This has been attributed to the long distances over which the order parameter is correlated in framework structures, and the consequent reduction in the region over which fluctuations are important

(Cowley, 1976).

In calcium-rich plagioclases the interplay (via strain) of the processes of ordering of Al and Si on the tetrahedral sites and the substitution of Na for Ca on the alkali sites with the displacive $I\bar{1}-P\bar{1}$ transformation of the framework results in changing transition behaviour. Therefore before turning to the displacive transition we shall briefly consider the process of Al/Si ordering in calcium-rich plagioclases.

3.1.1 The $C\bar{1}-I\bar{1}$ Al/Si Ordering Transition End-member anorthite has the composition $CaAl_2Si_2O_8$, and the 2:2 ratio of Al:Si allows it to order these tetrahedral cations so that (in the fully ordered state) each Si tetrahedron is surrounded by four Al neighbours, and vice-versa. This ordering of Al and Si on the tetrahedral sites in the plagioclase framework results in the lowering of symmetry from $C\bar{1}$ (disordered) to $I\bar{1}$ (ordered) and a unit cell with a 14 \AA repeat along the z-axis. The phase transition is accompanied by the loss of superlattice reflections (termed 'b' reflections: $h + k$ odd, l odd; see Bown and Gay (1958) for a description of the plagioclase reciprocal lattice geometry) which are observable by electron diffraction of quenched samples (Carpenter and McConnell, 1984). The superlattice intensities decrease continuously as the transition is approached from below and the transition temperature is strongly composition dependent. Extrapolation of the delineation of the phase boundary as a function of composition and temperature yields a T_c somewhere between 2000 K and 2250 K at the pure anorthite end-member (Carpenter and McConnell, 1984) and although this is above the melting point we can expect a steady increase in Al/Si order (defined by the order parameter Q_{od}) in

anorthite cooled in equilibrium below the melting point. The process of Al/Si ordering is slow, however, since it depends upon diffusion of Al and Si cations through the tetrahedral framework. Equilibrium values of Q_{od} are only obtained in crystals held at reasonably high temperatures for long periods of time.

Plagioclase crystallised from glass or from the melt may show quite low degrees of Al/Si order even at room temperature, since the kinetic barrier hinders ordering. The $I\bar{1}-P\bar{1}$ transition is rapid and reversible, however, so Q_{od} can take a wide range of values at the $I\bar{1}-P\bar{1}$ low temperature transition depending upon the thermal history of the crystal.

The process of Al/Si ordering induces a strain which Carpenter (1988) observes is proportional to the change in $\cos\gamma$, as in albite (Salje et al., 1985a). Unlike the Al/Si ordering process in albite, however, the $C\bar{1}-I\bar{1}$ transition in anorthite is associated with a critical point at the Brillouin zone boundary (equivalent to the 'b' Bragg reflections in diffraction experiments) and so the strain due to Al/Si order cannot couple directly to Q_{od} but instead couples quadratically, to Q_{od}^2 (we shall later see that this coupling between Al/Si ordering and strain has important consequences for the $I\bar{1}-P\bar{1}$ transition). In addition to the excess strain there is an excess enthalpy due to the order-disorder transition which has been measured as a function of composition in plagioclases by Carpenter et al. (1985). The measured excess enthalpy and derived T_c may be used together to determine the coefficients of Q_{od} in a Landau expansion for free energy, and Carpenter (1988) shows that the experimental data are consistent with a tricritical Landau model for the $C\bar{1}-I\bar{1}$ transition. A possible equilibrium phase diagram

of the plagioclases as a function of temperature is shown in Figure 3.2.

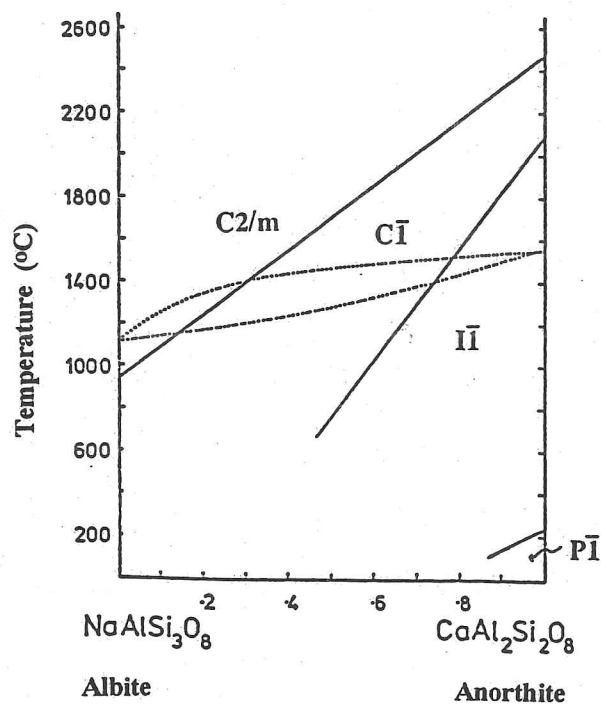


Figure 3.2(a) The phase diagram for plagioclase, after Carpenter (1988). The low-temperature 'e' structures at intermediate compositions are omitted and the diagram shows the predicted sequence of C2/m-C $\bar{1}$ -I $\bar{1}$ -P $\bar{1}$ for anorthite.

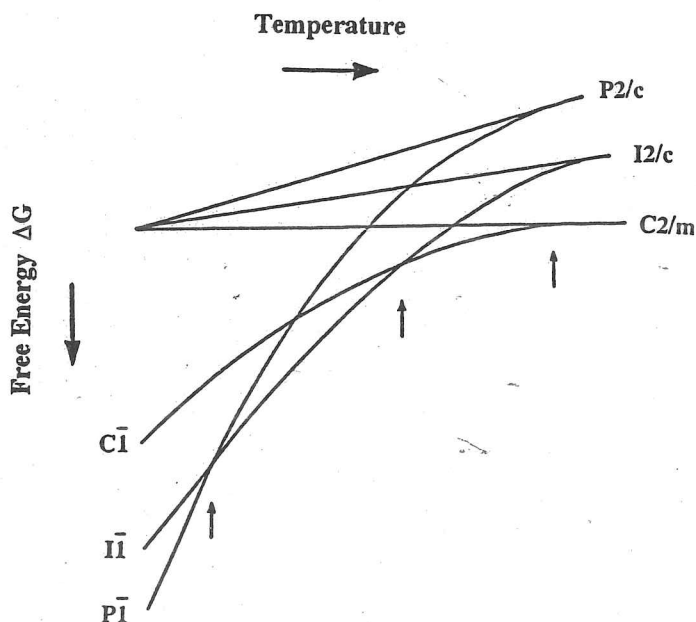


Figure 3.2(b) Schematic G-T curves for feldspar. Small arrows indicate phase transitions. C2/m-C $\bar{1}$ is the only ferroic transition, the others involve high-symmetry phases which are not the true paraphase.

3.1.2 The $I\bar{1}-P\bar{1}$ Transition in Pure Ordered Anorthite The room temperature phase of anorthite has triclinic symmetry with space group $P\bar{1}$. The crystal structure was determined by Kempster et al. (1962) and refined by Wainwright and Starkey (1971), by Czank (1973) and by Kalus (1978). The displacive phase transition from primitive to body-centred anorthite with increasing temperature was first described by Brown et al. (1963). It results in the disappearance of low temperature 'c' ($h + k$ even, l odd) and 'd' ($h + k$ odd, l even) primitive superlattice reflections which had been observed earlier by Laves and Goldsmith (1954) and which are associated with an anti-phase domain texture observable by dark field TEM (Laves et al., 1970; Czank et al., 1973; Müller et al., 1973). The 'c' and 'd' superlattice reflections correspond to the Z and Z' points on the boundary of the $I\bar{1}$ Brillouin zone, which become Γ points in the $P\bar{1}$ phase (Figure 3.3). The supergroup-subgroup relation between these two space groups indicates that the transition could be continuous. In fact the first experimental studies (Brown et al. 1963) indicated that the phase transition is continuous and reversible with $T_c \approx 510$ K in pure metamorphic anorthite (i.e. highly Al/Si ordered, low Na content) from the Val Paseda locality.

The equilibrium transition temperature T_c has since been determined from DSC measurements and is, indeed, 510 K according to Wruck (1986). The understanding of the mechanism of the phase transition was, for some time, muddled. Material related anomalies in the diffuseness of the 'c' and 'd' critical reflections had been observed by Laves and Goldsmith (1954) and attributed to ordering of Ca domains. Much speculation about the transition mechanism led to confusion, and Laves et al. (1970) and

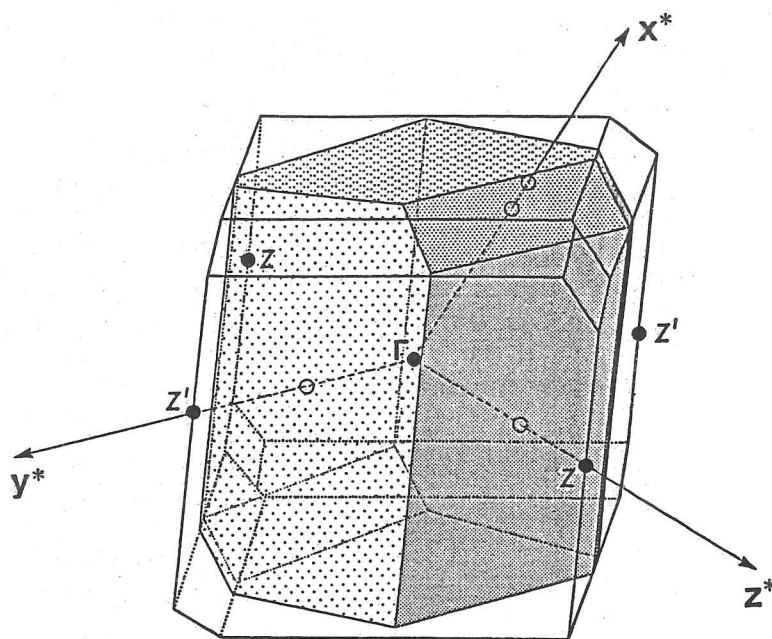


Figure 3.3 The $I\bar{1}$ (enclosing) and $P\bar{1}$ (shaded) Brillouin zones of Val Paseda anorthite, constructed from cell parameters at 510 K. The critical Z and Z' points become Γ points in the $P\bar{1}$ phase.

Czank (1973) reported that the symmetry-forbidden reflections (in the $I\bar{1}$ phase) still exist up to 1500°C. Foit and Peacor (1973) interpreted their high-temperature single-crystal X-ray data in terms of a primitive structure. This conflicted with the high-temperature ^{27}Al NMR measurements of the transition by Staehli and Brinkmann (1974), who found that the Al-site in the framework displayed a distinct and reversible symmetry change to $I\bar{1}$ above approximately 241°C. A clear distinction between the effect of dynamical and static X-ray and neutron scattering was, at last, made by Frey et al. (1977), however. These authors clearly showed that a phase transition takes place near $T_c = 510$ K and that residual scattering intensity at $T > T_c$ is due to elastic scattering in fully Al/Si ordered anorthite. Their results on the temperature evolution of the scattering intensities at $T < T_c$ are in full agreement with the findings presented here and also with those of Adlhart et al. (1980a).

Adlhart et al. (1980a) carried out the first quantitative investigation of the phase transition when they measured the intensities of superlattice reflections as a function of temperature by neutron and X-ray diffraction. They followed the behaviour of both the sharp and diffuse components of 'c' and 'd' type reflections and found that the intensity of the sharp part of the reflection, I_k , is a continuous and reversible function of temperature. The contribution to intensity due to diffuse scattering increases near T_c and arises from dynamical fluctuations of the order parameter for the transition, Q , in this region. I_k is proportional to $\langle Q \rangle^2$, the average correlated order (Bruce and Cowley, 1981; Schmahl and Redfern, 1988), and Adlhart et al.'s (1980a) data indicate that $I_k^2 \propto (T_c - T)$ (Figure 3.4a). This is the first hint that the transition in Val Paseda anorthite is tricritical since it implies $Q \propto (T_c - T)^\beta$ with $\beta = \frac{1}{4}$.

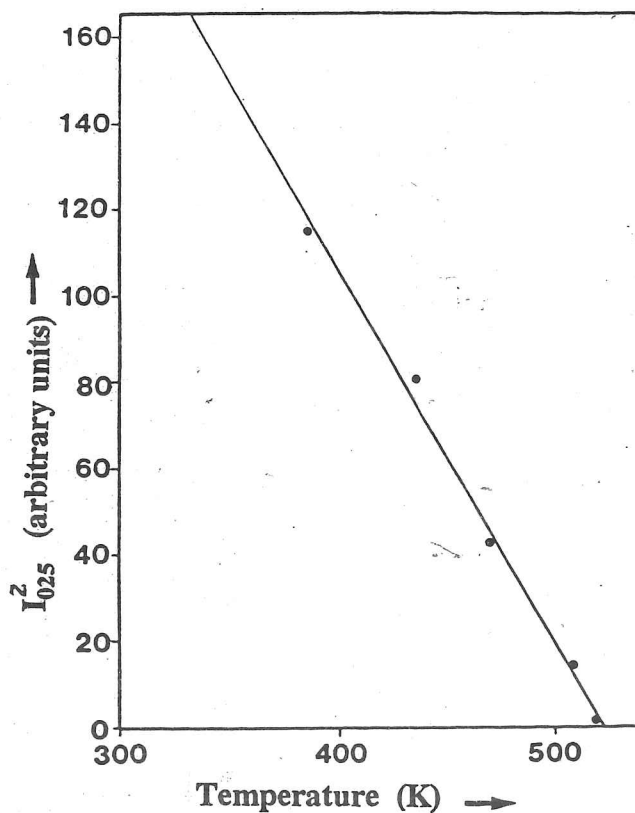


Figure 3.4(a) Temperature variation of the square of the intensity of elastic scattering of the 025 reflection in Val Paseda anorthite (data of Adlhart et al., 1980a).

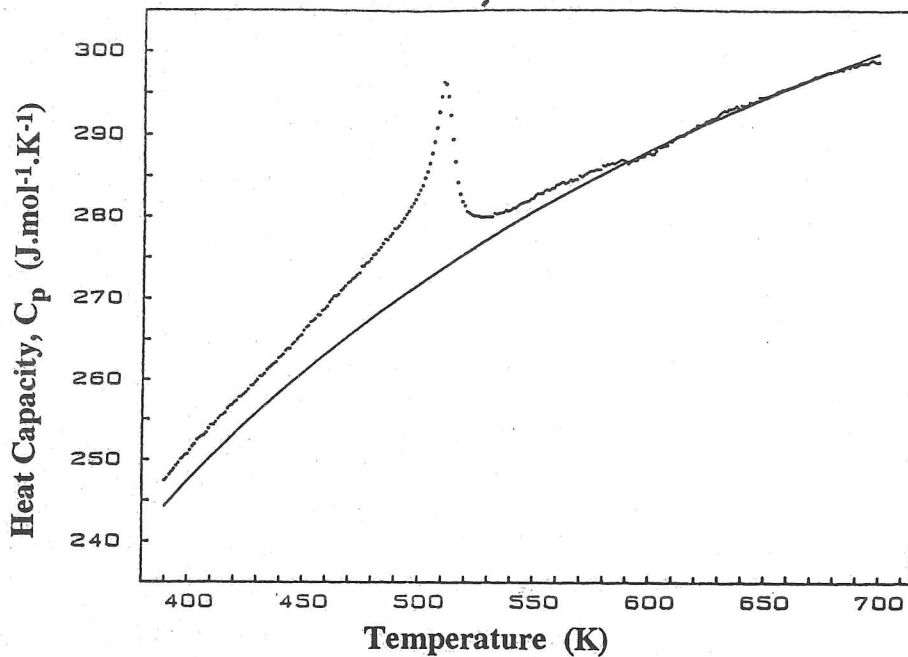


Figure 3.4(b) The specific heat anomaly at the $I\bar{1}\bar{1}$ - $P\bar{1}$ phase transition in Val Pasmada anorthite (from Wruck, 1986, with permission).

Measurements of the heat capacity C_p through the transition in Val Pasmada anorthite were made by Wruck (1986) (Figure 3.4b). A large λ -shaped anomaly is observed near T_c and the excess heat capacity below T_c due to the structural phase transition is found to be of the form $T_c(T_c - T)^{-\frac{1}{2}}$, thus the critical exponent $\alpha = \frac{1}{2}$ which again indicates that the $I\bar{1}\bar{1}$ - $P\bar{1}$ transition with temperature in Val Pasmada anorthite is tricritical.

It has long been realized that the displacive transition in anorthite exhibits features characteristic of ferroelastic behaviour despite the fact that the symmetry relations between the $I\bar{1}\bar{1}$ and $P\bar{1}$ phases do not require the development of a spontaneous strain. Newnham (1974) points to plagioclase as a mineralogical example of ferroelastic-type behaviour and mechanical twinning in anorthite had been demonstrated much earlier by Mügge and Heide (1931). It should, therefore, be possible to observe the behaviour of the elastic parameter, the

spontaneous strain, arising below the phase transition and link this to the order-parameter behaviour.

In this chapter, further experimental evidence for the predicted tricritical behaviour of the phase transition is presented, based on the observation of the temperature evolution of the spontaneous strain. The understanding of these observations rests on the theoretical approach of Salje (1987b). There it is shown that the phase transition is entirely related to a critical behaviour of symmetry equivalent Z and Z' points on the Brillouin zone boundary. In fact it is interesting to note that anorthite is the only end-member feldspar to show a zone boundary instability. The transition is of special interest in that it is an example of co-elastic behaviour, and the transition mechanism cannot simply be due to the ordering of Ca in a double potential (as this would not give rise to the spontaneous strain which is observed).

The description of the thermodynamic behaviour requires the use of two biquadratically coupled order parameters. One, Q^0 , corresponds to the rapid lattice distortion at the phase transition itself, the other, Q_{od} , corresponds to the degree of 'frozen in' Al/Si order arising from the high temperature $C\bar{1}-I\bar{1}$ symmetry reduction. Coupling between these two order parameters is strain-induced. The influence of Q_{od} explains the dependence of the $I\bar{1}-P\bar{1}$ transition on thermal history; annealing and quenching an anorthite will change the value of Q_{od} . Extrapolation of the data of Carpenter and Ferry (1984) indicates that the $C\bar{1}-I\bar{1}$ transition occurs near 2100 K which is over 400 K above the melting point (see Figure 3.2). Since the Al/Si disorder is an order parameter coupled to the $I\bar{1}-P\bar{1}$ transition,

this lower-temperature transition may be used as a tool for the study of the otherwise inaccessible high-temperature transition. In addition the sensitivity of the transition to Na and other impurities, and to thermal history indicates the potential usefulness of the $I\bar{1}-P\bar{1}$ transition for the thermodynamic characterisation of phases.

In order to understand the modifications of the transformation behaviour due to Al/Si disorder and Ca/Na substitution it is necessary to understand the critical behaviour of fully ordered, end-member anorthite. It is shown by Salje (1987b) that the transition temperature for pure Ca-feldspar depends explicitly on the degree of Al/Si order. The phase transition would occur at a temperature T_c for fully Al/Si disordered anorthite ($Q_{od}=0$) and is renormalized to an observed value T_c^* in partly or fully Al/Si ordered anorthite. Therefore in this chapter we confine ourselves to the study of pure $CaAl_2Si_2O_8$, and focus on the behaviour of Q^0 in the 'ideal' and simplest case. The discussion of the effects of albite in solid solution and the transition behaviour at high pressure is to be found in chapter 4. The results of lattice parameter refinements from X-ray powder patterns taken over a temperature range of over 1000 K across the transition are presented, and from these the temperature dependence of the spontaneous strain and its corresponding representation surface is calculated. The order parameter Q^0 is calculated for the temperature range considered and computed values of the coupling constants are given.

3.2 Experimental

Pure end-member Ca anorthite from the Val Paseda locality, South Tyrolia, obtained from the Harker Mineral Collection (number 3774) was used for this study. This is the same material as has been studied by Gay (1953), Wainwright and Starkey (1973), Frey et al. (1977) and more recently Carpenter et al. (1985), Wruck (1986), and Kirkpatrick et al. (1987). The anorthite content determined by electron microprobe varies between 99.5% and 100% An. This metamorphic anorthite is well ordered and is exactly the same specimen as that characterised by Carpenter et al. (1985), where details of the preparation and separation of the pure powder are given.

3.2.1 High-Resolution Powder X-ray Diffraction The anorthite was ground by hand under acetone in an agate mortar and mounted as a thin film pressed in a platinum loop in the furnace of a Huber 632 heating Guinier powder camera. A bent quartz monochromator selected $\text{CuK}\alpha_1$ radiation and reduced background intensity. Heating was controlled by a Huber 633 temperature controller. A chromel/alumel thermocouple was used, and throughout the whole temperature range its position relative to the sample remained constant. This allowed a relative temperature stability of better than 1 K, although absolute accuracy was less. Any systematic error was linear however, and a correction was facilitated using the value of T_c^* from Wruck (1986) and other known transition temperatures as fixed point. The controller allowed automatic film movement between each exposure. Further details of the measurement of high-temperature lattice parameters are given in appendix 1. Low-temperature lattice parameters were determined from similar Guinier

diffraction patterns carried out with the kind permission of Professor W Prandl at the low-temperature camera at the Institut für Kristallographie, Universität Tübingen. The details of the low temperature experimental procedure are presented in section 6.2.1.

An internal Si standard was used to correct for film shrinkage. Powder lines were measured using an Enraf-Nonius FR508V Guinier viewer, allowing measurement to within $0.010^\circ 2\theta$. Cell parameters were calculated by the least squares refinement using program 'CELL' with about forty reflexions, and indexed with the help of the calculated powder patterns of Borg and Smith (1969).

3.2.2 Lattice Parameters and Thermal Expansion The temperature evolution of the lattice parameters of Val Paseda anorthite is shown in Figure 3.5, and listed in Table 3.1. The data scatter gives an indication of the standard error, although the quoted standard error of the least squares refinement was less than this scatter. Above 600 K changes appear linear, and can be modelled by a simple linear thermal expansion. This thermal expansion has been extrapolated by least squares linear regression of the data above 600 K from the high-temperature $I\bar{1}$ phase to the $P\bar{1}$ low-temperature phase. These straight solid lines correspond to the lattice parameters to be expected in the absence of spontaneous strain arising from the transition, but we see that the phase transition induces anomalous thermal expansion behaviour of certain of the cell parameters. The dashed curves show the significant deviations of b , β , and γ which are observed below the transition temperature. It is remarkable that only the excess functions for these three lattice parameters show a

measurable temperature dependence, whereas the excess functions for a, c, and α are close to zero. This behaviour is not related to any particular symmetry constraints of the symmetry change at the phase transition process, rather it appears to be the result of the structural behaviour of the complicated anorthite lattice. These results for the lattice parameters are now interpreted in terms of the spontaneous strain which couples with the order parameter, Q^0 , of the transition.

VAL PASMEDA ANORTHITE

T(K)	a (Å)	b (Å)	c (Å)	alpha	beta	gamma	alpha*	beta*	volume
100	8.170	12.863	14.163	93.161	115.929	91.253	85.873	63.945	1334.856
128	8.169	12.867	14.164	93.174	115.906	91.245	85.865	63.968	1335.313
155	8.168	12.870	14.170	93.148	115.908	91.256	85.887	63.966	1336.050
184	8.172	12.870	14.166	93.165	115.900	91.249	85.872	63.974	1336.494
242	8.172	12.866	14.171	93.172	115.873	91.258	85.862	64.000	1336.885
254	8.176	12.871	14.173	93.167	115.838	91.272	85.862	64.034	1338.635
293	8.177	12.871	14.171	93.111	115.902	91.270	85.922	63.974	1337.858
354	8.181	12.878	14.171	93.106	115.866	91.270	85.930	64.010	1339.637
372	8.183	12.877	14.173	93.106	115.859	91.285	85.923	64.015	1340.117
390	8.186	12.880	14.178	93.115	115.872	91.287	85.911	64.002	1341.270
408	8.186	12.879	14.175	93.116	115.853	91.302	85.904	64.020	1341.219
426	8.185	12.878	14.171	93.119	115.847	91.301	85.901	64.026	1340.461
445	8.187	12.881	14.171	93.119	115.850	91.297	85.903	64.023	1341.035
463	8.187	12.876	14.174	93.110	115.831	91.301	85.913	64.042	1341.052
469	8.189	12.881	14.171	93.092	115.819	91.339	85.915	64.053	1341.735
475	8.188	12.880	14.173	93.089	115.795	91.335	85.921	64.077	1341.964
481	8.188	12.880	14.175	93.071	115.795	91.353	85.933	64.076	1342.158
487	8.189	12.881	14.176	93.083	115.779	91.363	85.916	64.091	1342.531
493	8.192	12.877	14.180	93.077	115.776	91.341	85.932	64.096	1343.201
499	8.192	12.878	14.180	93.093	115.771	91.338	85.917	64.101	1343.318
499	8.192	12.878	14.177	93.104	115.741	91.368	85.892	64.128	1343.305
511	8.194	12.878	14.179	93.089	115.735	91.391	85.898	64.134	1343.900
524	8.194	12.877	14.174	93.075	115.689	91.429	85.898	64.177	1343.684
536	8.193	12.877	14.171	93.040	115.675	91.434	85.934	64.193	1343.673
560	8.193	12.878	14.172	93.040	115.671	91.432	85.935	64.195	1343.828
566	8.197	12.882	14.176	93.034	115.701	91.455	85.930	64.166	1344.854
572	8.199	12.883	14.182	93.056	115.692	91.434	85.916	64.175	1345.959
578	8.199	12.886	14.182	93.048	115.703	91.420	85.931	64.165	1346.232
584	8.198	12.883	14.176	93.052	115.675	91.413	85.932	64.194	1345.534
584	8.198	12.886	14.182	93.036	115.710	91.440	85.935	64.158	1346.000
590	8.198	12.883	14.180	93.049	115.703	91.426	85.927	64.165	1345.648
596	8.198	12.882	14.179	93.042	115.711	91.431	85.932	64.157	1345.227
608	8.196	12.880	14.175	93.035	115.689	91.418	85.947	64.170	1344.897
633	8.200	12.879	14.179	93.047	115.703	91.367	85.959	64.172	1345.310
657	8.203	12.878	14.181	93.047	115.715	91.321	85.980	64.163	1346.070
681	8.199	12.881	14.186	93.062	115.692	91.342	85.954	64.182	1346.319
705	8.202	12.883	14.185	93.043	115.707	91.347	85.972	64.167	1346.820
730	8.202	12.883	14.185	93.069	115.712	91.321	85.955	64.162	1346.755
754	8.204	12.880	14.186	93.061	115.723	91.304	85.972	64.153	1346.997
778	8.204	12.884	14.188	93.042	115.728	91.284	85.992	64.149	1347.973
802	8.208	12.887	14.186	93.036	115.717	91.278	86.012	64.163	1348.256
827	8.210	12.887	14.184	93.032	115.709	91.248	86.032	64.173	1348.570
851	8.211	12.888	14.189	93.028	115.701	91.242	86.040	64.181	1349.490
875	8.211	12.887	14.187	93.023	115.701	91.212	86.059	64.184	1349.289
875	8.212	12.887	14.186	93.008	115.705	91.231	86.067	64.179	1349.179
911	8.214	12.895	14.190	93.019	115.713	91.228	86.056	64.171	1350.603
948	8.216	12.894	14.189	93.009	115.711	91.204	86.080	64.173	1350.822
984	8.217	12.896	14.190	93.009	115.702	91.182	86.090	64.186	1351.512
1021	8.218	12.898	14.193	92.982	115.712	91.170	86.124	64.167	1352.136
1057	8.222	12.901	14.200	92.976	115.723	91.124	86.153	64.169	1353.673
1093	8.222	12.901	14.201	92.969	115.724	91.136	86.155	64.168	1353.591
1130	8.225	12.905	14.197	92.963	115.731	91.143	86.158	64.161	1354.020
1166	8.224	12.902	14.195	92.982	115.728	91.094	86.161	64.166	1353.591
1202	8.230	12.911	14.206	92.962	115.747	91.097	86.180	64.148	1356.300

Table 3.1 Lattice parameters of Val Pasmada anorthite between 100 K and 1202 K.

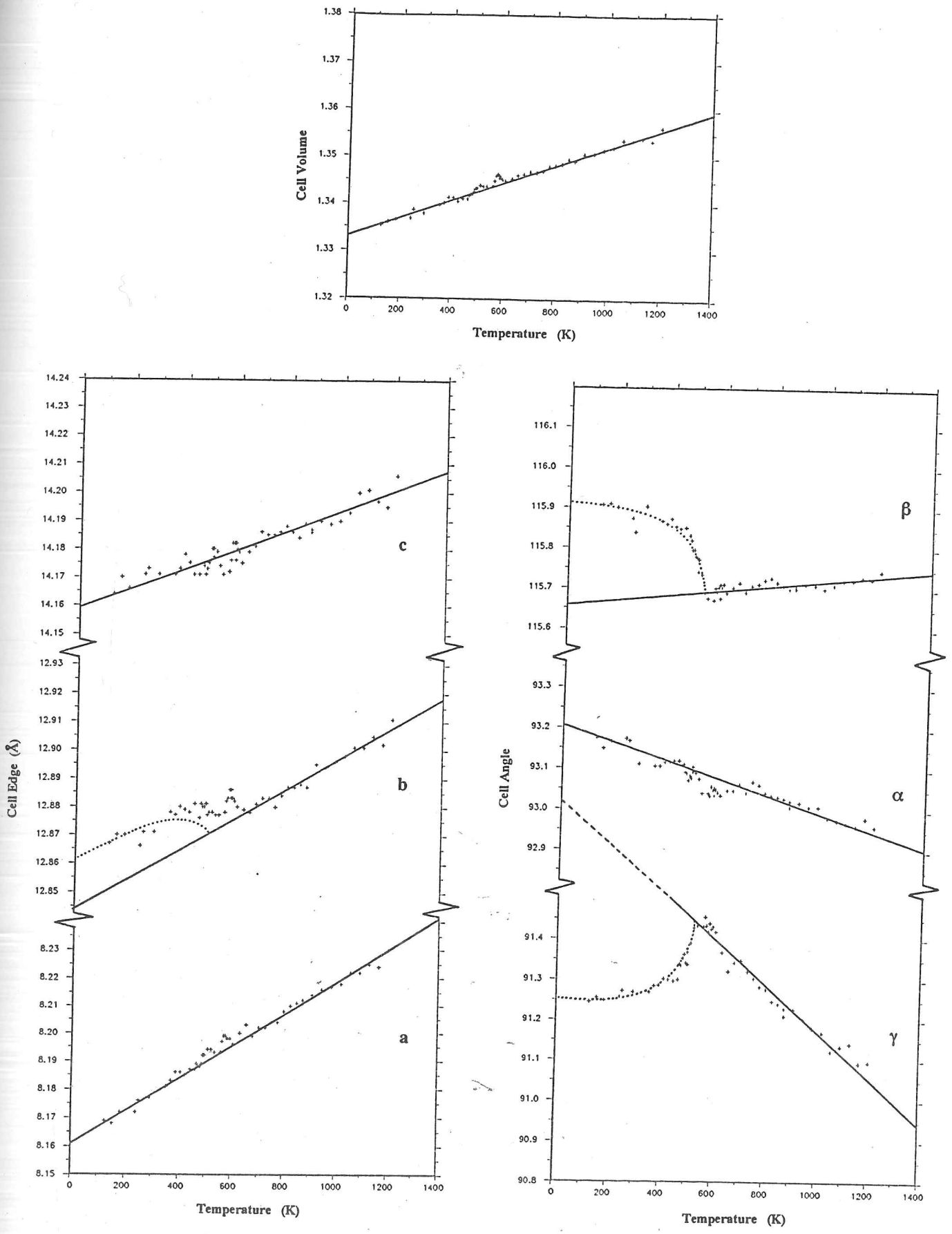


Figure 3.5 Temperature dependence of the lattice parameters of Val Pasmeda anorthite up to 1200 K. The $P\bar{1}$ "background" is shown by the solid lines, the deviations of b , β , and γ in the $P\bar{1}$ phase are indicated by dashed lines.

3.3 The Spontaneous Strain of the Phase Transition $\bar{I}\bar{1}-P\bar{1}$

The concept of spontaneous strain was first introduced into the description of structural phase transitions in feldspars by Salje (1985) and Salje et al. (1985a,b). As Tolédano and Tolédano (1980) have already pointed out, we can expect ferroelastic phase transitions to constitute the major part of the ferroic phase transitions inferred possible in Landau theory, and elastic transition behaviour is very common in minerals. The description of the high symmetry paraelastic phase is important in ferroelastic and co-elastic phase transitions, since the spontaneous strain must be measured relative to the lattice parameters of the paraelastic phase. Thus, by careful measurement of the lattice parameters in both the high-symmetry paraelastic phase and the low-symmetry elastic phase the evolution of the spontaneous strain may be determined.

The spontaneous strain at the $P\bar{1}-\bar{I}\bar{1}$ transition must now be calculated from the lattice parameters. For experimental purposes the spontaneous strain is best defined in a Cartesian coordinate system R_i ($i=1,2,3$) where the deformation in the low-temperature phase transforms a point at R_i to r_i with an elastic displacement vector $u_i = r_i - R_i$. The components u_i can be expressed as a function of the initial coordinates in a Lagrangian form, and the state of deformation of the body can be characterised by the symmetric polar second-rank tensor (Bhagavantam 1966, Nye 1957). This linear Lagrangian strain tensor is defined as

$$\epsilon_{ij} = \frac{1}{2} \left[\frac{du_i}{dr_j} + \frac{du_j}{dr_i} \right] \quad (3.1).$$

The underlying Cartesian coordinate system used for

triclinic feldspars is chosen for compatibility with the definition of the coordinate system in monoclinic feldspars (Salje et al., 1985b) and with the earlier work on elastic constants of plagioclase by Ryzhova (1964) to be:

R_2 : parallel to the crystallographic b axis

R_3 : parallel to the crystallographic c^* axis

R_1 : perpendicular to both.

The lattice parameters are related to the linear Lagrangian spontaneous strain tensor elements by the equations (Schlenker et al. 1978):

$$\epsilon_1 = \epsilon_{11} = \frac{a \cdot \sin \gamma}{a_0 \cdot \sin \gamma_0} - 1 \quad \{3.2\}$$

$$\epsilon_2 = \epsilon_{22} = \frac{b}{b_0} - 1 \quad \{3.3\}$$

$$\epsilon_3 = \epsilon_{33} = \frac{c \cdot \sin \alpha \cdot \sin \beta^*}{c_0 \cdot \sin \alpha_0 \cdot \sin \beta_0^*} - 1 \quad \{3.4\}$$

$$\begin{aligned} \frac{1}{2} \epsilon_4 = \epsilon_{23} = \frac{1}{2} & \left(\frac{c \cdot \cos \alpha}{c_0 \cdot \sin \alpha_0 \cdot \sin \beta_0^*} - \frac{b \cdot \cos \alpha_0}{b_0 \cdot \sin \alpha_0 \cdot \sin \beta_0^*} \right. \\ & \left. + \frac{\cos \beta_0^*}{\sin \beta_0^* \cdot \sin \gamma_0} \cdot \left(\frac{a \cdot \cos \gamma}{a_0} - \frac{b \cdot \cos \gamma_0}{b_0} \right) \right) \end{aligned} \quad \{3.5\}$$

$$\frac{1}{2} \epsilon_5 = \epsilon_{13} = \frac{1}{2} \left(\frac{a \cdot \sin \gamma \cdot \cos \beta_0^*}{a_0 \cdot \sin \gamma_0 \cdot \sin \beta_0^*} - \frac{c \cdot \sin \alpha \cdot \cos \beta_0^*}{c_0 \cdot \sin \alpha_0 \cdot \sin \beta_0^*} \right) \quad \{3.6\}$$

$$\frac{1}{2} \epsilon_6 = \epsilon_{12} = \frac{1}{2} \left(\frac{a \cdot \cos \gamma}{a_0 \cdot \sin \gamma_0} - \frac{b \cdot \cos \gamma_0}{b_0 \cdot \sin \gamma_0} \right) \quad \{3.7\}.$$

Where the subscript 0 denotes those parameters expected at low temperature by extrapolation of those in the $I\bar{1}$ phase.

The temperature dependence of the six tensor elements $\epsilon_1 \dots \epsilon_6$ is shown in Figure 3.6. Since strain is a symmetric tensor it may be referred to its principal axes, giving the principal strains. Each of the strain tensors calculated and shown in Figure 3.6 was diagonalised to give a matrix of

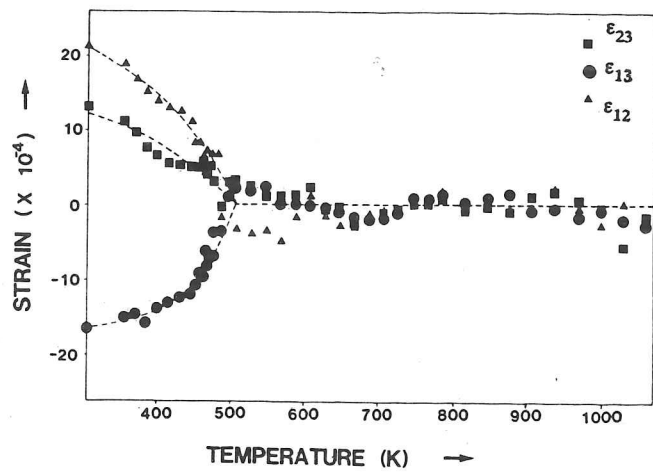
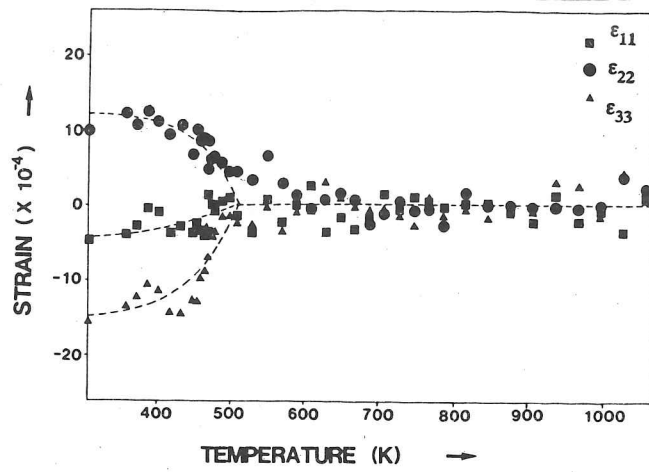


Figure 3.6 The temperature evolution of the spontaneous strain tensor elements $\epsilon_1 \dots \epsilon_6$.

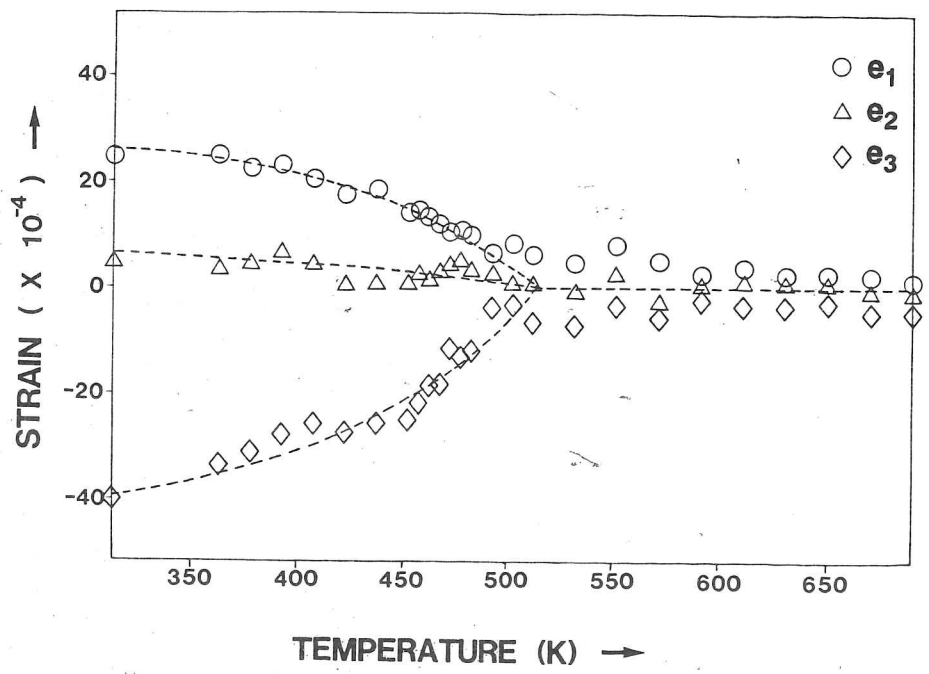


Figure 3.7 Temperature dependence of the diagonalised strain tensor components e_1 , e_2 , and e_3 .

eigenvalues and a matrix of eigenvectors using the Pascal program 'STRAINS' following the method of Jacobi in Ralston and Wilf (1960) (a listing of the source code is given in appendix 2). The three principal strains, e_1 , e_2 , and e_3 are along the principal axes: the three mutually perpendicular directions which remain perpendicular during deformation. These diagonal strain elements are shown in Figure 3.7. Within the limits of the experimental error e_2 remains zero below the transition temperature, whereas e_1 and e_3 oppose one another.

The representation surface defined by the equation

$$x_{ij} R_i R_j = 1 \quad \{3.8\}$$

is a hyperboloid of revolution. Although the orientation of the strain ellipsoid defined by the equation

$$\left(\frac{r_1^2}{1+e_1}\right)^2 + \left(\frac{r_2^2}{1+e_2}\right)^2 + \left(\frac{r_3^2}{1+e_3}\right)^2 = 1 \quad \{3.9\}$$

could be an explicit function of temperature the experimental results presented here clearly indicate that its principal axes remain constant. The $P\bar{1}$ cell is in a state of plane strain with respect to the $I\bar{1}$ cell, approximating to a pure shear along the direction of e_2 . Transferring the Cartesian coordinate system back onto the crystallographic axes the average Eigenvector of e_2 , the axis of minimal strain, corresponds to approximately [236] in the crystal and hardly changes with temperature. Structurally, this behaviour indicates that the crystal structure of anorthite in its $I\bar{1}$ phase is not only changed in such a way as to give rise to the doubling of the unit cell in $P\bar{1}$ at $T < T_c^*$ but also to shear of the structure along roughly the [236] direction. This orientation does not change with temperature although there

are no symmetry constraints to prevent it from doing so. This indicates that the coupling constants between Q^0 and the strain are temperature independent, since the fact that the orientation of the strain ellipsoid is unchanged (and only its magnitude varies with temperature) implies that the relative proportions of each strain tensor element remain constant.

3.4 Thermodynamic Calculations and Discussion

The experimental results are now interpreted in terms of the type of order parameter treatment presented in chapters 1 and 2.

3.4.1 The Landau Free-Energy Expansion The Landau potential for a Ca-rich plagioclase for the excess free energy due the $I\bar{1}-P\bar{1}$ transition is (Salje, 1987b):

$$\begin{aligned} \Delta G = & \frac{1}{2}\alpha(T-T_c - \gamma n_{Ab})Q^0{}^2 + \frac{1}{4}B_{eff}Q^0{}^4 + \frac{1}{6}cQ^0{}^6 \\ & + \sum \lambda_i \epsilon_i Q^0{}^2 + \frac{1}{2} \sum C_{ik} \epsilon_i \epsilon_k + \sum \zeta_i \epsilon_i Q_{od}^2 + \xi Q^0{}^2 Q_{od}^2 \\ & + \frac{1}{2}\alpha_{od}(T-T_c - \gamma_{od} n_{Ab})Q_{od}^2 + \frac{1}{4}b_{od}Q_{od}^4 + \frac{1}{6}c_{od}Q_{od}^6 \\ & + \xi_{od} n_{Ab} Q_{od} \end{aligned} \quad \{3.10\}$$

where n_{Ab} is the mole fraction of albite in solid solution and T_c is the critical temperature of the $I\bar{1}-P\bar{1}$ transition, which becomes renormalized to $T_c^* = T_c + \gamma n_{Ab}$ where γ is a constant representing the magnitude of (dT_c/dn_{Ab}) . λ_i and ζ_i are coupling constants linking the strain, ϵ_i , to the order parameters Q^0 and Q_{od} respectively. C_{ik} are the elastic constants, and come into the elastic energy term of the free energy expansion. ξ is the direct coupling constant between Q^0 and Q_{od} , since direct biquadratic coupling is permitted by symmetry, and ξ_{od} represents the direct coupling effect whereby albite substitution for anorthite necessarily increases the degree of Al/Si order (by the

coupled substitution $\text{Na} + \text{Si} = \text{Ca} + \text{Al}$).

This expression for free energy reveals that because the order parameter coupling in anorthite and Ca-rich plagioclase is biquadratic then this coupling, together with the influence of stress fields due to Na substitution and Al/Si disorder, changes both the critical temperature T_c and the fourth-order term of the expansion. This latter renormalization implies that Al/Si disorder and Na substitution change the order of the phase transition as well as the transition temperature (since the sign of the fourth-order term determines the transition character).

3.4.2 Strain Behaviour and Transition Character The variation of the strain parameters is explained in terms of strain induced coupling between the order parameter of the $\text{I}\bar{1}\text{-P}\bar{1}$ transition, Q^0 , and the order parameter of the $\text{C}\bar{1}\text{-I}\bar{1}$ Al/Si ordering transition, Q_{od} (see equation 3 in Salje, 1987b). This leads to the expression for strain in terms of both order parameters given by Salje (1987b):

$$\epsilon_i = (\Delta_i + S_{\epsilon Q_{\text{od}}}^i) Q_{\text{od}}^2 + (\delta_{i4} \Delta_4'' + \delta_{i6} \Delta_6'') Q_{\text{od}} + S_{\epsilon Q^0}^i Q^0{}^2 \quad \{3.11\}$$

Here the term in Q_{od}^2 is due to the coupling arising from the high-temperature $\text{C}\bar{1}\text{-I}\bar{1}$ transition, with a 'frozen in' degree of order Q_{od} . This transition occurs at around 2100 K according to Carpenter and Ferry (1984). The term in Q_{od} is the additional strain due to the monoclinic-triclinic transition to be expected above the $\text{C}\bar{1}\text{-I}\bar{1}$ transition, of the same form as at the $\text{C}2/m\text{-C}\bar{1}$ transition in albite (Salje et al. 1985a). The final term in the expression arises from the strain coupling to the $\text{I}\bar{1}\text{-P}\bar{1}$ order parameter Q^0 , where strain is proportional to $Q^0{}^2$.

Val Pasmada anorthite is highly ordered material with small

fluctuations in the degree of Al/Si order. We find that for this mineral $Q_{od} \approx 1$, and within the temperature range studied this value of Q_{od} is frozen in and remains constant (due to the kinetic barriers to Al/Si ordering). Thus the only temperature dependent term in equation 3.11 is $S_{\epsilon Q}^i Q^{o2}$. In other words, the effects observed in the behaviour of spontaneous strain through the transition reflect directly the behaviour of the order parameter for the $I\bar{1}-P\bar{1}$ transition, Q^o , and $\epsilon_i \propto Q^{o2}$. It is important to note, however, that this behaviour is not encountered for volcanic anorthite, or crystals containing Na, or for anorthites at high-pressure (see chapter 4). The critical exponent, β , of the order parameter may thus be obtained from the behaviour of the strain. Since $Q^o \propto (T^*-T)^\beta$, then $\epsilon_s \propto (T^*-T)^{2\beta}$.

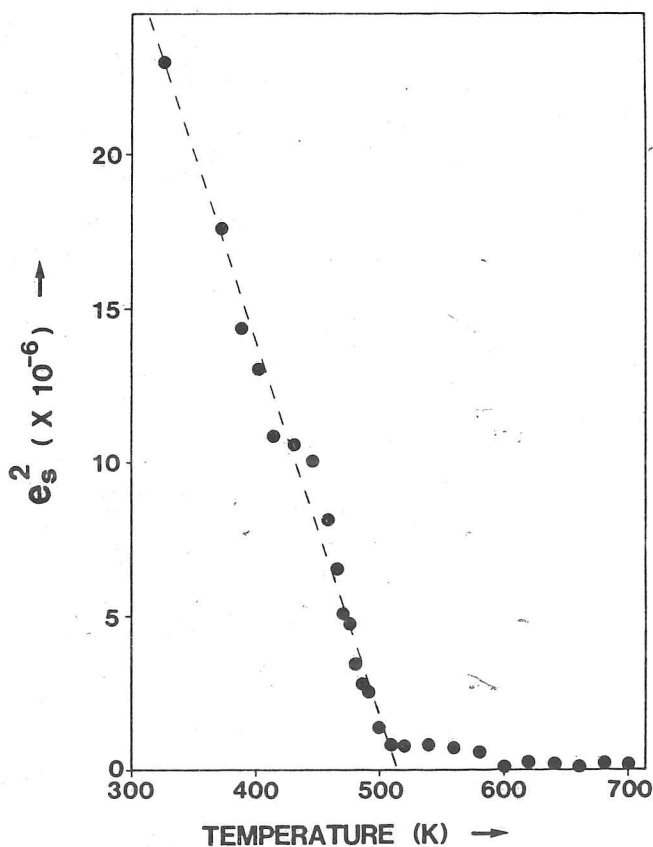


Figure 3.8 Variation with temperature of the square of the spontaneous strain below the $I\bar{1}-P\bar{1}$ phase transition in Val Pasmada anorthite. The linear dependence reflects the tricritical nature of the phase transition.

Here ϵ_s is the scalar spontaneous strain defined in the form adopted by Aizu (1970). Thus

$$\epsilon_s = \sqrt{\sum_i \epsilon_i^2} \quad \{3.12\}$$

Any physical property which transforms as ϵ_i will show the same critical dependence including the diagonal strain elements with $e_s = \sqrt{\sum_i e_i^2}$ which is proportional to $(T_c^* - T)^{2\beta}$. The relationship between e_s and T is shown in Figure 3.8 where a linear dependence is evident. Since $e_s^2 \propto (T_c^* - T)$ the critical exponent β is $\frac{1}{4}$ which indicates the tricritical nature of the $\bar{1}\bar{1}$ - $P\bar{1}$ transition in Val Pasmada anorthite. This result is in agreement with Wruck (1986) whose measurements of excess heat capacity on the same material also show a tricritical behaviour.

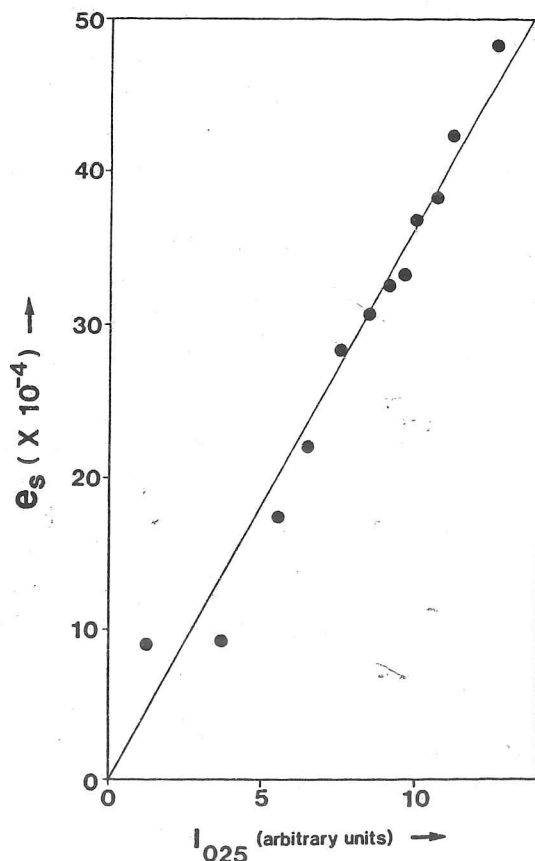


Figure 3.9 The linear dependence of spontaneous strain on scattering intensity of a critical reflection (data of Adlhart et al., 1980a). This results from a shared proportionality to the square of the order parameter.

Further evidence for tricritical behaviour is found in the neutron and X-ray scattering data of Frey et al. (1977), and Adlhart et al. (1980a). The internal consistency of the data of Adlhart et al. (1980a) and the findings presented here is demonstrated in Figure 3.9 where the linear correlation between the spontaneous strain and the intensity of the 025 reflexion (which both reflect the same temperature evolution of Q^0) is shown.

At a tricritical point the fourth order term in the Landau expansion for free energy becomes zero. For Val Paseda anorthite exhibiting tricritical behaviour the order parameter below T_c^* for the $I\bar{1}-P\bar{1}$ transition becomes

$$Q^0 = \left(\frac{a}{c}(T_c^* - T)\right)^{\frac{1}{4}} \quad \{3.13\}$$

Therefore, if we know T_c^* we are able to calculate the order parameter at any temperature. The value for T_c^* determined by Wruck (1986) is 510 K, which is in agreement with the results of Adlhart et al. (1980a), Frey et al. (1977), and Staehli and Brinkmann (1974). Since $Q^0 = 1.0$ at $T = 0$ K

$$\frac{c}{a} = T_c^* = 510 \text{ K} \quad \{3.14\}$$

and

$$Q^0 = (1 - T/510) \quad \{3.15\}$$

which gives the final temperature dependence of Q^0 .

The coefficients $S_{\epsilon Q}^1$ in equation 3.11 have been calculated from the slopes of ϵ_1 against Q^0 , allowing the determination of ϵ_1 at all temperatures if Q_{od} is known:

$$\begin{aligned}
\varepsilon_1 &= f_1(Q_{od}) - 0.765 \times 10^{-3} Q^0 \\
\varepsilon_2 &= f_2(Q_{od}) + 1.381 \times 10^{-3} Q^0 \\
\varepsilon_3 &= f_3(Q_{od}) - 2.907 \times 10^{-3} Q^0 \\
\varepsilon_4 &= f_4(Q_{od}) + 2.062 \times 10^{-3} Q^0 \\
\varepsilon_5 &= f_5(Q_{od}) - 3.471 \times 10^{-3} Q^0 \\
\varepsilon_6 &= f_6(Q_{od}) + 4.072 \times 10^{-3} Q^0
\end{aligned}
\tag{3.16}$$

where in each case

$$f_i(Q_{od}) = (\Delta_i + S_{eQod}^i) Q_{od}^2 + (\delta_{i4} \Delta_4'' + \delta_{i6} \Delta_6'') Q_{od} \tag{3.17}$$

Similarly the diagonal strain elements may be described in terms of a function of Q^0 and Q_{od} analogous to equation 3.11 giving the following dependence on Q^0

$$\begin{aligned}
e_1 &= F_1(Q_{od}) + 4.166 \times 10^{-3} Q^0 \\
e_2 &= F_2(Q_{od}) + 0.771 \times 10^{-3} Q^0 \\
e_3 &= F_3(Q_{od}) - 7.223 \times 10^{-3} Q^0
\end{aligned}
\tag{3.18}$$

where in each case

$$F_i(Q_{od}) = (\Delta_i + S_{eQod}^i) Q_{od} + (\delta_{i4} \Delta_4'' + \delta_{i6} \Delta_6'') Q_{od} \tag{3.19}.$$

Using these equations it is now possible to determine the value of Q^0 in fully ordered anorthite end member feldspars at any temperature. Further studies of anorthites with varying degrees of Al/Si order will allow determination of the other coupling constants between the strain and Q_{od} , and in a following chapter we discuss the influence of Al/Si disorder on the values of $f_i(Q_{od})$.

The application of Landau theory is thus seen to explain the behaviour of the spontaneous strain in anorthite below 510 K, predicting the observed tricritical behaviour and allowing the

determination of quantitative relationships between the strain and the order parameter.

3.4.3 Strain Energy of the Transition Now the strain behaviour at the transition is determined it should be possible to calculate the strain energy this contributes to the free energy of stabilisation of the $P\bar{1}$ phase, and compare this with the measured excess free enthalpy of the transition. The total enthalpy of Val Pasmada anorthite and the excess heat capacity has been measured by Wruck (1986). The baseline enthalpy of the high temperature phase is calculated from integration of Wruck's (1986) heat capacity measurements between 390 K and 699 K:

$$\begin{aligned} H^{\circ} &= 0.369 \times T - 42.4105 \times \ln T + 107.973/T \Big|_{390}^{699} \\ &= 85.35913 \text{ kJ.mol}^{-1} \end{aligned} \quad \{3.20\}$$

and Wruck's (1986) value of the measured enthalpy at 390 K is $86.7056 \text{ kJ.mol}^{-1}$, thus the excess enthalpy is $\Delta H = H - H^{\circ} = 1.3465 \text{ kJ.mol}^{-1}$ at this temperature.

The excess energy due to strain is given by $\frac{1}{2} \sum_{ik} C_{ik} \epsilon_i \epsilon_k$. Values for C_{ik} for Val Pasmada anorthite at 390 K are not available, but the measurements of Ryzhova (1964) on $\text{Ab}_{44}\text{An}_{56}$ at room temperature may be used as a first estimate. The values of ϵ_i at 390 K are, approximately: $\epsilon_1 = -4 \times 10^{-4}$, $\epsilon_2 = 11 \times 10^{-4}$, $\epsilon_3 = -13 \times 10^{-4}$, $\epsilon_4 = 18 \times 10^{-4}$, $\epsilon_5 = -30 \times 10^{-4}$, and $\epsilon_6 = 32 \times 10^{-4}$. These values imply a strain energy at 390 K due to the $I\bar{1}$ - $P\bar{1}$ transition of approximately 56 J.mol^{-1} , or only about 4% of the total excess enthalpy at this temperature due to the transition. This is less than the strain energy associated with some other co-elastic transitions, for example in NaNO_3 (chapter 6, Reeder et al., 1988). Although the spontaneous strain may not, at first glance,

appear particularly significant in terms of the energy it releases, strain is nonetheless very important since it provides a means of coupling other processes which themselves can be most significant energetically.

CHAPTER 4

CHANGING TRANSITION CHARACTER IN Ca-RICH PLAGIOCLASES

4.1 Introduction

The application of Landau theory has proved successful in the thermodynamic treatment of the calcium end-member anorthite (chapter 3 and Redfern and Salje (1987)). In this chapter the influence of Na incorporated into the anorthite structure by solid solution with albite shall be considered. In particular the effect of compositional change as well as state of Al/Si order on the order-parameter behaviour at the $\overline{I1}-\overline{P1}$ will be discussed. Indications that plagioclase composition has a significant bearing on the structural properties of feldspars were brought to light some time ago: the dependence of twinning on the composition and degree of Al/Si order was outlined by Starkey (1967) and Borg and Heard (1969). The correlation between structural effects and composition has commonly been used for determinative purposes: extensive studies of the lattice parameters and optical indicatrices of plagioclases have proved their worth as measures of the structural and compositional state of the material (Kroll, 1983; Stewart and Ribbe, 1983). As yet, there has been no unified approach to the interpretation of these data, and the situation appears somewhat muddled by the sheer wealth of information on these aspects of plagioclase behaviour. We shall see that the consideration of the underlying co-elastic nature of feldspars draws together the observations made, since the spontaneous strain associated with the displacive transitions is directly related to twin, indicatrix, and lattice parameter properties. The relationships between structural state and these

measured physical properties may then be considered in terms of the coupling between the ferroelastic phase transitions and Al/Si ordering processes occurring in plagioclases.

So far we have only considered the end-member anorthite from Val Paseda. By selecting a natural anorthite which contains slightly more sodium and has a different thermal history the influence of sodium content and Al/Si disorder on the $I\bar{1}-P\bar{1}$ transition can be investigated. The diffraction experiments, heat capacity, and lattice parameter measurements which had been made with Val Paseda anorthite have been repeated on samples of volcanic anorthite from Monte Somma which contain some albite in solid solution.

Adlhart et al. (1980b) again measured intensities of 'c' and 'd' superlattice reflections in Monte Somma anorthite, observing that the sharp reflections get continuously weaker and become spread out near T_c^* . The behaviour of I_k with $(T_c^* - T)$ is nearly linear unlike that seen in Val Paseda anorthite. Wruck's (1986) measurements of C_p for Monte Somma anorthite reveal a smeared out transition with no λ anomaly, but instead a second-order step in C_p at T_c . These results indicate that the $I\bar{1}-P\bar{1}$ transition with temperature in calcium rich plagioclases away from the end-member anorthite is second-order with critical exponents $\beta = \frac{1}{2}$ and $\alpha = 0$. T_c^* appears lower than in the end-member anorthite, and the smearing out of the transition can be related to the inhomogeneity of sodium content in the crystals. It is thus apparent that changing sodium content affects both T_c and the thermodynamic character of the transition.

The changing transition character will be explained in this chapter in terms of strain-coupling: coupling between phase

transitions in feldspars appears to be effected by strains which are able to operate over long correlation lengths as they are transmitted through the framework structure. Hence the Al/Si order (described by the order parameter Q_{od}) inherited from the $C\bar{1}-I\bar{1}$ transition may influence the $I\bar{1}-P\bar{1}$ transition (described by the order parameter Q^o) by strain-coupling between the order parameters.

Salje (1987b) has already predicted that disordering of the Al and Si over the tetrahedral sites and substitution of Na for Ca (which itself reduces Al/Si order by coupled substitution) should renormalize the transition temperature T_c^* and alter the thermodynamic character of the $I\bar{1}-P\bar{1}$ phase transition. The studies by Adlhart et al. (1980b) and Wruck (1986) tend to substantiate the model proposed by Salje (1987b). In this chapter, the temperature evolution of one of the essential thermodynamic parameters of the $I\bar{1}-P\bar{1}$ displacive transition, the spontaneous strain, is described in Na-bearing anorthites. The temperature evolution of this strain is interpreted in terms of coupling to the other phase transitions occurring in Ca-rich plagioclases

4.2 Strain Behaviour in Monte Somma Anorthite

4.2.1 Measurement of Lattice Parameters The anorthite used for this study was obtained from the Harker mineral collection and originates from the Monte Somma locality in Italy; it was found in rapidly cooled limestone ejecta at Vesuvius. This is the same volcanic sample as characterised by Carpenter et al. (1985), and the composition of single crystals from this sample ranges from $An_{97}Ab_3$ to An_{100} and the average composition of a powder is around $An_{98}Ab_2$. Despite its thermal history, the sample is still

relatively well ordered (Angel et al., 1989a). Separated powder was ground and mixed with silicon as an internal standard. High- and low-temperature lattice parameters were measured between 2 K and 1100 K using a Guinier powder camera by exactly the same method as is described in chapters 2, 3 and 6 and appendix 1.

MONTE SOMMA ANORTHITE

T(K)	a (Å)	b (Å)	c (Å)	alpha	beta	gamma	alpha*	beta*	volume
23	8.164	12.863	14.162	93.113	115.940	91.285	85.910	63.934	1333.540
53	8.165	12.868	14.162	93.125	115.937	91.275	85.902	63.937	1334.331
69	8.164	12.871	14.162	93.119	115.941	91.273	85.910	63.934	1334.478
90	8.165	12.870	14.166	93.118	115.939	91.278	85.909	63.935	1334.823
110	8.166	12.871	14.168	93.122	115.940	91.276	85.905	63.934	1335.231
137	8.167	12.873	14.170	93.145	115.942	91.262	85.886	63.932	1335.832
165	8.168	12.873	14.168	93.118	115.934	91.268	85.914	63.941	1335.907
193	8.173	12.877	14.167	93.125	115.908	91.252	85.915	63.967	1337.357
305	8.181	12.879	14.180	93.130	115.903	91.257	85.907	63.972	1340.053
317	8.181	12.881	14.180	93.144	115.897	91.265	85.889	63.978	1340.392
330	8.182	12.883	14.181	93.145	115.893	91.255	85.892	63.982	1340.978
342	8.184	12.886	14.181	93.108	115.888	91.296	85.914	63.985	1341.684
354	8.185	12.885	14.185	93.120	115.892	91.272	85.912	63.982	1342.085
354	8.184	12.882	14.177	93.162	115.846	91.280	85.863	64.026	1341.195
366	8.186	12.881	14.178	93.138	115.845	91.271	85.895	64.029	1341.637
378	8.187	12.883	14.181	93.146	115.843	91.275	85.884	64.030	1342.247
390	8.186	12.882	14.182	93.155	115.833	91.281	85.872	64.039	1342.222
402	8.190	12.881	14.180	93.118	115.831	91.296	85.906	64.042	1342.532
414	8.185	12.883	14.178	93.141	115.801	91.289	85.885	64.071	1342.217
426	8.187	12.881	14.178	93.141	115.799	91.300	85.880	64.073	1342.301
440	8.187	12.881	14.181	93.126	115.778	91.305	85.895	64.094	1342.833
450	8.187	12.883	14.182	93.122	115.780	91.316	85.894	64.091	1343.005
463	8.189	12.881	14.182	93.121	115.771	91.346	85.882	64.099	1343.326
475	8.191	12.880	14.179	93.103	115.760	91.358	85.896	64.110	1343.427
475	8.196	12.882	14.178	93.099	115.735	91.342	85.911	64.137	1344.619
487	8.191	12.881	14.177	93.120	115.738	91.345	85.885	64.131	1343.514
493	8.192	12.880	14.176	93.100	115.734	91.372	85.896	64.135	1343.521
499	8.192	12.882	14.180	93.110	115.728	91.352	85.894	64.143	1344.283
499	8.198	12.883	14.182	93.109	115.742	91.328	85.905	64.130	1345.219
505	8.192	12.885	14.180	93.117	115.717	91.345	85.890	64.153	1344.592
511	8.192	12.884	14.179	93.130	115.704	91.331	85.883	64.166	1344.575
517	8.192	12.882	14.186	93.139	115.718	91.316	85.880	64.153	1344.875
523	8.196	12.884	14.181	93.124	115.699	91.305	85.902	64.174	1345.473
523	8.198	12.882	14.182	93.109	115.733	91.320	85.909	64.139	1345.414
530	8.191	12.887	14.186	93.098	115.691	91.370	85.900	64.178	1345.510
536	8.193	12.887	14.187	93.110	115.721	91.338	85.901	64.151	1345.673
542	8.194	12.887	14.189	93.116	115.707	91.319	85.903	64.165	1346.222
548	8.195	12.887	14.188	93.108	115.698	91.333	85.907	64.173	1346.421
548	8.199	12.881	14.181	93.109	115.718	91.288	85.926	64.156	1345.558
554	8.195	12.889	14.191	93.134	115.694	91.303	85.893	64.178	1346.810
560	8.196	12.889	14.192	93.147	115.699	91.277	85.891	64.175	1347.167
566	8.195	12.882	14.185	93.112	115.707	91.308	85.903	64.168	1347.470
572	8.202	12.885	14.179	93.067	115.739	91.318	85.957	64.136	1346.198
596	8.202	12.886	14.182	93.066	115.728	91.306	85.965	64.148	1346.569
621	8.203	12.888	14.183	93.055	115.726	91.297	85.982	64.151	1347.108
645	8.204	12.889	14.186	93.070	115.729	91.277	85.975	64.149	1347.763
669	8.205	12.885	14.184	93.071	115.752	91.256	85.982	64.126	1346.926
669	8.207	12.892	14.188	93.059	115.747	91.276	85.986	64.131	1348.401
693	8.207	12.888	14.184	93.078	115.737	91.237	85.985	64.143	1347.811
693	8.209	12.892	14.191	93.066	115.755	91.257	85.987	64.123	1349.035
717	8.207	12.888	14.190	93.051	115.757	91.236	86.013	64.124	1348.245
717	8.210	12.895	14.192	93.050	115.736	91.254	86.008	64.144	1349.749
742	8.208	12.891	14.191	93.051	115.744	91.234	86.015	64.137	1348.944
742	8.211	12.895	14.194	93.037	115.743	91.247	86.025	64.138	1350.184
754	8.214	12.892	14.195	93.033	115.741	91.235	86.035	64.141	1350.407
814	8.216	12.894	14.195	93.055	115.739	91.203	86.026	64.144	1351.115
875	8.217	12.898	14.197	93.045	115.740	91.184	86.046	64.145	1351.808
936	8.218	12.899	14.200	93.041	115.721	91.166	86.061	64.166	1352.631
996	8.222	12.901	14.202	93.041	115.730	91.130	86.078	64.159	1353.544
1057	8.225	12.906	14.201	93.028	115.742	91.071	86.120	64.151	1354.415
1117	8.229	12.905	14.205	93.031	115.756	91.017	86.142	64.141	1355.335
1178	8.233	12.909	14.212	93.036	115.731	90.994	86.149	64.168	1357.408
1239	8.234	12.912	14.214	93.035	115.727	90.984	86.154	64.172	1358.155
1299	8.240	12.915	14.219	93.018	115.736	90.955	86.188	64.166	1359.783

Table 4.1 Lattice parameters of Monte Somma anorthite between 23 K and 1299 K.

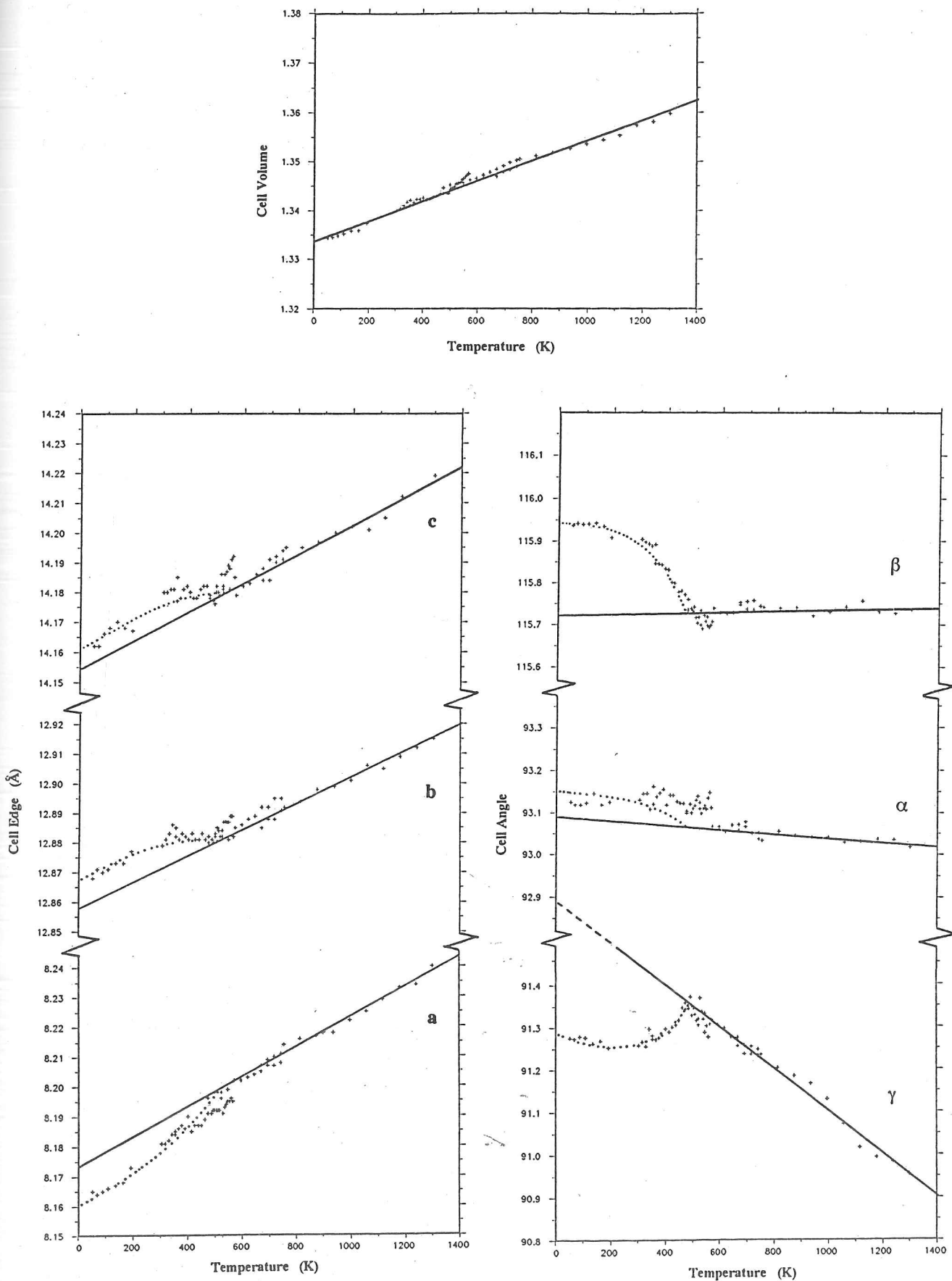


Figure 4.1 The lattice parameters of Monte Somma anorthite from 23 K to 1299 K. Solid lines show the I1 lattice parameters, dotted lines serve as a guide to the eye of the deviations from I1 in the P1 phase.

The lattice parameters of Monte Somma anorthite are presented in Table 4.1 and temperature evolution of these lattice parameters is shown in Figure 4.1. In each case the solid line shows the linear least squares fit to the high temperature $I\bar{1}$ lattice parameters above 600 K. Deviations from the low temperature extrapolation of this line in the $P\bar{1}$ phase are indicated by the dotted line. As observed for Val Pasmeda anorthite (chapter 3) the displacive $I\bar{1}$ - $P\bar{1}$ transition in Monte Somma anorthite results in marked deviations in the thermal expansion of some lattice parameters. The thermal expansions of Monte Somma anorthite and Val Pasmeda anorthite are not identical however; the former shows larger deviations of a , c and α in the $P\bar{1}$ phase and the slopes of β and γ in Monte Somma directly below the transition are smaller than the equivalent slopes for Val Pasmeda anorthite. These observations may be explained in terms of the theory of spontaneous strain and order parameter coupling at the $I\bar{1}$ - $P\bar{1}$ transition introduced in chapter 3.

4.2.2 Spontaneous Strain and the Order Parameter in $P\bar{1}$ Anorthite

The anomalous behaviour of the lattice parameters in the $P\bar{1}$ phase arises from the distortion associated with the displacive phase transition $P\bar{1}$ - $I\bar{1}$, as seen in Val Pasmeda anorthite (Redfern and Salje, 1987; chapter 3). Applying the same analysis as described in detail in section 3.3 the six elements of the spontaneous strain tensor have been calculated in Monte Somma anorthite at all temperatures below T_c^* . Each of these strain tensors has been diagonalised to give the three principal strain elements of the strain quadric; e_1 , e_2 and e_3 . The temperature evolution of these principal strain elements for Monte Somma anorthite is shown in Figure 4.2.

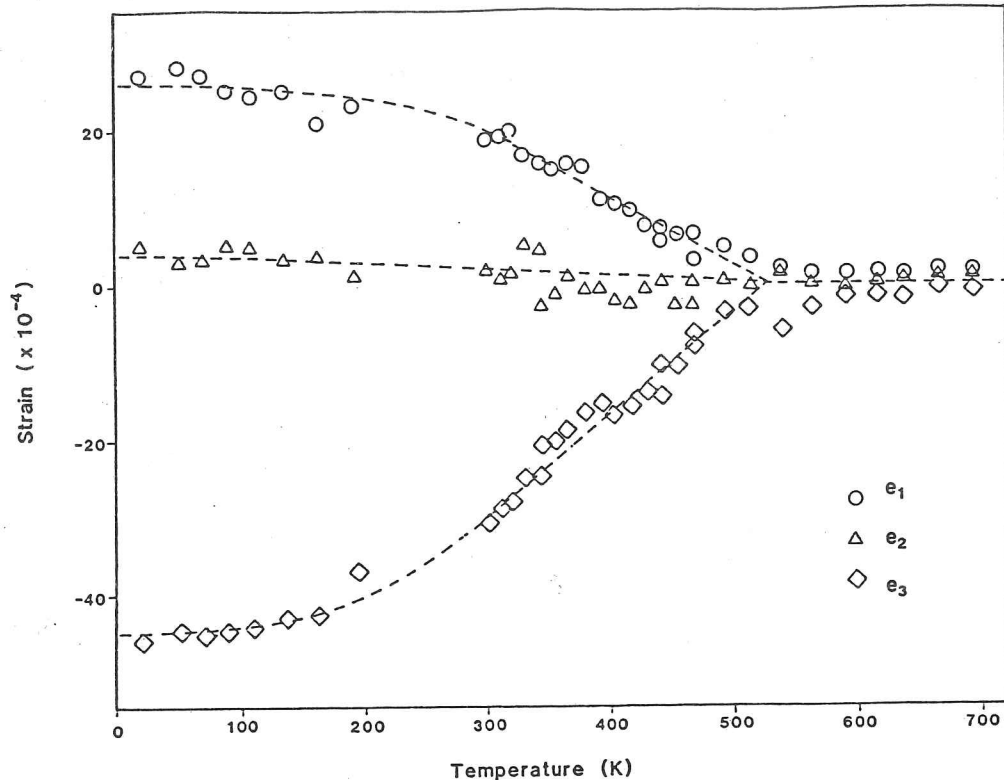


Figure 4.2 Temperature evolution of the principal spontaneous strains below the $\text{I}\bar{1}$ - $\text{P}\bar{1}$ phase transition in Monte Somma anorthite.

The temperature dependent behaviour of the principal strains in Monte Somma anorthite is quite different from that observed in Val Paseda anorthite (chapter 3). The magnitudes and directions of these three strain elements are different in the two anorthites. We again observe, however, that as in Val Paseda anorthite the strain quadric of Monte Somma anorthite does not change orientation as the temperature changes, although it is a different orientation to that in Val Paseda anorthite. This again indicates that the deformation pattern is independent of temperature and only the deformation amplitude increases as the square of the order parameter. The strain quadric is intimately linked to the refractive index indicatrix via the elasto-optic effect. It is not surprising to see a dependence of its orientation on chemical composition; such a dependence of optical indicatrix orientation has long been known (see for

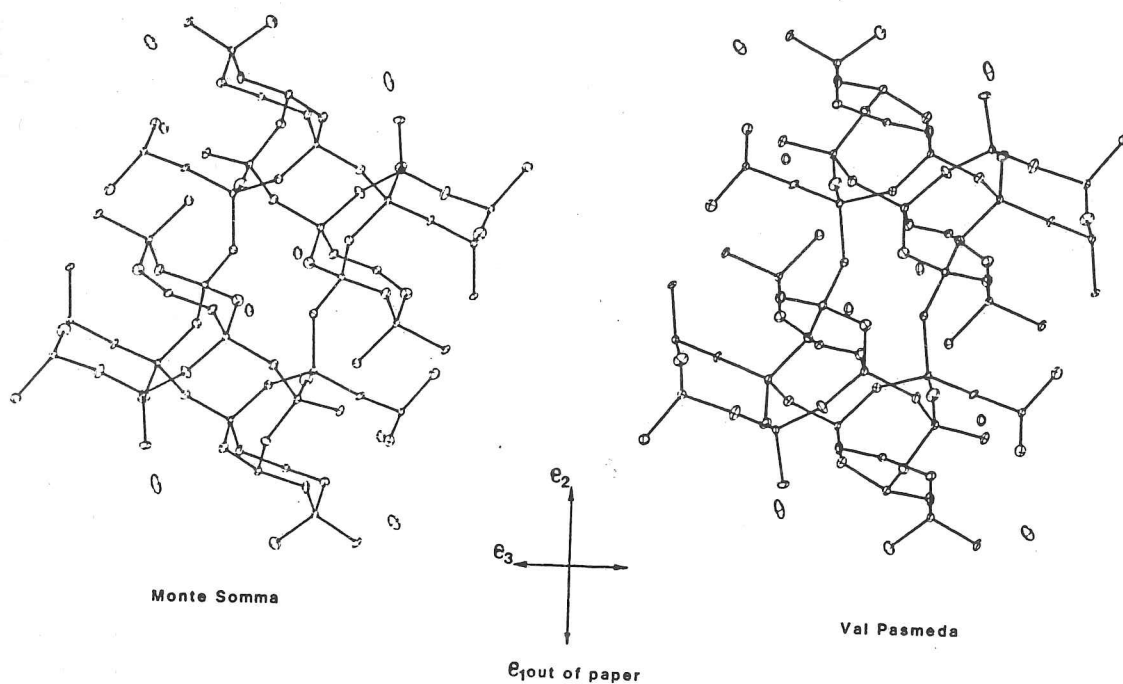


Figure 4.3 The structure of anorthite (refinement of Kalus, 1978) projected parallel to the principal axes of the strain ellipsoids for both Monte Somma and Val Pasmada anorthite, demonstrating the dependence of strain tensor orientation on Na-content, and its complex relationship to the crystal structure. T-O bonds only are shown.

example Smith, 1958).

The strain quadrics of both Monte Somma and Val Pasmada anorthite are shown projected onto the anorthite structure in Figure 4.3. In this figure, the crystal structure of anorthite has been plotted using the program ORTEP in an orientation which coincides with the principal strains. This is achieved by referring the structural data of Kalus (1978) to the same cartesian coordinate system as that of the strain tensor and then rotating the structure about these axes by angles corresponding to the direction cosines given in the matrix of Eigenvectors for the principal strains. Any relationship between the strain orientation and crystal structure is not obvious, but the variation in orientation between the two anorthites studied is

apparent.

The behaviour of the lattice parameters and spontaneous strain may be understood in terms of the thermodynamic behaviour of plagioclase feldspars by considering the Landau model for the free energy of plagioclase feldspars outlined in chapter 3. The importance of the spontaneous strain lies in its role in providing a coupling mechanism between the degree of Al/Si order, Q_{od} , and the essential thermodynamic parameter of the $I\bar{1}-P\bar{1}$ transition, Q^0 . Coupling between these two order parameters is biquadratic through the spontaneous strain. Since the strain couples to $Q^0{}^2$ it provides an indirect measure of the behaviour of Q^0 and in chapter 3 the spontaneous strain was used to determine the temperature dependence of Q^0 for Val Paseda anorthite. The spontaneous strain may be expressed in terms of both order parameters in the manner given in equation 3.11. The observed temperature evolution of the strain is due solely to the temperature dependence of Q^0 . Other anorthites with different values of Q_{od} would, however, be expected to show different strain behaviour due to the quadratic coupling between ϵ_i and Q_{od} . This scalar spontaneous strain has been calculated for Monte Somma anorthite and is shown in Figure 4.4. Within 300 K of T_c^* the strain ϵ_s is a linear function of temperature. Thus ϵ_s (T_c^*-T) and the critical exponent $\beta = \frac{1}{2}$ as is expected for a second-order phase transition obeying Landau theory. In contrast tricritical behaviour was observed in Val Paseda anorthite, with $\beta = \frac{1}{4}$ (chapter 3; Wruck, 1986). This indicates that the increased Na content and the lower degree of Al/Si order in Monte Somma anorthite have effectively altered the fourth order coefficient B_{eff} , renormalizing it to more positive values in

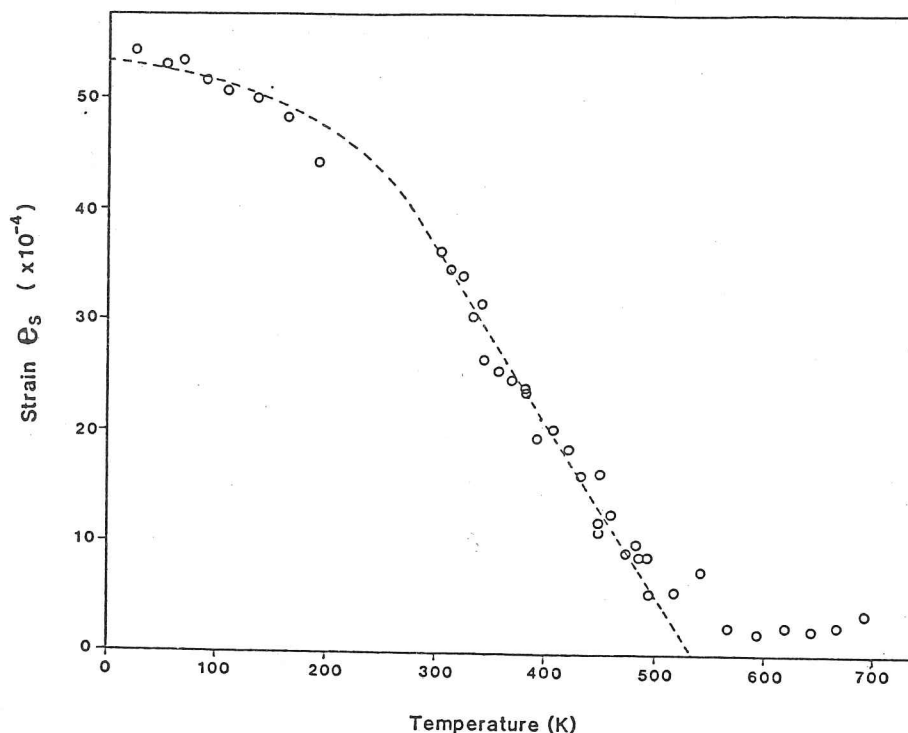


Figure 4.4 Temperature evolution of the scalar spontaneous strain (e_s) in Monte Somma anorthite. The linear dependence above 200 K reflects the second-order nature of the transition.

equation 3.10 above, and the thermodynamic behaviour has moved from being tricritical for Val Paseda to second-order for Monte Somma. The change in B_{eff} has an additional effect on the thermodynamic behaviour at the $\overline{I1}-\overline{P1}$ transition since it leads to renormalization of T_c^* . The spontaneous strain behaviour indicates that the transition temperature for Monte Somma anorthite is 530 ± 10 K compared with $T_c^* = 510$ K for Val Paseda anorthite.

4.2.3 Comparison with Val Paseda and Saturation The thermodynamic behaviour of the $\overline{P1}$ phase of Val Paseda and Monte Somma anorthites can be compared directly by considering the temperature evolution of Q^0 for each material. This order parameter is directly proportional to $\epsilon_s^{1/2}$ which we have already determined. The relevant normalized order parameters have therefore been calculated from the strain behaviour and are shown

in Figure 4.5 where the order parameter is plotted against reduced temperature $t = (T_c^* - T)/T_c^*$. The steeper increase of Q^0 near $t=0$ for Val Paseda (where $Q^0 \propto t^{\frac{1}{4}}$) compared with Monte Somma (where $Q^0 \propto t^{\frac{1}{2}}$) is apparent. The order parameter in Monte Somma anorthite only follows the behaviour predicted by Landau theory down to around 250 K, below which it saturates to a value of around 0.75. Saturation in the Val Paseda anorthite is not as obvious. This is not surprising, however, since should it occur at similar temperatures to Monte Somma the order parameter would already be around 0.9 due to the tricritical behaviour followed in Val Paseda anorthite. Saturation of the order parameter must be

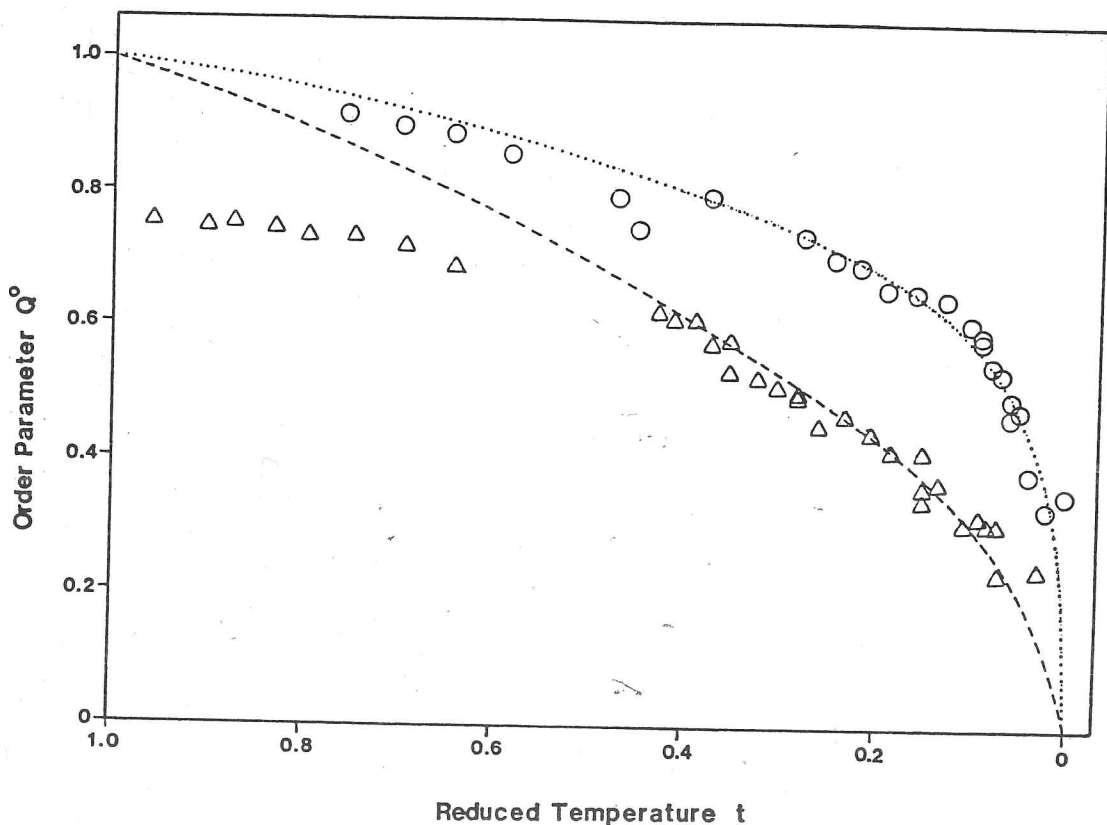


Figure 4.5 Normalized order parameter behaviour of Monte Somma (triangles) and Val Paseda (circles) anorthite derived from spontaneous strain data. Val Paseda anorthite behaves according to a tricritical model (dotted line) whereas Monte Somma anorthite follows second-order behaviour (dashed line). Order parameter saturation is apparent for Monte Somma anorthite at $t > 0.6$ (corresponding to $T < 200$ K).

expected since the gradient term dQ/dT must be zero at 0 K by simple thermodynamic considerations. Similar order parameter saturation has been observed in other co-elastic materials; in chapter 6 flattening of the spontaneous strain in NaNO_3 below 70 K is reported and the effects of order parameter saturation are discussed in greater detail. It is not immediately obvious, however, why the spontaneous strain should saturate at temperatures as high as around 200 K in anorthite. Local strain fields associated with heterogeneities in Si/Al order and Na 'point defects' may interact with the macroscopic strain preventing further distortion at lower temperatures. As such the Na point defect would act either as a local defect perturbation to the order parameter, or if the Na distribution were appropriate it may act as an effectively homogeneous field conjugate to Q^0 . The rôle of defects and their influence on displacive phase transitions is further considered in the discussion of K-bearing cordierites in the next chapter (and Redfern et al. 1989a). For the moment we may simply postulate that the plagioclase framework structure cannot tolerate the relatively high degree of distortion that the Landau model predicts would arise as 0 K is approached.

4.2.4 Magnitude of Coupling to other Transitions In addition to the study of the structural distortion in the $P\bar{1}$ phase we might also speculate about the role of Al/Si disorder on the lattice parameters of the high-temperature $I\bar{1}$ phase. According to equation 3.11, we find that the spontaneous strain taken with respect to the highest possible symmetry of the feldspar structure, which is $C2/m$, is described by two terms. The first term is proportional to Q_{od} (that is $(\delta_{i4}\Delta_4'' + \delta_{i6}\Delta_6'')Q_{od}$) and is

related to the symmetry change $C2/m-C\bar{1}$. The second term is described by the first part of equation 3.11 (that is $(\Delta_i + S_{\epsilon Q_{od}}^i)Q_{od}^2$) and is related to the hypothetical phase transition $C\bar{1}-I\bar{1}$. This part of the spontaneous strain involves all six strain components. Experimentally, it is found that the major difference between the lattice parameters in the $I\bar{1}$ phase of anorthite from Monte Somma and Val Paseda (comparing Figure 3.5 and Figure 4.1) is revealed as a parallel shift of γ by almost 0.1° . The maximum strain component is, therefore, ϵ_6 . This experimental result may indicate that the strain induced by the $C2/m-C\bar{1}$ phase transition is larger than that of the $C\bar{1}-I\bar{1}$ phase transition. We can then roughly estimate the order of magnitude of Δ_6'' and Δ_4'' if we assume that Q_{od} (Val Paseda) is close to unity (e.g. 0.95) and Q_{od} (Monte Somma) is reduced to approximately 0.8. These values are shown by Carpenter (1988) to be reasonable estimates using a tricritical model to calculate Q_{od} . Putting these numbers into equation 3.11 we find, as orders of magnitude:

$$\Delta_4'' \ll \Delta_6'' = \frac{\delta x_6}{\delta Q_{od}} = 0.012 \quad \{4.1\}.$$

Thus the temperature dependent behaviour of the lattice parameters not only reveals the character of the (relatively) low-temperature $I\bar{1}-P\bar{1}$ transition but also allows an estimate of the coupling constants associated with the high temperature $C2/m-C\bar{1}$ transition. This is despite the fact that the $C2/m-C\bar{1}$ transition does not occur in nature since melting takes place in the $I\bar{1}$ phase. Nevertheless this hypothetical phase transition does have a significant influence on the lattice parameters, as

indicated here. It is apparent that strain coupling between successive phase transitions plays a dominant rôle in the thermodynamic behaviour of plagioclase feldspars at high-temperature.

4.3 The $I\bar{1}$ - $P\bar{1}$ Transition at High-Pressure

Recent work (Angel et al., 1988) has demonstrated that the $I\bar{1}$ - $P\bar{1}$ phase transition in anorthite which has been reported in this thesis at high temperature and 1 bar also occurs at room temperature and elevated pressure; above 26 kbar the $P\bar{1}$ structure of Val Paseda anorthite undergoes a first-order transformation to a structure with $I\bar{1}$ symmetry. In anorthites with up to 16 mol % albite component in solid solution, the behaviour at pressure is also first-order, whereas we have seen that at elevated temperature the transition is second-order for such Ca-rich plagioclases away from end-member anorthite. We shall now demonstrate that these observations are entirely consistent with the Landau model for the phase transition, and that the tricritical behaviour in pure anorthite described in chapter 3 represents the boundary between a set of second-order transitions in Ca-rich plagioclases at atmospheric pressure (as described in section 4.2 above and Redfern et al., 1988), and a set of first-order transitions in plagioclases at high pressure and room temperature.

The structure determination of the high-pressure phase (Angel, 1988) has shown that it has the same $I\bar{1}$ symmetry as the high-temperature phase of anorthite. Indeed, thermodynamic arguments (Angel and Ross, 1988) suggest that the two structures are the same phase. At this high-pressure displacive phase

transition, Q^0 , is again coupled to the spontaneous strain, ϵ , arising as a result of the transition. Angel et al. (1989b) therefore, used the spontaneous strain as a thermodynamic parameter to chart the order parameter behaviour in exactly the same manner as was first used on anorthite in this thesis. As we have observed in the phase transition at elevated temperature, one of the principal strains in anorthite at high-pressure is close to zero; the low symmetry $P\bar{1}$ structure is approximately in a state of plane strain with respect to the high symmetry $I\bar{1}$ structure.

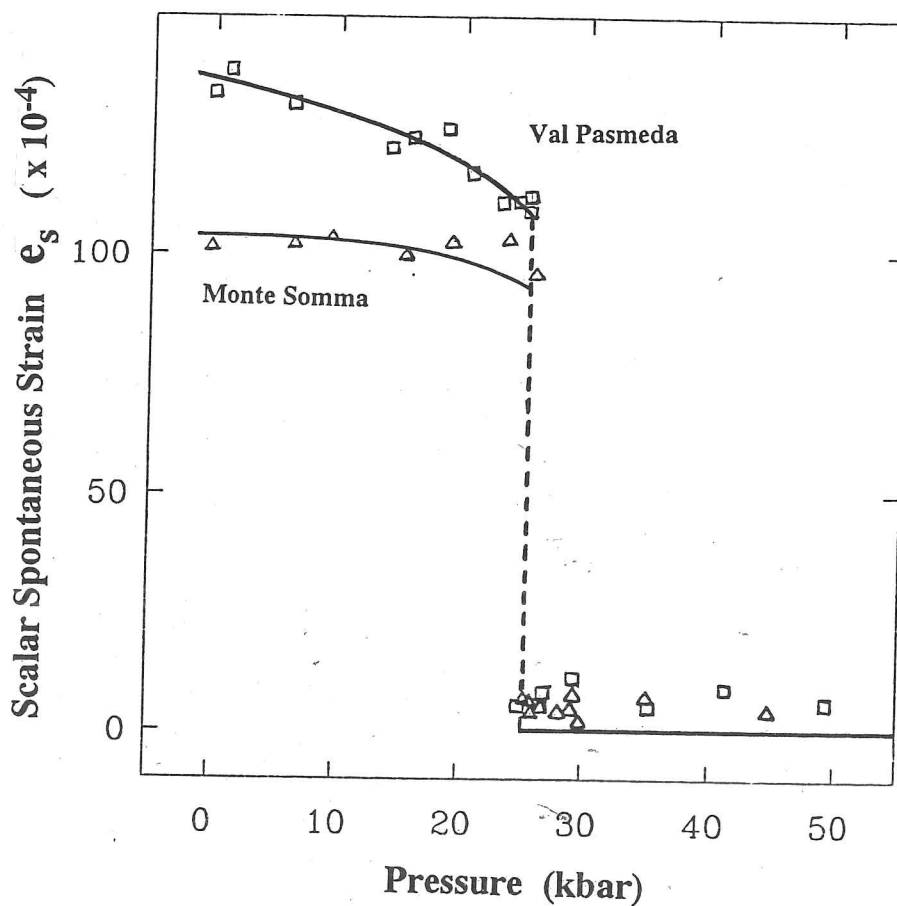


Figure 4.6 Scalar spontaneous strain below the $I\bar{1}$ - $P\bar{1}$ phase transition at pressure (data of Angel et al., 1989b) demonstrating the strongly first-order character of this transition at pressure.

The scalar strain of the $P\bar{1}$ phase with respect to the $I\bar{1}$ phase has been calculated from the high-pressure data of Angel et al. (1989b) for both samples, and Figure 4.6 shows the pressure dependence of this scalar strain, which is proportional to Q^2 . The discontinuous and very strongly first-order character of the phase transition is obvious in both Monte Somma anorthite and Val Paseda anorthite. The maximum scalar strain as well as the first order step at the transition point is somewhat larger for Val Paseda anorthite than for Monte Somma anorthite. We shall discuss the significance of these observations in the next section.

The compositional dependence of the transition pressure has been derived from the reversals of the phase boundary at varying compositions. Angel et al. (1989b) found that the transition pressure increases with albite content. They also noted that the magnitude of the first-order step at the transition decreases as we move toward more albite rich samples. Extrapolating the composition dependence of this first order step, Angel et al. (1989b) observed that the step disappears in samples with $N_{Ab} \geq 16\%$.

We have seen that the atmospheric pressure $I\bar{1}$ - $P\bar{1}$ phase transition in pure anorthite is tricritical (chapter 3; Wruck, 1986; Redfern and Salje, 1987), and in plagioclases with some albite in solid solution the same phase transition is second-order (section 4.2; Wruck, 1986; Redfern et al., 1988). It may at first, therefore, be rather surprising to find such a large discontinuity and hysteresis in the order parameter at P_{Tr} (the transition pressure) through the $I\bar{1}$ - $P\bar{1}$ transition in the same anorthites at high pressure, indicative of strong first-order

character. Why should changes in Na-content and Al/Si order result in such very different transition behaviour in various regions of P-T-X space?

The changing character of the $I\bar{1}-P\bar{1}$ phase transition in plagioclases may be fully understood in terms of the renormalisation of the relevant coefficients in the Landau expansion for free energy, G. The influences of Al/Si disorder, Na-Ca replacement, inhomogeneity, and potential at the Ca-site may be treated together as a single independent parameter, a local stress field. This approach allows the free energy to be approximated as a simple function of Q^0 , the displacive order parameter. In this approximation Salje (1987b) gave the free energy as:

$$\Delta G(Q^0) = \frac{1}{2}AQ^0{}^2 + \frac{1}{4}\left(B - \frac{d^2}{C}\right)Q^0{}^4 + \frac{1}{6}cQ^0{}^6 \quad \{4.2\}$$

where B, and c are constants, d is a function of Q_{od} , and C represents the elastic constants. The coefficient of the first term in this expansion, A, vanishes at the phase transition. The coefficient of the fourth-order term in the expansion can be replaced by B_{eff} which is dependent on Q_{od} , Na content (degree of albite solid solution) and form of the potential at the Ca-site. The results of section 4.2 show that decreasing the Na content (N_{Ab}) at atmospheric pressure changes B_{eff} from some positive value to smaller values, until at An_{100} $B_{eff}=0$ ($c>0$) so that the phase transition with temperature changes from second order (for $N_{Ab}>0$) to tricritical (at $N_{Ab}=0$) (chapter 3). Further reduction of B_{eff} would lead to a first-order phase transition ($B_{eff}<0$, $c>0$), but this is not observed on the temperature-composition equilibrium phase diagram since it would correspond

to an anorthite with greater than 100% Ca or greater than 100% Al/Si order (both obviously unattainable and without real physical meaning), or a change in the Ca-potential well (which has not been observed). Nonetheless, the tricritical behaviour in Val Paseda anorthite must mark the boundary between second-order and first-order behaviour (Landau and Lifschitz, 1954).

To understand the thermodynamic behaviour of plagioclases under pressure and relate it to the existing Landau theory we must first consider the form that the order parameter, Q^0 , is expected to take as a function of pressure. We have already seen, from the experimental results of Angel et al. (1989b), that since the strain, ϵ , is proportional to Q^{0^2} we can chart the order parameter experimentally with pressure. With temperature as a variable we find that for continuous phase transitions the order parameter may be expressed as:

$$Q^0 \propto |T_c - T|^\beta \quad \{4.3\}$$

If we consider the behaviour of Q^0 as a function of pressure at constant temperature we expect:

$$Q^0 \propto |P - P_c|^\beta \quad \{4.4\}$$

for continuous transitions. Here the critical exponent β takes the same values as above. In the case of the first-order transition observed in anorthite at pressure the equivalent form of the order parameter is somewhat more complicated. The transition occurs at some P_{Tr} which is greater than P_c in the case of anorthite, and there is a step in Q^0 at the transition proportional to $|P_{Tr} - P_c|^{\frac{1}{2}}$. The size of this step is indicative of how strongly first-order the transition is, in particular we

expect the step in Q^0 to increase as B_{eff} moves to larger negative values. Below P_{Tr} we expect Q^0 to increase gradually. The form of the order parameter (observed in terms of spontaneous strain in Figure 4.6) for both Monte Somma anorthite and Val Paseda anorthite reflect these features.

First-order behaviour at the $I\bar{1}-P\bar{1}$ transition in anorthite might result from a variety of causes. It would be expected on the application of an external shear stress parallel to and opposing the shear of the spontaneous strain, such a stress acts as the conjugate field to the displacive order parameter, Q^0 . In the absence of an external field first order behaviour would result if the fourth order coefficient, B_{eff} , became negative. The Ca split position in $I\bar{1}$ anorthite at atmospheric pressure is observed to differ dramatically from the same site in the high-pressure $I\bar{1}$ phase (Angel, 1988); high-temperature $I\bar{1}$ anorthite has a shallow Ca potential well with split sites, the high-pressure phase has a significantly sharper well and Ca sits on a single site. The coupling between Q^0 and the Ca potential must change as the form of the Ca-site changes. Salje (1987b) points out that there is coupling between the fast phonon movements of the lattice and the slow relaxation of the Ca position. In real anorthite crystals the Z and Z' points on the Brillouin zone boundary are non-equivalent due to inhomogeneity and the order parameter Q^0 comprises two contributions Q_c^0 and Q_d^0 , which may be related to the structure factors of the 'c' and 'd' reflections (see equation 5 of Salje, 1987b). It is the part Q_d^0 which is sensitive to the disorder on the Ca sites, and it is this part of Q^0 which will differ in the two cases of ambient pressure and high-pressure results. For this reason alone we would expect

renormalisation of B_{eff} in equation 4.2 above in anorthite under pressure, and a switch to first-order behaviour. In a naïve way the high pressure structure of anorthite shows those structural features associated with an increasing Ca-content, but extrapolated beyond the anorthite end-member, and may be considered simplistically as a 'super-saturated Ca anorthite'. The effect of coupling to the monoclinic-triclinic displacive transition may also become more important at high pressure, and this would renormalize the fourth-order term in the Landau expansion (move B_{eff} to negative values). Thus we should expect to find first-order behaviour in some regions of P-T-X space, as indeed the results of Angel et al. (1989b) confirm. The boundary between first- and second-order behaviour should be a line of phase transitions in pressure-temperature-composition space and the tricritical transition in pure anorthite at 510 K and 1 bar is a point on this line. The data of Angel et al. (1989b) show that as we increase N_{Ab} the step at the phase transition at pressure decreases, in other words $|P_{\text{Tr}} - P_{\text{c}}|$ decreases, until at approximately 84 mol% anorthite the transition becomes continuous and $P_{\text{c}} = P_{\text{Tr}}$. At this point the phase transition changes again from first-order to second-order, and this must mark another point on the line of tricritical phase transitions. We note that in both the suite of samples studied by Angel et al. (1989b) and in samples studied through the transition at high-temperature (Redfern et al., 1988) the effect of increasing N_{Ab} is the same: namely to make B_{eff} more positive.

4.4 Conclusions: the P-T-X Phase Diagram

The experimental observations of the $I\bar{1}$ - $P\bar{1}$ phase transition in calcium-rich plagioclases show second-order, tricritical, and first-order behaviour dependent upon temperature, composition, and pressure. It is possible to bring together all the results described here and construct a phase diagram for the $I\bar{1}$ - $P\bar{1}$ transition in P-T-X space (Figure 4.7). We see that the phase boundary between primitive and body-centred plagioclase is a surface of phase transitions, and the experimental observations put some constraints on the locus of this surface. Figure 4.7, therefore, can only be said to describe the essential topology of

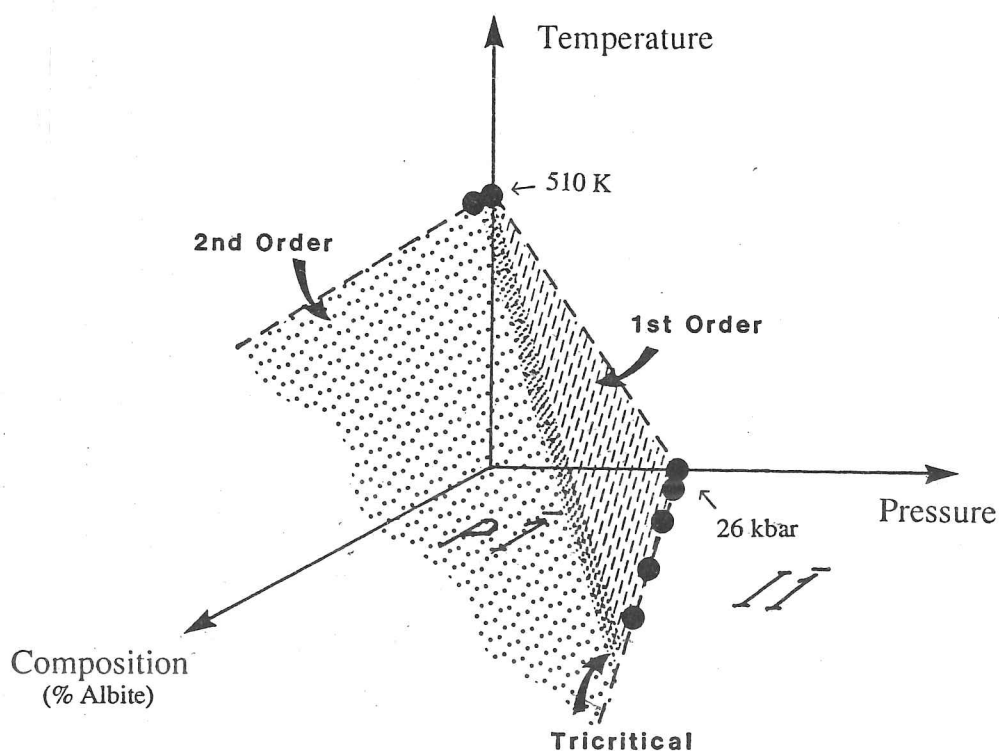


Figure 4.7 Schematic P-T-X phase diagram showing the topology of the boundary between the $I\bar{1}$ and $P\bar{1}$ Ca-rich plagioclases. The stippled surface represents a surface of second-order phase transitions, the hatched area a surface of first-order phase transitions. The heavier shaded line between these two areas represents the line of tricritical phase transitions. Filled circles show points on the phase transition surface determined by experiment (this work and Angel et al., 1989b).

the phase relations; further work must be carried out in high-temperature high-pressure cells to chart the P-T planes of the phase diagram. Despite this, the line of tricritical phase transitions must join the two points at (510 K, 100 % anorthite, 1 bar) and (300 K, 84 % anorthite, 42 kbar) as shown. The $P\bar{1}$ phase occurs in a region near the origin at the anorthite end-member. As we move away from this origin to higher pressures or temperatures we eventually cross the surface of phase transitions into the $I\bar{1}$ phase. The thermodynamic character of the phase transition will depend on where we cross this surface, and the geometry of this surface may be simply related to changes in B_{eff} which directly affects the form of the empirical Landau potential in equation 4.2. This phase diagram for plagioclases is the only example the author knows in which a line of tricritical phase transitions has been charted in P-T-X space. Tricritical phase transitions have been observed in other systems on changing composition, pressure and temperature, for example tricritical behaviour is found as a function of T and X in the solid-solution series $\text{Pb}_3(\text{P}_{1-x}\text{V}_x\text{O}_4)_2$ (Wadhawan and Glazer, 1981) and as a function of P and T in ND_4Cl (Yelon et al., 1974).

The rôle of strain-induced order parameter coupling is crucial in the understanding of the complex coupled processes at phase transitions in feldspars, such as $I\bar{1}-P\bar{1}$. We see that such co-elastic behaviour leads to renormalization of certain Landau coefficients and changing transition behaviour at the $I\bar{1}-P\bar{1}$ transition providing the opportunity to observe multicritical phenomena in a single system. Changes in coupling between the displacive order parameter and Ca potential well renormalize the fourth-order coefficient of the overall Landau potential leading

to a switch from second-order behaviour through tricritical to first-order behaviour. These changes in transition behaviour with temperature and pressure have significant implications for the thermodynamic properties of plagioclase feldspars in the Earth's crust. The study of phase transitions in mineral systems can thus be seen to yield results which are not only significant in the understanding of the stability of geological materials, but which also further our awareness of the importance of material-related properties and their influence on phase transition behaviour.

CHAPTER 5

HEXAGONAL-ORTHORHOMBIC TRANSITION IN Mg-CORDIERITE

5.1 Mg-Cordierite: a Kinetic Problem

So far Landau theory is seen to provide a satisfactory basis for the description of the thermodynamic equilibrium behaviour of As_2O_5 and Ca-rich plagioclase. We have seen that Landau theory is particularly useful for the description of elastic behaviour at phase transitions in crystals with a framework structure. Can these ideas be extended to the description of time-dependent phenomena arising in kinetic experiments?

The polymorphic phase transition in Mg-cordierite ($\text{Mg}_2\text{Al}_4\text{Si}_5\text{O}_{18}$) has been described within the framework of equilibrium Landau theory but studied in non-equilibrium metastable samples. The transformation from the high-temperature hexagonal structure (P6/mcc) to the low-temperature orthorhombic structure (Cccm) is, in two respects, quite different to those phase transitions discussed in the preceding chapters. Firstly, the transition has been studied as a function of time as the samples approach equilibrium from a non-equilibrium state. Secondly, the transition between the high- and low-temperature forms must be first-order under equilibrium conditions, since the symmetry relations imply the presence of a third-order term in the Landau expansion (it is an example of a symmetry-driven first-order phase transition, as described in 1.2.4).

5.1.1 Cordierite Structure and Stability The structure of Mg-cordierite comprises a framework of Al, Si tetrahedra with Mg^{2+} in octahedral coordination. Although not traditionally classed as a framework silicate, cordierite may sensibly be described as such

since each tetrahedron is corner-linked to four nearest neighbours. Under equilibrium conditions, pure magnesium cordierite is orthorhombic at room temperature and transforms to hexagonal symmetry above approximately 1450°C (Schreyer and Schairer, 1961; Smart and Glasser, 1977; Putnis, 1980). The hexagonal structure (Figure 5.1) contains tetrahedral sites of two types: six T_2 sites per formula unit forming six-membered rings on (001), the rings being connected by T_1 linking tetrahedra to form channels parallel to the z-axis. There can be no long-range Al/Si order in the hexagonal structure; ordering of Al and Si on the tetrahedral sites (which become subdivided into non-equivalent $T_{1,1}$, $T_{1,6}$, $T_{2,1}$, $T_{2,3}$, and $T_{2,6}$ sites) leads to the orthorhombic polymorph (Gibbs, 1966; Meagher and Gibbs, 1977; Cohen et al., 1977; Carpenter et al., 1983).

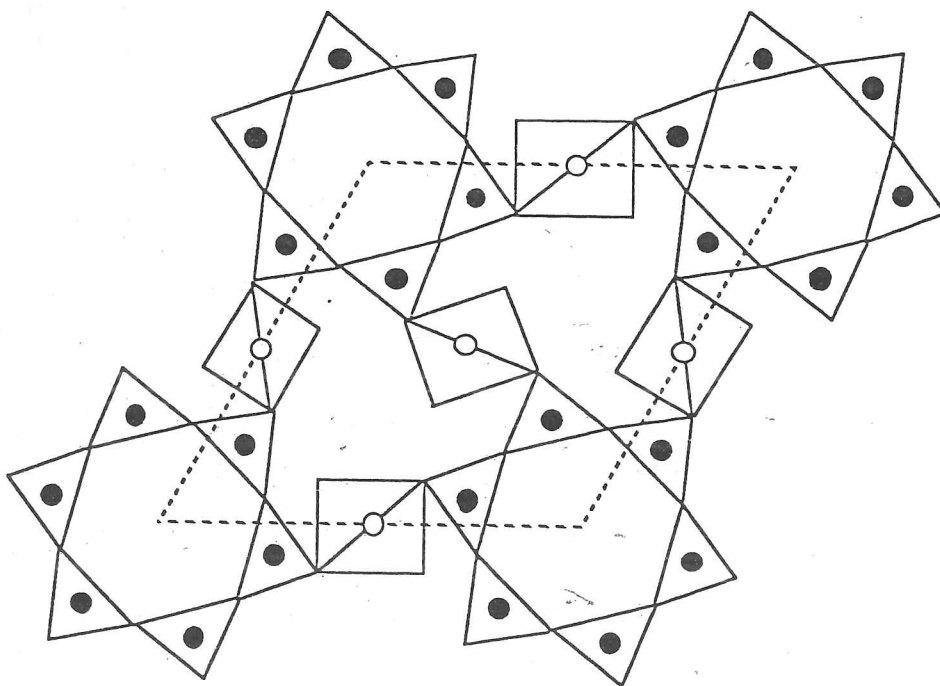


Figure 5.1 The tetrahedral framework of hexagonal cordierite. The tetrahedra in the ring sites (●) are designated T_2 , and those outside the ring (○) are designated T_1 .

The ordering of Al and Si below 1450°C in cordierite is kinetically hindered in the annealing experiments described below, but the study of the temperature-dependent equilibrium behaviour of cordierite around this phase transition is experimentally difficult because of the high temperatures involved. Most studies have centred on the investigation of the ordering process as a function of annealing time in cordierites crystallised from glass and annealed at temperatures below T_c . These studies have revealed that the same phases evolve as a function of time (Schreyer and Schairer, 1961). It is found that the first cordierite phase to crystallise from the glass is hexagonal, and further annealing leads to the development of a modulated structure, which in turn transforms to the true low-temperature orthorhombic equilibrium phase (Putnis et al., 1987; Salje, 1987a; Güttler et al., 1989). It is known from group-theoretical considerations that under equilibrium conditions the latter transition must be first-order (McConnell, 1985; Salje, 1987a)

The ordering of Al and Si and the transformation to orthorhombic symmetry is accompanied by distortions of the unit-cell parameters, and the distortion index Δ was introduced by Miyashiro (1957) as a measure of the distortion of the orthorhombic cell with respect to the hexagonal cell. The orthorhombic distortion was long regarded as analagous to the degree of Al/Si order, but we can see that this is only true if the degree of Al/Si order and the strain are linearly coupled. In this chapter we test the assumption that the Δ index can be used as a convenient measure of the degree of cationic order and present the results of an investigation into the spontaneous

strain behaviour of cordierites (measured by high-resolution X-ray powder diffraction using the Δ index) of known degree of Al/Si order. It will be shown that previous reports (for example, Putnis and Bish, 1983) that the Δ index varies continuously with degree of Al/Si order (despite the first-order character of the transition) are misleading and result from X-ray diffraction data of insufficient resolution. The high-resolution synchrotron X-ray diffractometry reported here leads to an improved and different interpretation of the transformation mechanism. The results are presented within the framework of the coupled order parameter theory described by Salje and Devarajan (1986).

The discussion of pure Mg-cordierite is extended in section 5.4 where the influence of channel-filling potassium is considered. In particular the potassium is considered in terms of a defect with an associated stress field on the lattice. We will investigate the effect such added potassium has on the transition behaviour, on the structure, and on the form of the Landau potential.

5.1.2 Landau Theory of Cordierite Before turning to K-bearing cordierite let us first consider the phase transition behaviour in pure Mg-cordierite. The theoretical description of the $P6/mcc-Cccm$ transition in cordierite has been presented by Salje (1987a). Two order parameters may be employed for the Landau theoretical description: the degree of long-range Al/Si order is represented by the order parameter Q_{od} , and the degree of macroscopic structural distortion is represented by the order parameter Q . Thus the orthorhombic distortion (traditionally measured by the Δ index) is expressed in the Landau expansion in

terms of the displacive order parameter, Q , which is zero when $\Delta = 0$ and increases in the same way as Δ with time in annealing experiments. Q_{od} should be zero in the totally disordered hexagonal phase. The experimental work presented in section 5.2 and discussed in section 5.3 probes the nature of the coupling between Q and Q_{od} .

The space group relations imply that the transition is associated with the Γ point of the Brillouin zone and the active representation of the order parameters is E_{2g} in $P6/mcc$. This is a two-dimensional representation with components corresponding to monoclinic as well as orthorhombic symmetry. Salje (1987a) expresses the two components as q_1 and q_2 , and $q_{od,1}$ and $q_{od,2}$ respectively. In addition, each order parameter may be defined on a local length scale as well as a macroscopic length scale. X-ray diffraction experiments would, for instance, probe the order parameters on a long length scale (a few hundred \AA), whereas Raman and infrared experiments can shed light on the behaviour of order on a local length scale (a few tens of \AA). The relationships between these various order parameters and the possible point-group symmetries of cordierite are tabulated by Güttler et al. (1989). For our purposes a description employing just one Al/Si order parameter, Q_{od} , and the orthorhombic distortion, q_1 (which we also occasionally refer to simply as Q), will suffice.

It is now possible to formulate the Landau potential for pure orthorhombic Mg-cordierite ignoring local monoclinic fluctuations (which are represented by q_2). Following the approach of Salje (1987a), we write this as an excess free energy:

$$\Delta G(Q_{od}, q_1) = \frac{1}{2}a^*_{od}Q_{od}^2 + \frac{1}{3}b_{od}Q_{od}^3 + \frac{1}{4}c_{od}Q_{od}^4 + \frac{1}{2}aq_1^2 + \frac{1}{3}bq_1^3 + \frac{1}{4}cq_1^4 + \lambda Q_{od}q_1 \quad \{5.1\}$$

where a^*_{od} , b_{od} , c_{od} , a , b , and c are the normal Landau coefficients for the expansion containing a cubic term and including fourth-order. The last term in this expansion results from bilinear coupling (Salje and Devarajan, 1986) between q_1 and Q_{od} which operates at the hexagonal-orthorhombic transition in cordierite, and λ is the coupling constant. This equation predicts the first-order behaviour and formation of a modulated phase during annealing of originally hexagonal Mg-cordierite (Salje, 1987a).

5.1.3 The Measurement of Q_{od} and Q Many of the recent experiments have given information concerning the various order parameters. In particular NMR has been successfully applied to annealed cordierite samples since the local environment of the Si atom varies with annealing time and this can be correlated with the number of Al-O-Al linkages (Putnis and Angel, 1985) which in turn is directly related to Q_{od} (Salje, 1987a). The structural order parameter Q can be directly linked to the distortion index, Δ .

In the hexagonal-orthorhombic transformation the (211) peak in the hexagonal structure splits into the (131), (421) and (511) peaks of the orthorhombic structure. The distortion index defined by Miyashiro (1957) is given by:

$$\Delta = 2\theta_{131} - \frac{2\theta_{511} + 2\theta_{421}}{2} \quad \{5.2\}.$$

It should therefore be possible to determine all necessary information regarding the structural distortion in cordierite by

careful measurement of the time dependent behaviour of the (211) hexagonal peak. Comparison of the time dependent behaviour of Q with that of Q_{od} should reveal the nature of coupling between Q and Q_{od} .

5.2 Experimental Investigation of Mg-Cordierite

All experiments were carried out on samples prepared from stoichiometric Mg-cordierite glass in the manner described by Putnis (1980). A suite of crystalline specimens was kindly provided by Dr A Putnis. These had been prepared by annealing the glass in air at temperatures of 1180°C, 1290°C and 1400°C: the details of treatments for each sample are given in Table 5.1. These run products were studied using synchrotron X-ray powder diffraction. The same samples had previously been characterised using T.E.M. and magic angle spinning N.M.R. by Putnis et al. (1985).

5.2.1 Synchrotron X-ray Powder Diffraction: Pure Mg-Cordierite

The cordierite samples weighing around 20 mg each were ground by hand in an agate mortar and loaded into quartz glass capillaries of 0.3 mm internal diameter. These capillary samples were mounted in Debye-Scherrer geometry on a purpose-built spinning goniometer head on the high-resolution Stoe 2-circle diffractometer at station 9.1 of the synchrotron radiation source, Daresbury, England. The spinning frequency was 5 Hz and the rotation axis of the samples was carefully aligned to coincide with the 2θ axis of the diffractometer by means of a fixed optical telescope.

Synchrotron radiation of peak energy 3.5 GeV was monochromated using a channel-cut Si (111) monochromator and

careful measurement of the time dependent behaviour of the (211) hexagonal peak. Comparison of the time dependent behaviour of Q with that of Q_{od} should reveal the nature of coupling between Q and Q_{od} :

5.2 Experimental Investigation of Mg-Cordierite

All experiments were carried out on samples prepared from stoichiometric Mg-cordierite glass in the manner described by Putnis (1980). A suite of crystalline specimens was kindly provided by Dr A Putnis. These had been prepared by annealing the glass in air at temperatures of 1180°C, 1290°C and 1400°C: the details of treatments for each sample are given in Table 5.1. These run products were studied using synchrotron X-ray powder diffraction. The same samples had previously been characterised using T.E.M. and magic angle spinning N.M.R. by Putnis et al. (1985).

5.2.1 Synchrotron X-ray Powder Diffraction: Pure Mg-Cordierite

The cordierite samples weighing around 20 mg each were ground by hand in an agate mortar and loaded into quartz glass capillaries of 0.3 mm internal diameter. These capillary samples were mounted in Debye-Scherrer geometry on a purpose-built spinning goniometer head on the high-resolution Stoe 2-circle diffractometer at station 9.1 of the synchrotron radiation source, Daresbury, England. The spinning frequency was 5 Hz and the rotation axis of the samples was carefully aligned to coincide with the 2θ axis of the diffractometer by means of a fixed optical telescope.

Synchrotron radiation of peak energy 3.5 GeV was monochromated using a channel-cut Si (111) monochromator and

careful measurement of the time dependent behaviour of the (211) hexagonal peak. Comparison of the time dependent behaviour of Q with that of Q_{od} should reveal the nature of coupling between Q and Q_{od} .

5.2 Experimental Investigation of Mg-Cordierite

All experiments were carried out on samples prepared from stoichiometric Mg-cordierite glass in the manner described by Putnis (1980). A suite of crystalline specimens was kindly provided by Dr A Putnis. These had been prepared by annealing the glass in air at temperatures of 1180°C, 1290°C and 1400°C: the details of treatments for each sample are given in Table 5.1. These run products were studied using synchrotron X-ray powder diffraction. The same samples had previously been characterised using T.E.M. and magic angle spinning N.M.R. by Putnis et al. (1985).

5.2.1 Synchrotron X-ray Powder Diffraction: Pure Mg-Cordierite

The cordierite samples weighing around 20 mg each were ground by hand in an agate mortar and loaded into quartz glass capillaries of 0.3 mm internal diameter. These capillary samples were mounted in Debye-Scherrer geometry on a purpose-built spinning goniometer head on the high-resolution Stoe 2-circle diffractometer at station 9.1 of the synchrotron radiation source, Daresbury, England. The spinning frequency was 5 Hz and the rotation axis of the samples was carefully aligned to coincide with the 2θ axis of the diffractometer by means of a fixed optical telescope.

Synchrotron radiation of peak energy 3.5 GeV was monochromated using a channel-cut Si (111) monochromator and

monochromatic radiation of 1.4725 \AA was used for all measurements. The second monochromator crystal was slightly tilted to avoid higher order scattering. The excellent mechanical stability of the instrument eliminated any significant errors in 2θ positions, but nonetheless high-purity Si was used as an internal standard. The positions of the Si lines were used to verify the wavelength calibration of the incident radiation. In addition the peak widths of the Si lines served as an indication of the instrumental peak profile in the configuration described.

The monitored primary intensity was 11400 cps (measured by flow counter) and was stable to within 0.2 percent during the course of the experiments (28 h). As line profile measurements rather than absolute intensity measurements were the purpose of this investigation, no absolute calibration of the intensity data was needed. An energy dispersive EG&G detector was employed with a small energy window to reduce background scattering. Since all measurements were wavelength dispersive no further use of the energy dispersive facility was made. The maximum level of background scattering when no sample was in place was found to be 50 cps with a vertical beam width of around 2 mm, scattering from the quartz capillary increased this to over 300 cps.

The angular resolution of the diffractometer was tested by scanning the (111) line of the internal Si standard. The long 2θ arm (specimen to detector distance = 650 mm) and high mechanical stability of the instrument at station 9.1 lead to a very good angular resolution, allowing attainment of line widths (FWHM) as small as $0.03^\circ 2\theta$ (also dependent on sample characteristics). This compares with a typical minimum FWHM of around $0.07^\circ 2\theta$ on standard two-circle X-ray powder diffractometers. The small

instrumental line width also means that the instrumental line function may, in many instances, reasonably be approximated as a delta-function (thus avoiding the need to consider instrumental convolution effects). These features make this powder diffractometer ideally suited for the study of relative changes in line profiles and peak broadening and splitting. In particular the experimental determination of small orthorhombic lattice distortions in cordierite requires the high-resolution diffraction data typically obtainable at a synchrotron source.

5.2.2 Results from Diffractometry Typical observed diffraction patterns of cordierite samples through the transition are shown in Figure 5.2. They clearly demonstrate the good angular resolution of the diffractometer and the excellent signal to noise ratio. It must further be emphasised that the very narrow profiles were encountered for all cordierite samples independent of their annealing temperature and times. These findings are in complete contrast to earlier reports on line broadening effects observed with standard Philips two-circle diffractometers (Putnis, 1980; Putnis and Bish, 1983).

The observed scattering profile of the (211) line of hexagonal cordierite (Figure 5.2a) is almost identical to the instrumental resolution function of the powder diffractometer at the Daresbury synchrotron source. This implies that the correlation length in cordierite is large, even for samples that have only just crystallised from glass after very short annealing times. The deconvoluted effective correlation lengths were calculated by assuming that the silicon standard linewidth corresponds to infinite correlation length (that is, all line broadening is due to instrumental linewidth) and then applying

Temp(°C) Time(min) Sample Δ Index

1400	15	135	
1400	30	136	
1400	60	137	
1400	165	138	0.224
1400	360	139	0.242
1400	3900	140	0.235
1280	60	022	
1280	120	019	
1280	282	018	0.228
1280	480	020	0.222
1280	1308	015	0.243
1280	2760	017	0.244
1280	10050	021	0.248
1280	28740	016	0.247
1180	135	012	
1180	240	009	
1180	480	013	
1180	1500	010	
1180	9750	011	0.242
1180	23100	014	0.248

Table 5.1 Cordierite samples investigated, and distortion indices of orthorhombic cordierites.

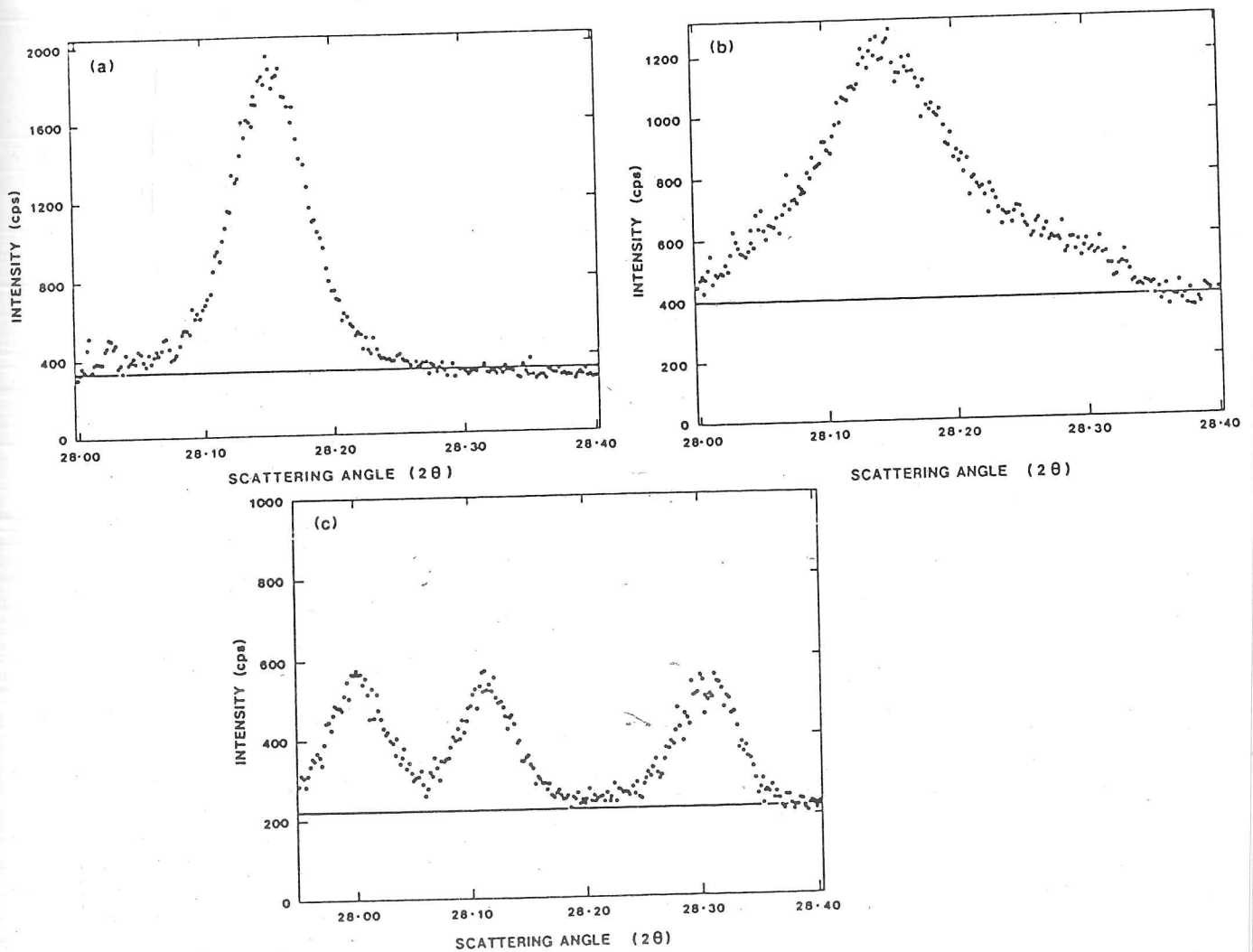


Figure 5.2 Synchrotron X-ray diffraction patterns over a narrow range of 2θ angles. (a) The 211 peak of hexagonal cordierite. (b) The 211 peak of modulated cordierite. (c) The 511, 421, and 131 peaks of orthorhombic cordierite.

the corrections given by Arora and Umadevi (1982) to the measured linewidths. The deconvoluted effective correlation lengths for hexagonal cordierites just crystallised from glass are always greater than 300 Å.

In cordierite that has been annealed for sufficiently long times a new feature is observed. The spectrum shown in Figure 5.2b shows the sharp (211) peak of the hexagonal phase superposed by a broad scattering profile which is almost symmetric about the hexagonal peak. The scattering angles are different from those of the orthorhombic form (Figure 5.2c) and cannot be confused with a partial transformation of hexagonal cordierite into orthorhombic cordierite. The line profile is identical to that expected from satellite reflections arising from a modulated structure. This "side intensity" may be interpreted in one of two ways. It could arise from a range of modulation wavevectors without a unique length, but varying continuously from very low values (below the resolution of this experiment) to a maximum value of around $4.0 \times 10^{-3} \text{ \AA}^{-1}$ (corresponding to 0.175° in 2θ space). The corresponding minimum wavelength of the modulation is 250 Å. Alternatively in a recent neutron HRPD study of the same samples carried out by Dove et al. (1989), the side intensity of Figure 5.2b due to structural modulation has been explained in terms of the predicted positions of twelve satellite reflections arising from a modulation of single wavelength 385 ± 35 Å. Either interpretation is possible: it is not possible to sensibly differentiate between these two scenarios in the light of the evidence from existing scattering experiments alone and attempts to measure satellite intensities by TEM have proved unsuccessful. The number of free parameters for a fit of so many

satellite reflections, which may themselves be composite, to one peak profile from powder diffraction is too great to allow a unique conclusion to be drawn. In either case it is apparent that the structural transformation between hexagonal and orthorhombic cordierite is precursored by an intermediate structural state different from either. The line profiles of X-ray diffraction strongly suggest a well-defined structural state characterised by a hexagonal matrix with lower-symmetry modulations.

The Δ index for each of the annealed orthorhombic samples was calculated according to equation 5.2 and is given in Table 5.1. Although the Δ index defined by equation 5.2 assumes $\text{CuK}\alpha_1$ radiation and is dependent on the wavelength of X-rays employed, the small difference in wavelength between $\text{CuK}\alpha_1$ radiation and the radiation selected at Daresbury does not significantly alter the Δ index values. The difference in wavelengths leads to a difference in $\Delta 2\theta$ of 0.02° at $28.2^\circ 2\theta$. The orthorhombic phase appears abruptly as three peaks (131, 511 and 421) in place of the hexagonal 211 peak. The annealing time over which the modulated structure and the orthorhombic structure coexist is very short compared to the time scale of Al/Si ordering at these temperatures. The orthorhombic phase appears with an almost fully distorted structure and with a distortion index close to that of the final equilibrium state. The distortion index from these measurements has a maximum value of 0.25, whereas orthorhombic cordierites with shortest annealing times give a minimum Δ index value of 0.22. The distortion index does not, therefore, change continuously with time and the previous data of Putnis (1980) were presumably of insufficient resolution. The

large discontinuity in Δ index occurs at all three annealing temperatures, in each case suggesting a nucleation and growth mechanism for the formation of orthorhombic cordierite from the modulated structure.

5.3 Coupling Between Q and Al/Si Ordering

We can see from the synchrotron data that the hexagonal-modulated-orthorhombic transition in cordierite leads to a structural distortion, and this may be used as one measure of the transition: the order parameter Q . At the same time the process of annealing and transformation leads to increased ordering of Al and Si on the tetrahedral sites of the framework. The degree of Al/Si order for each of the samples has been determined by ^{29}Si magic-angle spinning NMR (Putnis and Angel, 1985; Putnis et al., 1987) which enables the evaluation of the number of Al-O-Al bonds per formula unit (N). For total statistical disorder Putnis and Angel (1985) showed that $N = 3.3$. This corresponds to totally disordered hexagonal cordierite with $Q_{\text{od}} = 0$. The hexagonal cordierites described here are shown (Putnis et al., 1987) to have less than half that number of Al-O-Al bonds, and are therefore already substantially ordered. Q_{od} is normalized to 1 for complete order and 0 for complete disorder; it has been related to N by Salje (1987a), who gives the order parameter as:

$$Q_{\text{od}} = \langle 1 - (N/3.3) \rangle^{\frac{1}{2}} \quad \{5.3\}.$$

The lattice distortion is defined by the order parameter Q which is determined by the spontaneous strain (chapter 1). The distortion of the cordierite structure is described by two strain parameters e_1 (which corresponds to an orthorhombic distortion)

and e_2 (which corresponds to a monoclinic distortion); we shall assume $e_2=0$ in the orthorhombic phase (Salje, 1987a). The line splitting between the (131), (421) and (511) reflections is proportional to the structural deformation along the a and b axes of the orthorhombic phase. The hexagonal unit cell can be described by equivalent orthorhombic axes with $a_0 = \sqrt{3}b_0$, and $\gamma = 90^\circ$. If the orthorhombic lattice parameters in the true orthorhombic annealed specimens are a and b then the strain e_1 must be expressed with respect to the super-symmetry hexagonal structure. These para-phase lattice parameters (denoted by subscript 0) are related to the distorted cell parameters by $b_0 = a_0/\sqrt{3} \approx \frac{1}{2}b + \frac{1}{2}a/\sqrt{3}$ so the spontaneous strain can be expressed in terms of the orthorhombic lattice parameters alone:

$$e_s = \frac{ab - \frac{a^2}{\sqrt{3}}}{ab + \frac{a^2}{\sqrt{3}}} \quad \{5.4\}.$$

The spontaneous strain is proportional to the splitting of the powder lines and is therefore also proportional to the distortion index Δ . Thus the Δ index, normalized to 1 for $\Delta = 0.25$ (the maximum distortion) may be used as the order parameter Q. The distortion index is also convenient to use as the order parameter Q because it is a familiar parameter in the cordierite literature.

In thermodynamic equilibrium, cordierite can be expected to transform between the hexagonal and orthorhombic forms via uniquely defined paths of Q and Q_{od} . There should be a relation between both order parameters. We must now address the question of how far the order parameter Q_{od} and Q reflect each other in the kinetic experiment described here. To what extent is Al/Si ordering, described by Q_{od} , involved in the structural distortion

described by Q ? Does one or other of the order parameters drive the phase transition uniquely, or are they coupled directly? In order to answer these questions we must investigate the correlation between Q and Q_{od} for all the structural states represented in the suite of samples. For each annealing time and temperature the order parameters Q , determined from the synchrotron measurements, and Q_{od} determined from NMR are plotted on an order parameter vector diagram for the transition (Figure 5.3).

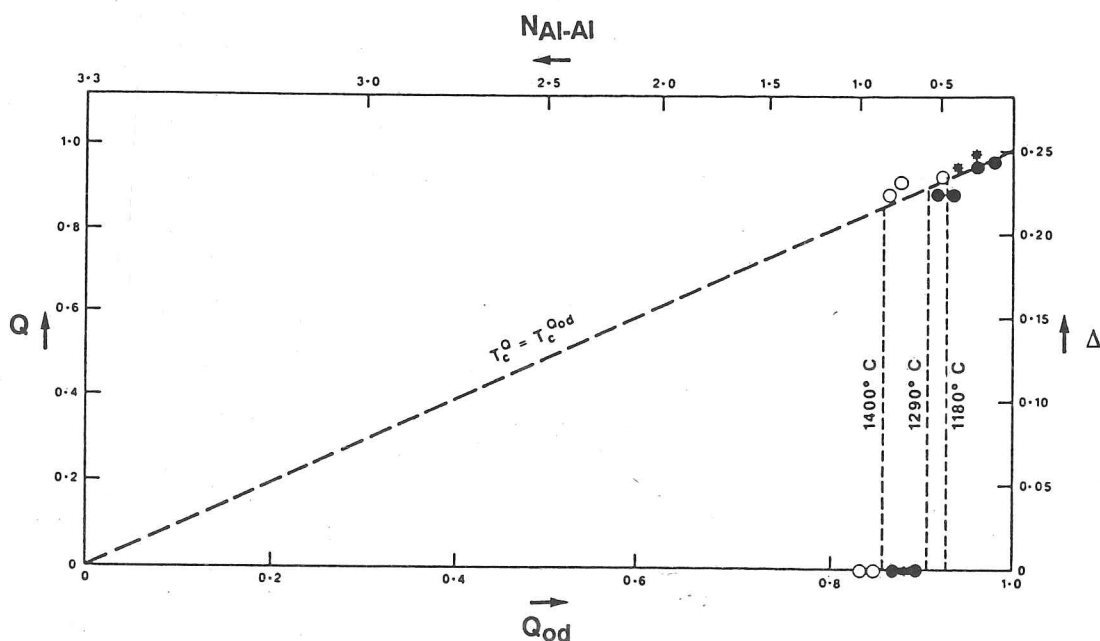


Figure 5.3 The experimentally determined variation of the order parameter Q , defined by the Δ index from X-ray diffraction, plotted against the order parameter Q_{od} , defined by the number of Al-O-Al bonds (from NMR data of Putnis et al., 1987) during the annealing sequence. Open circles represent samples annealed at $1400^\circ C$, filled circles correspond to $1290^\circ C$, stars represent samples annealed at $1180^\circ C$. The short dashed lines show the discontinuities in Q (and Δ) on transition from modulated to orthorhombic cordierite. The long dashed line shows the theoretical behaviour of Q and Q_{od} if the transition was a bilinearly coupled process with identical critical temperatures for Al/Si ordering and framework distortion (Salje, 1987a).

Salje (1987a) showed that if Q_{od} is the driving order parameter and Q is coupled linearly then all data points describing the structural states of cordierites should lie on the dashed straight line. In this case the critical temperature at which cordierite is expected to fully disorder (T_C^{od}) and the extrapolated critical temperature at which the orthorhombic phase would transform to hexagonal (if there were no intervention of a modulated state, or melting and so forth) should be identical. The results from the X-ray diffraction experiments clearly show, however, that although this linear relation holds within experimental error for all samples with orthorhombic symmetry it is broken by the abrupt transformation of the orthorhombic form into modulated cordierite (with decreasing Q_{od}). The strongly first-order transformation between the orthorhombic phase and the modulated phase is not equivalent to the theoretical phase transition between an orthorhombic phase and a totally disordered hexagonal phase with $Q_{od} = 0$ and $Q = 0$.

The structural phase transition between modulated and orthorhombic cordierite is characterised by a spontaneous increase in Q . The order parameter Q_{od} , on the other hand, does not reveal any singularity at the phase transition point. Both order parameters Q and Q_{od} show a strong correlation in the orthorhombic phase where they follow exactly the predictions of Landau theory with bilinear coupling. The phase transition appears to be triggered by a critical value of Q_{od} which is in turn dependent on the particular annealing temperature. The temperature dependence of the critical value of Q_{od} can be attributed to the temperature dependence of the elastic constants (Salje, 1987a) and thus the temperature dependence of the

critical strain energy needed for the orthorhombic distortion. The stepwise behaviour of Q does not imply a stepwise behaviour of Q_{od} , which changes continuously from hexagonal, through modulated, to orthorhombic cordierite.

5.4 The Influence of Potassium

Natural cordierites invariably accommodate additional elements within the structure (for a recent summary see Schreyer, 1985). In most cases H_2O molecules are present in the large channels which run parallel to the z axis, which often contain sodium and occasionally potassium. For this reason it was decided to investigate the influence of the presence of potassium on the structural phase transition in Mg-cordierite. The results of a study of the hexagonal-orthorhombic phase transition in a synthetic cordierite of the composition $K_{0.2}Mg_2[Al_{4.2}Si_{4.8}O_{18}]$ are presented. The addition of potassium directly affects the Al/Si ordering behaviour, since the substitution of $K+Al$ for $\square+Si$ which operates here necessarily alters the Al:Si ratio from that in pure Mg-cordierite. The phase transition is triggered by a critical degree of Al/Si order (Q_{od}) which causes a sudden distortion of the structure and breaks the hexagonal symmetry leading to the orthorhombic structure. Additional effects may be introduced by local strains due to the incorporation of potassium. The local stress field associated with such a point defect (in this case a potassium atom in a channel) may act as the conjugate field to Q and alter the phase transition behaviour and character.

Using the techniques and theory developed to describe the transition behaviour of pure Mg-cordierite (as detailed above)

let us now address the influence of additional channel-filling potassium (and hence changed Al:Si ratio) on the transition. Both orthorhombic long-range distortions and the local distortions of the structure have been studied as a function of annealing time in a suite of K-bearing Mg-cordierites (by synchrotron X-ray powder diffraction and hard-mode infrared spectroscopy respectively).

5.4.1 X-ray Diffraction Experiments The samples used for this study were synthesised at the Institute of Mineralogy at the Ruhr University, Bochum and kindly provided by W Schreyer. The samples were prepared from cordierite glass of the given stoichiometric composition according to the method described by Wolfsdorff (1983). A suite of crystalline specimens was obtained by annealing the glass in air at 1290°C for varying times before quenching. Samples annealed for 15 min, 30 min, 1 hr, 2 hr 6 min, 4 hr 42 min, 10 hr, 20 hr, and 46 hr 48 min were selected for infrared and synchrotron X-ray investigation.

Sample preparation was identical to that described in 5.2.1 and powder diffraction patterns were again collected at station 9.1 of the synchrotron radiation source, Daresbury with the diffractometer operating in identical geometry. Again the quartz capillary samples were rotated in the beam at the axis of the instrument and at the same frequency. The only experimental differences between data collection on the potassium-bearing samples and measurements of pure Mg-cordierite were that for the experiments on K-bearing cordierite the monochromator crystal was He-cooled and set to obtain radiation of wavelength 1.5406 Å. The incident beam flux was higher due to the incorporation of a new wiggler magnet directly before beamline 9 at the synchrotron

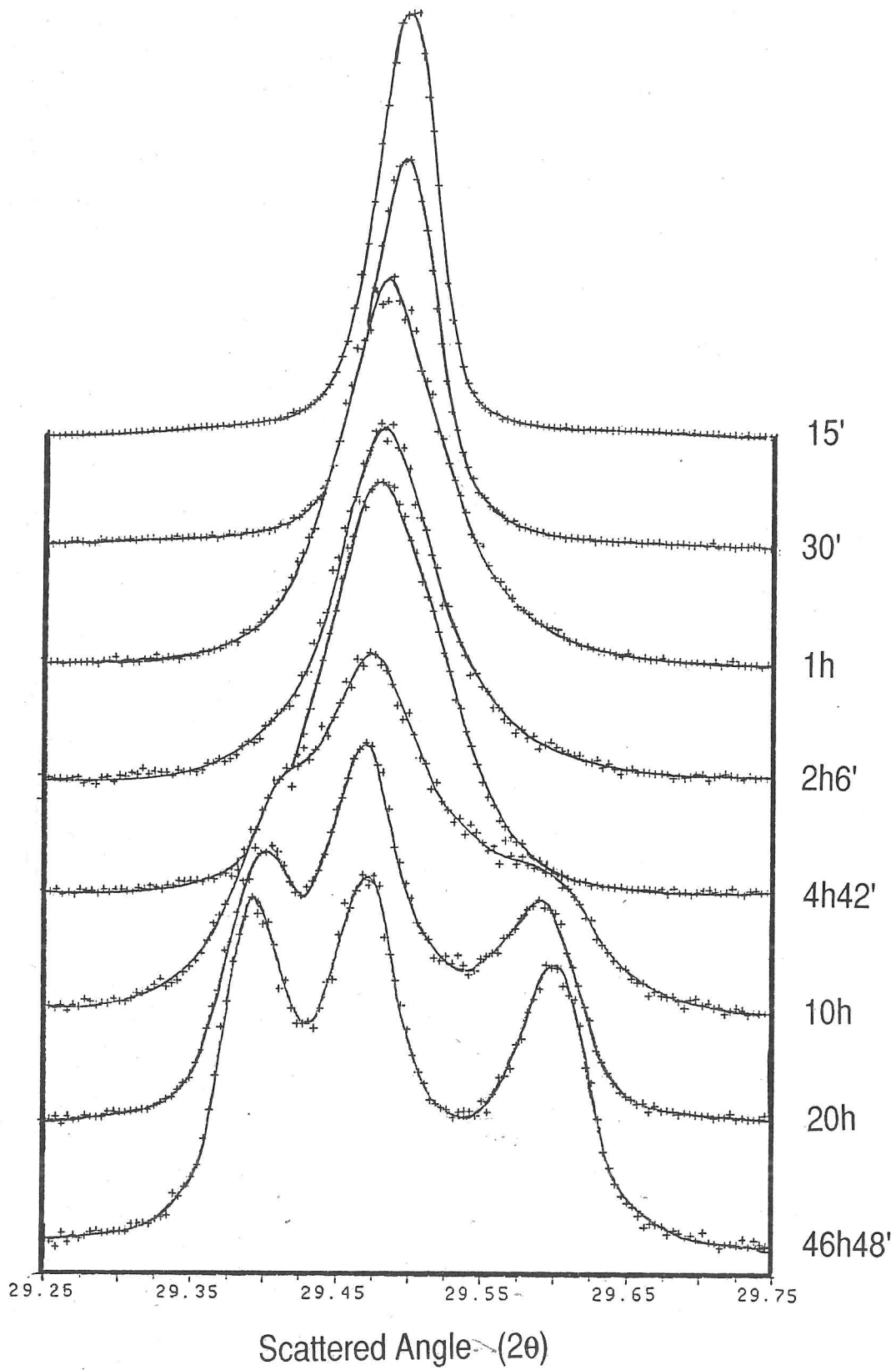


Figure 5.4 Synchrotron X-ray diffraction profiles of the suite of K-bearing Mg-cordierites showing the splitting of the 211 hexagonal peak (top) to the 511, 421 and 131 peaks of the orthorhombic phase.

source. In addition since there was no need for energy-dispersive measurement, a scintillation counter was employed as the detector. These additional measures improved the signal at the detector and the counting statistics. Diffraction experiments were performed at room temperature over a range of 29.25 to $29.75^\circ 2\theta$ by step scan with a step size of $0.002^\circ 2\theta$ and a counting time of 5 seconds per step.

The measurements of hexagonal K-bearing cordierite yielded a 211 peak which was fitted with a Gaussian profile to 95% accuracy (using the diffraction data handling package 'GENIE' developed at Rutherford Appleton Laboratories). The higher incident beam flux obtainable with a cooled monochromator crystal leads to improved signal-to-background ratio, as can be seen from the experimental results (Figure 5.4).

5.4.2 Hard-mode Infrared Measurements Infrared spectra of the powdered cordierite samples were obtained using a standard KBr pellet technique. All samples were prepared in a similar fashion: dried for 24 hours at 100°C before being milled for 30 minutes in a Spex micromill and mixed in the same mill (without the grinding balls) for 30 minutes with similarly dried KBr in a ratio of 1:300 sample to KBr. Each pellet weighed 200 mg and was pressed under vacuum in a polished die to give optically transparent pellets. Great care was taken to ensure, as nearly as possible, identical conditions for the preparation of each sample pellet.

The spectra were recorded at room temperature under vacuum on a Bruker 113v Fourier-transform infrared spectrometer. Spectra were measured in transmission in the range 1400 to 400 cm^{-1} and in each case were calculated from 512 sample scans

at a resolution of 2 cm^{-1} using an Aspect 3000 computer. Band-profile analysis was carried out on the same computer, fitting Voigt profiles to the measured spectra by least-squares refinement. The maximum R-factor of the fitting procedure was 0.03% giving errors of $\pm 0.2 \text{ cm}^{-1}$ in the linewidths (FWHM) and around 10% for the computed integrated intensities. The absolute frequency of the absorption bands was obtained to a similar accuracy of $\pm 0.2 \text{ cm}^{-1}$.

The use of hard-mode infrared spectroscopy (HMIS) in this study follows the same approach as that of Güttler et al. (1989). In this method the absolute values of absorption frequency are dependent upon sample characteristics, but the structural effects of the phase transition are characterised by relative changes in band frequencies, intensities and half-widths.

5.4.3 Strain Behaviour from Diffractometry In section 5.3 we related the index, Δ , directly to Q for the case of pure Mg-cordierite and found that in this case $Q \approx 4\Delta$ for Δ measured with Cu radiation. Using the same approach for the investigation of the K-bearing samples described here, the macroscopic strain behaviour of K-bearing cordierites is obtained by careful measurement of the evolution of the (211) hexagonal peak through the suite of annealed samples.

The observed diffraction patterns between 29.25 and $29.75^\circ 2\theta$ are shown in Figure 5.4. At the shortest annealing time the hexagonal (211) peak is sharp and intense (peak intensity of 25000 cps) and near-Gaussian (by least squares fit to Voigt profile). With longer annealing, the (211) peak becomes noticeably and significantly broadened. This broadening corresponds to the development of a modulated phase, analogous

with that observed in pure Mg-cordierite. The width of the (211) peak corresponding to the modulated phase remains constant upon further annealing.

The modulated phase appears as a precursor to the orthorhombic structure of K-bearing Mg-cordierite during the course of a kinetic experiment. The orthorhombic phase is identified in the X-ray scattering experiments here by the three distinct peaks which are apparent in samples annealed for 10 h or more (Figure 5.4). As has been seen in pure Mg-cordierite when the orthorhombic phase first appears it is already almost totally distorted with respect to the hexagonal cell. The orthorhombic cordierite obtained at the longest annealing time is not much more distorted. The distortion index in K-bearing cordierites does not change continuously with annealing, but undergoes a sudden discontinuity from zero to 0.155 on the transformation from modulated to orthorhombic cordierite (as observed on the length scale of X-ray experiments). Since the transition from modulated to orthorhombic is first-order we expect a limited regime of coexistence of phases. This is observed in the spectra of the sample annealed for 10 hours shown in Figure 5.4.

The distortion indices of the K-bearing cordierites measured here show a maximum value of $\Delta = 0.17$. This is significantly less than the maximum distortion index measured in pure Mg-cordierite of 0.25 (section 5.3, above). The minimum non-zero value of the distortion index measured in this suite of samples is 0.155 whereas it is 0.22 in Mg-cordierite. The measured Δ indices for the three orthorhombic K-bearing cordierites studied are 0.155 (10 hours), 0.16 (20 hours), and 0.17 (46 hours 48 minutes). Hence the structural distortion in K-bearing

cordierites is always less than in orthorhombic pure Mg-cordierite samples. The behaviour, however, follows the same trends in both sets of samples. In K-bearing cordierite the distortion index changes discontinuously at some annealing time between 4 and 10 hours. The large discontinuity in distortion index suggests a nucleation and growth mechanism for the formation of orthorhombic K-bearing cordierite from the modulated phase, as in pure Mg-cordierite.

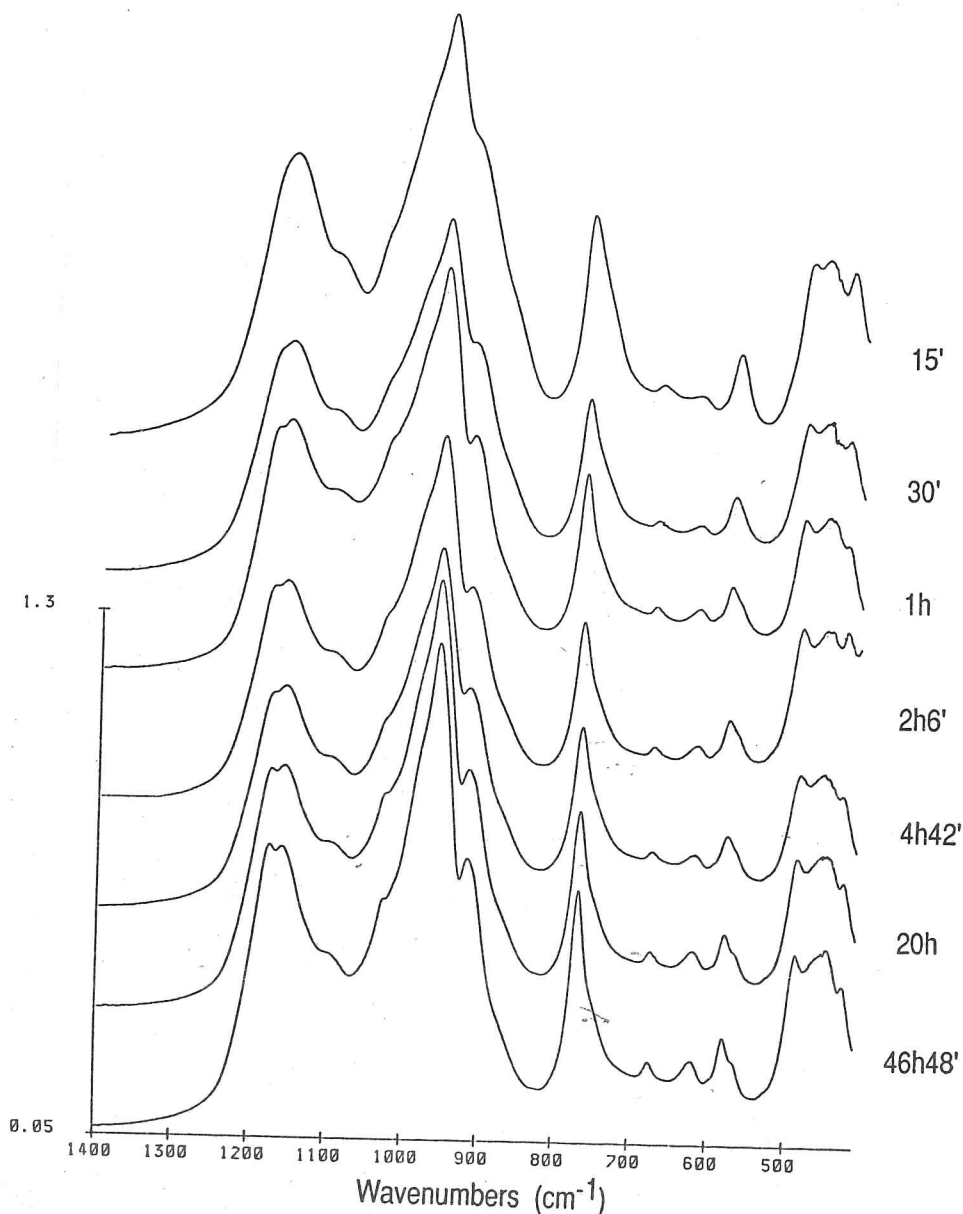


Figure 5.5 Infrared spectra of annealed synthetic K-bearing cordierites.

5.4.4 Results from Hard-mode Infrared Spectroscopy Infrared spectra of the suite of annealed K-bearing Mg-cordierites are shown in Figure 5.5. Additional bands appear with increasing annealing time, among others they include one on the high-energy side of the 580 cm^{-1} mode. The results from line profile analysis of this band are shown in Figure 5.6. The fit shown represents the best agreement with the measured data by

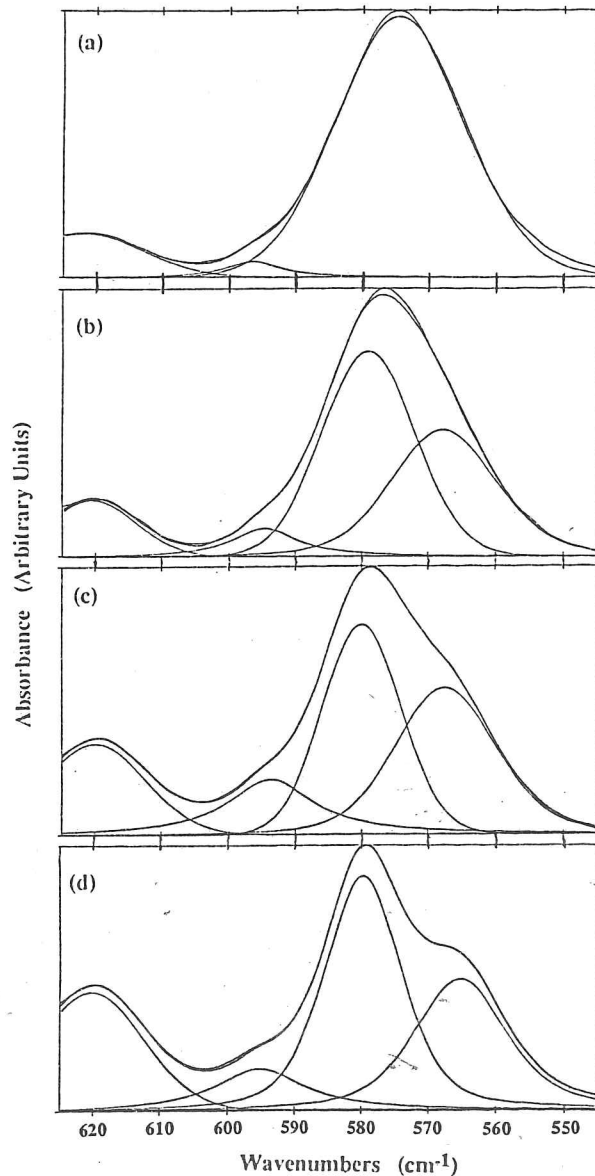


Figure 5.6 Results of absorption-band profile analysis of K-bearing cordierites crystallised from glass and annealed for (a) 15 min, (b) 30 min, (c) 1 hour, and (d) 46 hours 48 min.

simulation using the minimum necessary component bands. The fit of all spectra was identical, in the case where the mode intensity of the band near 566 cm^{-1} could be fitted as zero it was omitted from the spectrum fit. Splitting of the 580 cm^{-1} mode is clearly seen in samples annealed for longer than 15 min. This splitting results directly from changing selection rules on the structural phase transition from the high symmetry $P6/mcc$ hexagonal phase to a phase with orthorhombic symmetry (space group $Ccmm$). No further splitting or additional bands are observed with longer annealing. These results are in essential agreement with the results of earlier studies by Langer and Schreyer (1969) and Güttler et al. (1989).

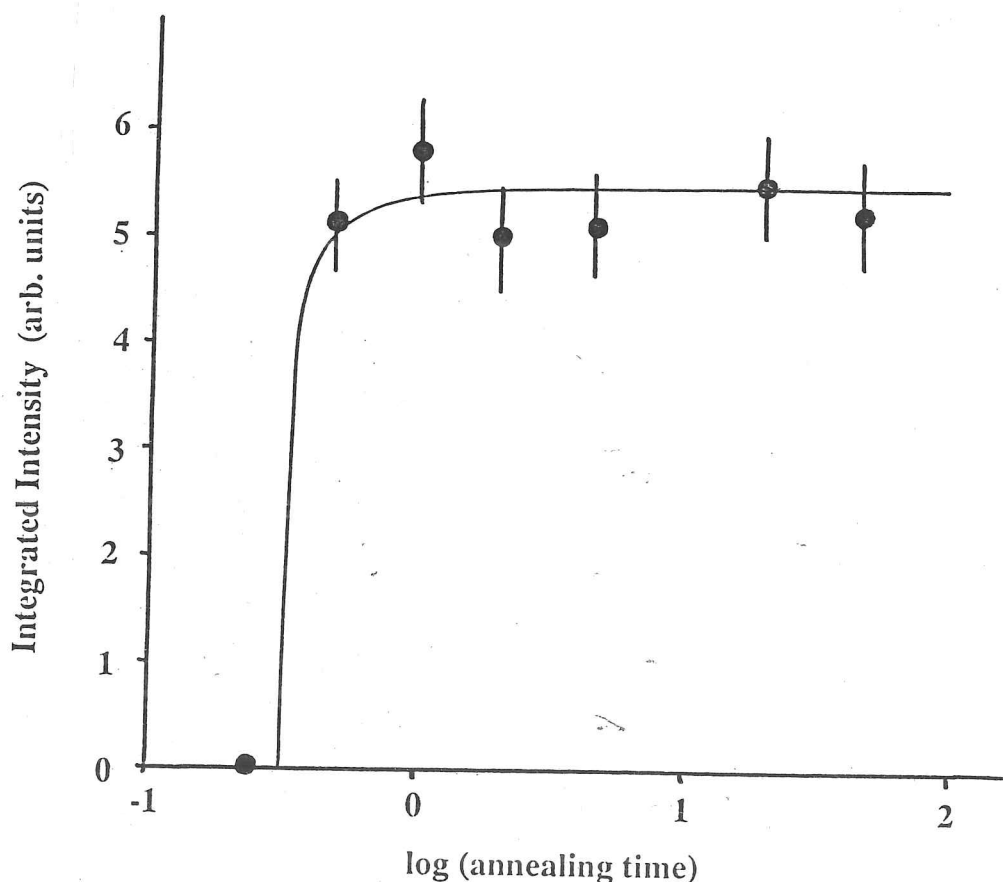


Figure 5.7 Time evolution of the integrated intensity of the infrared mode near 566 cm^{-1} in K-bearing cordierite.

The intensity of the additional side band at 566 cm^{-1} is shown as a function of annealing time in Figure 5.7. We see a stepwise increase in intensity of this band, which does not change after 30 min. Thus, the hexagonal K-cordierite must have changed before this time to the modulated state with orthorhombic symmetry on the length scale probed by the 580 cm^{-1} mode. We have already seen that on the length scale probed by X-ray diffraction the samples at these shorter annealing times (up to 4 hours) appear hexagonal or modulated. In this respect the behaviour of this suite of samples is identical to that observed for pure Mg-cordierite (Güttler et al., 1989). The stepwise transition from hexagonal to modulated cordierite (at the same local length scale) is underlined by the behaviour of the peak frequency of the 770 cm^{-1} band, shown in Figure 5.8.

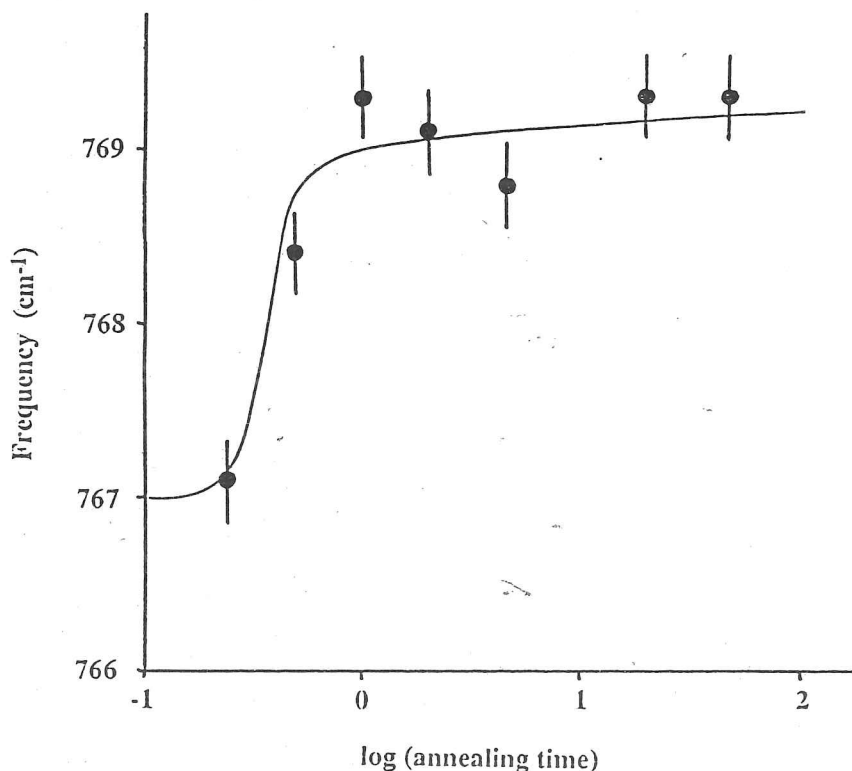


Figure 5.8 Frequency shift of the infrared mode near 770 cm^{-1} shown as a function of \log (annealing time) for the suit of K-bearing cordierites.

5.4.5 Potassium as a Defect Stress Field The Landau model for free energy of Mg-cordierite (section 5.1.2) describes the stability of the orthorhombic form of cordierite in terms of the degree of Al/Si order on the tetrahedral sites (Q_{od}), the distortion of the lattice away from hexagonal symmetry (the spontaneous strain and Q). The model may be extended to take account of the influence of channel-filling cations such as potassium. All of these structural features influence one another and couple to each other through the strain that arises in the structure as the lattice relaxes in response to them, and they may all be incorporated into one expression for the excess free energy of the orthorhombic phase with respect to the hexagonal phase.

The experimental results presented in this section indicate that the structural states of the potassium-bearing samples are essentially the same as in pure Mg-cordierite (in particular the order parameters Q_{od} and Q are non-linearly coupled in modulated and hexagonal cordierites, and the Δ index changes discontinuously). The two essential differences are: firstly, that the highest degree of Al/Si order is lower than in the K-free material (that is, the maximum value of Q_{od} is less than unity) and, secondly, that the maximum spontaneous strain is also reduced from a distortion index of 0.25 to 0.17. There are experimental indications that phase mixtures of coexisting cordierites occur over limited periods of annealing time. The 10-hour sample shows modulated and orthorhombic cordierite in coexistence, and the peak intensities of the diffraction pattern of the 20-hour sample may also be interpreted in terms of a similar phase mixture. It should be borne in mind, however, that

inhomogeneity in K-distribution and grain size would also lead to line broadening which could account for the diffraction profile of the 20 hour sample. Whatever the extent of coexistence actually is, the results seem to imply that the effect of doping with potassium cannot simply be described as local defect perturbations of the cordierite lattice, as in the Ornstein-Zernicke formalism (Levanyuk et al., 1979; Salje, 1988; Strukov et al., 1980; Salje, 1987a). Rather, it appears that the defect concentration is sufficiently high that the combined local stress fields of all the individual potassium atoms act as an effectively homogeneous field (rather than a purely local field). This is convenient since this homogeneous stress field due to the potassium defects may then be treated in the Landau formalism of cordierite as a simple homogeneous field, conjugate to the order parameter. In this case the Landau potential of equation 5.1 is re-written as (Redfern et al., 1989a):

$$\Delta G(Q_{od}, q_1) = \frac{1}{2}a_{od}^* Q_{od}^2 + \frac{1}{3}b_{od} Q_{od}^3 + \frac{1}{4}c_{od} Q_{od}^4 + \frac{1}{2}a q_1^2 + \frac{1}{3}b q_1^3 + \frac{1}{4}c q_1^4 + \lambda Q_{od} q_1 + H Q_{od} + h q_1 + \frac{1}{2}g_{od} (\nabla Q_{od})^2 + \frac{1}{2}g (\nabla q_1)^2 \quad \{5.5\}.$$

The last four terms represent the proposed coupling with the conjugate fields H (conjugate to Q_{od}) and h (conjugate to q_1) due to incorporation of potassium, and the fluctuational Ginzburg terms (arising from the gradient energy of the order parameters). The relative stabilities, microstructures, and kinetic behaviour of cordierite depend on the magnitude and spatial homogeneity of H and h. In particular, in the treatment presented here H and h are assumed (as a first approximation) to be homogeneous fields opposing Q_{od} and q_1 (hence the addition of potassium results in

reduced Al/Si order and Δ index in the orthorhombic phase, compared to those values observed in pure Mg-cordierite). In other words the addition of potassium hinders the development of the orthorhombic phase during an annealing experiment. Comparing the diffraction data of the pure Mg-cordierite 1280°C samples with that of the 1290°C K-bearing suite, it is apparent that the K-bearing sample annealed for 4.7 hours is modulated whereas the pure Mg-cordierite sample annealed for the same time has an orthorhombic distortion index of 0.228. Indeed, spatial variation of the conjugate stress fields associated with potassium defects can lead to relative stabilisation of the modulated form, as has been pointed out by Michel (1984). The interval of annealing times over which modulated cordierite is found is expected to increase for K-bearing samples with respect to pure Mg-cordierite (Salje, 1987a). In addition the equilibrium transition temperature of potassium-bearing cordierite can be expected to be lowered if H and h oppose Q_{od} and q_1 . Quantitative assessment of the kinetic behaviour requires the experimental determination of H and h . Indirect evidence for the strength of H has still to be obtained from NMR spectroscopy which could be used to determine the maximum degree of Al/Si order in K-bearing cordierite, allowing the calculation of H in the limit of homogeneous fields. It is, nonetheless, apparent that the introduction of defects such as potassium within the cordierite structure is a very significant influence on the stability and kinetic behaviour of cordierite. This is a general feature of those elastic phase transitions in which the defect stress field acts as the conjugate field to the order parameter.

5.5 Synopsis and Conclusions

The application of high-resolution synchrotron X-ray powder diffractometry to the problem of the hexagonal-orthorhombic transition in cordierite reveals the weaknesses and faults of past interpretation. In particular these new studies of the distortion index in cordierite have revealed that Δ is not a sensible measure of the degree of Al/Si order, except in the orthorhombic phase (where, in any case, it hardly changes at all) since coupling between Q and Q_{od} is highly non-linear during most of the ordering process. It seems that at the hexagonal-orthorhombic transition in cordierite the alumino-silicate framework distortion is not the driving order parameter of the transition, but is a structural feature triggered by some critical degree of Q_{od} . In this sense the nature of the order parameter coupling in cordierite appears quite different from coupling in the plagioclase feldspars.

The rôle of additional potassium has been considered in terms of a 'defect' stress field, and in fact the potassium incorporated into the structure has been seen to act as an effectively homogeneous stress on the lattice, opposing the transition to orthorhombic symmetry. The transition behaviour, studied by X-ray diffraction and hard-mode infrared spectroscopy, appears exactly analagous to that of pure Mg-cordierite in that orthorhombic cordierite evolves from hexagonal via a stepwise transition from the modulated structure. The concept of the conjugate field to Q and Q_{od} has been introduced to explain the observations within the framework of Landau theory. This potassium-induced field reduces the maximum attainable orthorhombic distortion, Δ , and stabilises (to some unspecified

extent) the modulated structure.

We see that Landau theory may be applied to the study of time-dependent transition phenomena and kinetic experiments by the assumption that equilibrium is approached, as a function of time, via a continuous sequence of metastable states, which may themselves be treated as equilibrium states corresponding to higher temperatures. Thus the Landau potential may be used to shed light on kinetically driven processes, since the gradient of the potential is the driving force for the transformation. This approach has recently been investigated theoretically by Salje (1989), who shows that such an extension of Landau theory leads to the formulation of well known kinetic rate laws.

CO-ELASTICITY AND ORIENTATIONAL DISORDER IN THE CALCITE STRUCTURE6.1 Introduction

It would be rather limiting if the applications of Landau theory in mineralogy were restricted to cationic site ordering processes in framework silicates. Although these materials do comprise a very significant part of the Earth's crust, several interesting and important transition phenomena occur in other mineral systems and for this reason it would be instructive to apply the concepts discussed in the preceding chapters to a problem outside the realm of framework silicates. One such problem is the nature and thermodynamic influence of the orientational order/disorder transition which occurs at high temperature in the calcite structure. We shall see that this phase transition has significant implications for the form of the calcite/aragonite phase equilibrium boundary, and also that its strong co-elastic character enables the study of saturation phenomena as the mineral approaches absolute zero. The orientational order/disorder transition occurs not only in calcite (CaCO_3) but also in sodium nitrate (NaNO_3), an isostructural material. The orientational order/disorder phase transition in calcite occurs at around 980°C which is above the decarbonation temperature at atmospheric CO_2 pressures, and the study of this transition is not without practical difficulties. In contrast, the orientational order/disorder transition in NaNO_3 occurs at the more manageable temperature of around 280°C . For this reason, NaNO_3 is used as a model analogue compound in the study of this phase transition and in this chapter we shall

investigate the spontaneous strain behaviour at low temperatures below the phase transition in NaNO_3 in order to explore the basic character of the transition. Following this, we shall investigate the thermodynamic influence of the analagous transition in CaCO_3 by direct measurement of the excess enthalpy of ordering in calcite at high temperatures through the transition.

6.1.1 Orientational Order/Disorder in Sodium Nitrate The structural phase transition in NaNO_3 at 549 K was first observed by Kracek (1931) and attributed to some manner of rotation of the NO_3 groups around the 3-fold axis (Kracek et al., 1931). Since that time considerable effort has been expended trying to characterise the nature of the transition utilising numerous techniques, including vibrational spectroscopy (Brehat and Wynke, 1985), specific heat measurements (Reinsborough and Wetmore, 1957), and X-ray and neutron diffraction (Strømme, 1969; Paul and Pryor, 1972; Terauchi and Yamada, 1972). General agreement still prevails that the transition involves different states of orientational ordering of the NO_3 groups.

The low-temperature form of NaNO_3 is isostructural with calcite (space group $R\bar{3}c$), and the primitive unit cell is an acute rhombohedron containing two NaNO_3 formula units (Figure 6.1). At room temperature, NO_3 groups in adjacent layers are related by 180° rotation around the 3-fold axis, and so the relevant pair correlation is perfectly antiparallel. Based on diffraction evidence (Strømme, 1969; Paul and Pryor, 1972; Terauchi and Yamada, 1972), the space group of the high-temperature form is $R\bar{3}m$, with a primitive rhombohedral cell containing one formula unit of NaNO_3 . In the hexagonal

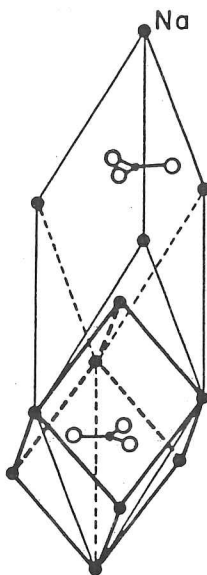


Figure 6.1 The rhombohedral cell of NaNO_3 (isostructural with CaCO_3). Closed circles indicate Na positions (Ca in calcite). The heavy outline shows the high-temperature $R\bar{3}m$ unit cell.

description used throughout this chapter, the unit cell of the high-temperature form is halved in length along the c-axis.

Several authors suggested that in the high-temperature phase NO_3 groups are randomly distributed between the two low-temperature orientations (for example, Paul and Pryor, 1972; Terauchi and Yamada, 1972). The precise structure of the high-temperature phase was not established however. Although it seemed clear that the perfectly antiparallel pair correlation is lost in the transition, the details remained obscure. Moreover, the years of intensive research failed to determine whether the transition was continuous or discontinuous until the experiments of Reeder et al. (1988) and other related studies attempted to determine a consistent set of critical exponents associated with the transition.

In section 6.2 the results of low-temperature X-ray diffraction experiments are reported and the magnitude and

temperature dependence of the spontaneous strain below room temperature are determined. The coupling of strain with the macroscopic order parameter is discussed. Related results of optical birefringence (Poon and Salje, 1988), specific heat measurements (Wruck and Salje, 1987), hard-mode Raman spectroscopy (Poon, 1988), high-temperature lattice parameter measurements (Reeder et al., 1988), and X-ray critical and diffuse scattering (Schmahl, 1988) for the same material are reported elsewhere.

6.1.2 Orientational Order/Disorder in Calcite The initial interest in NaNO_3 stemmed from its isostructural relationship to CaCO_3 . The temperature- and pressure- dependent behaviour of CaCO_3 is of fundamental geological and chemical significance, involving as it does several intriguing polymorphic phase transitions as well as the much studied calcite/aragonite phase boundary. Attention has focussed on the slope of this phase boundary which Johannes and Puhan (1971) found to be continuously varying with a significant change in slope between the low-temperature low-pressure part and the high-temperature high-pressure regime. Previous work has attempted to explain this change in slope by invoking a possible phase transition within calcite which could lead to the required changes in thermodynamic parameters.

The first indications of the existence of such a high-temperature phase transition came from Boeke (1912) who noticed changes in the heating and cooling curves of calcite at 975°C . This anomaly was confirmed by Eitel (1923) and further investigated by Cohen and Klement (1973) whose careful DTA work placed the transition near 985°C at atmospheric pressure,

increasing to around 1000°C at 5 kbar. This is undoubtedly the same transition as Chang (1965) observed by X-ray diffraction during his study of the $\text{CaCO}_3\text{-SrCO}_3$ and $\text{CaCO}_3\text{-BaCO}_3$ systems. Chang (1965) recorded the gradual disappearance of 113 Bragg peaks which relate to the transformation from the low-temperature space group $R\bar{3}c$ to the high-temperature form of calcite, space group $R\bar{3}m$ (termed α -calcite by Boeke (1912)). This loss of the c glide plane is a consequence of rotational disorder of the CO_3 groups, as evinced in the single crystal X-ray study of Markgraf and Reeder (1985). Their high-temperature structure refinements demonstrate increased thermal motion due to rigid body motion of the CO_3 groups. These results confirm the temperature dependent decrease of I_{113} , as do the X-ray data of Mirwald (1979). Most recently Dove and Powell's (1989) high-temperature neutron scattering experiments on pure calcite have shown that the temperature evolution of I_{113} , of I_{211} and of the spontaneous strain follows tricritical Landau behaviour with $T_c = 987 \pm 5^\circ\text{C}$. The order parameter, Q , for the transition which is a measure of the degree of orientational order in calcite, is expected to follow the behaviour shown in Figure 6.2 and is proportional to

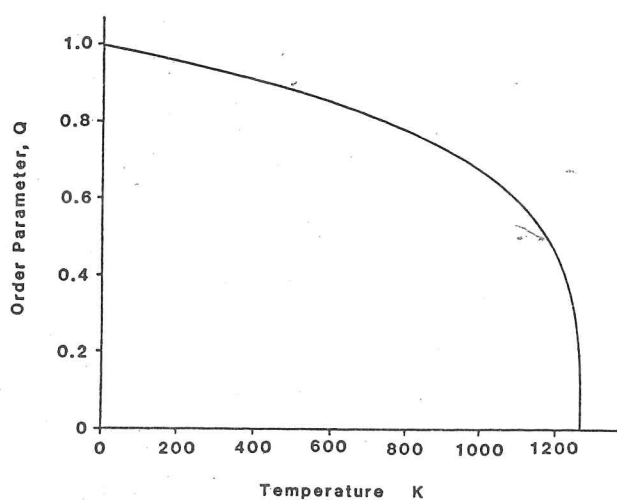


Figure 6.2 The equilibrium temperature-dependent behaviour of the orientational order parameter below the $R\bar{3}m\text{-}R\bar{3}c$ transition in calcite according to a tricritical model.

\sqrt{I}_{113} : Salje and Viswanathan (1976) first suggested that gradual orientational disordering in calcite would give rise to the observed curvature of the calcite/aragonite boundary. This is because the tricritical behaviour at the $R\bar{3}c-R\bar{3}m$ transition implies gradual and continuous ordering of calcite below T_c (Figure 6.2) and therefore a continuous increase in the stability of calcite with respect to aragonite with increasing temperature. In section 6.3 it will be argued that the well known curvature of the calcite/aragonite phase boundary in the P/T diagram is, indeed, the result of orientational disorder in calcite.

The situation became somewhat confused, however, when Mirwald (1979) reported a second high-temperature phase transition in calcite at 800°C giving rise to a third, intermediate, phase which he denoted calcite IV. The DTA experiments which Mirwald (1976) described by no means provide unequivocal evidence of such a transition. In fact the X-ray diffraction data of Mirwald (1979) are inconsistent with such a transition and more obviously indicate the behaviour of the order parameter Q associated with the $R\bar{3}c-R\bar{3}m$ phase transition at 987°C. Reinterpretation of Mirwald's (1979) c lattice parameter data in terms of the spontaneous strain arising below the $R\bar{3}c-R\bar{3}m$ transition shows they are entirely consistent with those expected from continuous disordering rather than a second transition at 800°C (see Dove and Powell, 1989). It seems that Mirwald's (1976, 1979) observations relate more consistently to the increased disorder of the CO_3 groups within the still $R\bar{3}c$ calcite above 800°C but below T_c (987°C). In other words calcite IV is not a true phase, and calcite retains $R\bar{3}c$ symmetry until the phase transition first reported by Boeke (1912).

Experimental results relating to the structural changes in calcite near 987°C are sparse, probably due to the practical difficulties arising from the significant decomposition of calcite above around 700°C under the CO₂ pressures characteristic of ambient conditions. Single crystal neutron diffraction is, however, currently being carried out by Dove and co-workers. The transition at 987°C is beyond the upper temperature limit of operation for a conventional differential scanning calorimeter. This, coupled with the problems associated with the high temperature reaction $\text{CaCO}_3(\text{s}) = \text{CaO}(\text{s}) + \text{CO}_2(\text{g})$, has precluded direct measurement of the heat capacity of calcite through the postulated orientational order-disorder transition. Low-temperature heat capacity measurements were made by Stavely and Linford (1969), however, and further extended to 775 K by Jacobs et al. (1981). Here we present the results of direct measurements of the enthalpy of calcite by transposed-temperature-drop calorimetry up to 1325 K. These data enable quantitative determination of the enthalpy changes associated with the process of orientational disorder, and we investigate the direct influence of this additional energy contribution on the calcite/aragonite phase boundary.

6.2 Strain in Sodium Nitrate at Low Temperature

Before turning to the influence of orientational disorder on the calcite/aragonite phase boundary let us first consider the effect such disorder has on the lattice parameters in the calcite structure, even a very long way below the phase transition temperature. We shall address this effect through the study of the lattice parameters of sodium nitrate below room temperature.

This study will also yield information on the nature of order-parameter saturation in the calcite structure.

6.2.1 Materials and Methods The NaNO_3 used for the study of strain behaviour at low temperatures was generously provided by Prof. Patrick J. Herley of the State University of New York at Stony Brook. The clear single crystals occur as cleavage rhombs up to several centimetres, which were grown from seeds in aqueous solution at 50°C using reagent grade chemicals. Uniform growth conditions were maintained throughout, resulting in high-purity crystals with few imperfections. X-ray topography has shown that the material is homogeneous with low dislocation densities (P.J. Herley, pers. comm.).

Low-temperature lattice parameter measurements were carried out using asymmetric transmission Guinier X-ray powder diffraction geometry at the Institut für Kristallographie, Universität Tübingen, by kind permission of Professor W Prandl. The details of the low-temperature Guinier camera developed at Tübingen are given by Irhinger (1982). Silicon was used as an internal standard. The NaNO_3 was crushed and ground by hand with the silicon under acetone in an agate mortar. The sample was deposited as a powder on silicon grease spread thinly on an aluminized Mylar foil held in a circular disc and in good thermal contact with the cold finger. The specimen disc was rotated within the beam during all exposures by means of a magnetically coupled motor. A liquid helium circulating cryostat with CTI Cryogenics model 21 SC cryocooler refrigerator was used to obtain stable temperatures down to 22 K. The thermal contact between the cold finger and the sample is improved by around 1 atm pressure of helium gas. Temperature measurement was carried out

by means of a calibrated Si p/n junction located on the cold finger near the sample. A 6 kW Rigaku rotating-anode Cu X-ray source was used with a bent germanium monochromator selecting $K\alpha_1$ radiation.

The powder diffraction patterns were recorded on single-emulsion film held in the film cassette of the camera. The sample temperature was first set to 22 K, and when stabilised the exposure was made as the sample slowly returned to room temperature at a constant heating rate whilst the film cassette moved synchronously. Positions of 11 lines ranging from 23 to $58^\circ 2\theta$ were determined on an Enraf-Nonius film reader with an estimated precision of $0.01^\circ 2\theta$. Corrections for film shrinkage and any other systematic errors were made using the line positions of the internal standard. Corrected line positions were used to refine by least squares the hexagonal cell parameters at each temperature. Precisions calculated from least-squares method are approximately 1 part in 25000.

T	a (Å)		c (Å)		v (Å ³)	
22 K	5.0658	0.0005	16.5490	0.0031	367.7911	0.0882
29 K	5.0660	0.0005	16.5540	0.0028	367.9234	0.0817
37 K	5.0654	0.0005	16.5487	0.0027	367.7237	0.0791
45 K	5.0648	0.0003	16.5503	0.0017	367.6778	0.0482
55 K	5.0653	0.0004	16.5480	0.0023	367.6966	0.0664
64 K	5.0651	0.0003	16.5478	0.0019	367.6566	0.0534
75 K	5.0650	0.0003	16.5532	0.0018	367.7633	0.0518
85 K	5.0651	0.0005	16.5645	0.0028	368.0321	0.0807
96 K	5.0652	0.0004	16.5751	0.0025	368.2827	0.0728
107 K	5.0660	0.0005	16.5803	0.0027	368.5081	0.0782
118 K	5.0664	0.0004	16.5906	0.0024	368.8021	0.0687
129 K	5.0660	0.0005	16.6009	0.0029	368.9748	0.0838
141 K	5.0662	0.0004	16.6062	0.0021	369.1257	0.0602
153 K	5.0665	0.0005	16.6224	0.0027	369.5283	0.0777
164 K	5.0669	0.0005	16.6338	0.0029	369.8331	0.0822
175 K	5.0672	0.0004	16.6414	0.0025	370.0439	0.0717
185 K	5.0670	0.0004	16.6478	0.0023	370.1542	0.0657
196 K	5.0678	0.0004	16.6637	0.0024	370.6271	0.0688
206 K	5.0675	0.0002	16.6772	0.0012	370.8924	0.0348
215 K	5.0671	0.0003	16.6878	0.0020	371.0611	0.0574
225 K	5.0686	0.0005	16.7094	0.0027	371.7647	0.0772
234 K	5.0695	0.0003	16.7221	0.0016	372.1807	0.0468
245 K	5.0699	0.0005	16.7405	0.0030	372.6531	0.0845
256 K	5.0708	0.0006	16.7518	0.0034	373.0329	0.0974
270 K	5.0700	0.0006	16.7759	0.0034	373.4476	0.0962
284 K	5.0694	0.0004	16.7900	0.0025	373.6788	0.0704
298 K	5.0697	0.0005	16.8118	0.0030	374.1992	0.0866
302 K	5.0684	0.0003	16.8197	0.0019	374.1880	0.0528

(one standard deviation error given)

Table 6.1 Low-temperature lattice parameters of NaNO_3 .

6.2.2 Lattice Parameter Results Unit cell data from 22 K to 302 K are reported in Table 6.1, and the variation of a and c with temperature up to and above the transition temperature are shown in Figure 6.3 where the high-temperature X-ray data collected by R.J. Reeder (Reeder et al., 1988) are incorporated with these results. The larger unit cell of the low-temperature form has been used for the high-temperature form for consistency in reporting values. Comparison of the a and c cell parameters (Figure 6.3) demonstrates the large anisotropy of expansion noted by previous workers. The direction of largest expansion is along the c -axis, which increases uniformly from about 75 K to near 450 K. Thermal expansion coefficients at 100, and 300 K are 4.8, and $10.4 \times 10^{-5} \text{ K}^{-1}$, respectively. These values are in good agreement with previous work (Ibrahim et al., 1986; Krishna Rao

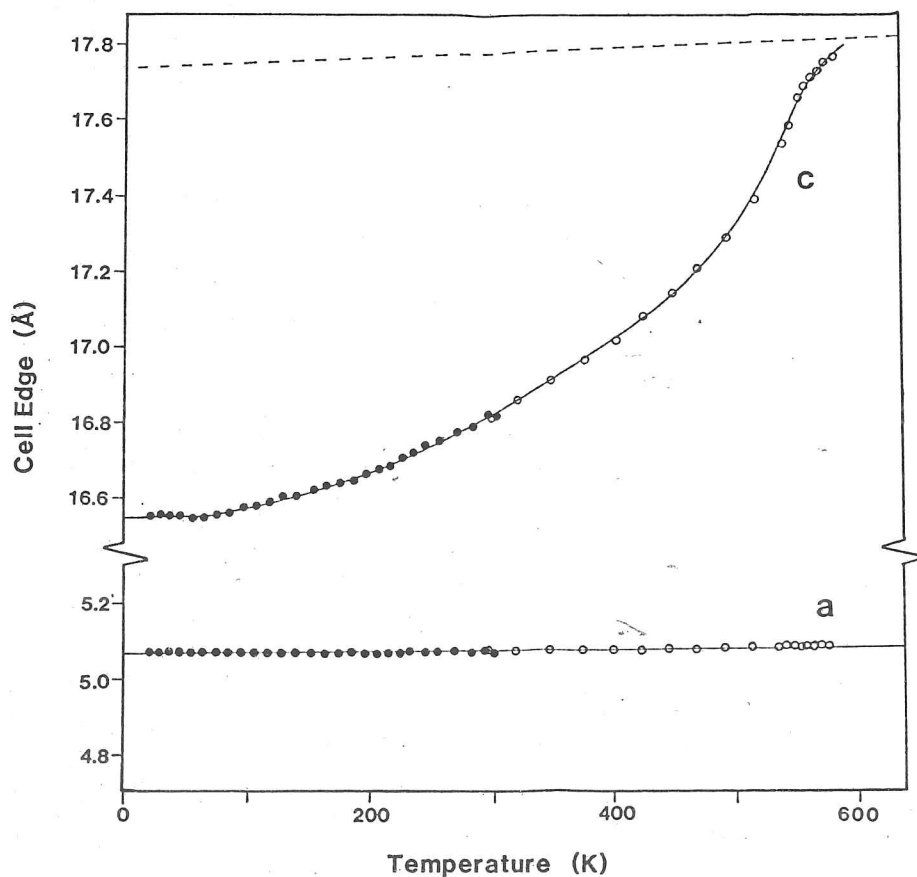


Figure 6.3 Lattice parameters of NaNO_3 . Filled circles show the data from this work, open circles are the data of Reeder et al., 1988 at high-temperature.

and Satyanarayana Murthy, 1970). The measurements of Reeder et al. (1988) show that above roughly 460 to 480 K, the expansivity increases rapidly and at T_c , a distinct anomaly is observed, just as has been seen in calcite (Dove and Powell, 1989).

Below approximately 70 K, the c cell dimension does not change with temperature. The low-temperature interferometry study of Ibrahim et al. (1986) was restricted to temperatures greater than 80 K, and thus saturation of the cell parameters has not been observed previously. Such saturation is to be expected from a consideration of simple thermodynamics as absolute zero is approached. Landau theory predicts that the derivatives of free energy take some non-zero value at 0 K, in which case it would be favourable to reduce temperature below 0 K. The derivatives must be zero at absolute zero and therefore as we approach absolute zero Landau theory will fail, as we have observed in NaNO_3 and previously in anorthite. The structural barriers to further strain at very low temperatures are as yet unclear.

Saturation in the a cell dimension, although much less distinct, is also observed below 70 K. Above this temperature, expansion in the a-axis direction increases only very slightly with temperature, in agreement with other workers (cf. Krishna Rao and Satyanarayana Murthy, 1970; Ibrahim et al., 1986); thermal expansion coefficients range from $0.4 \times 10^{-5} \text{ K}^{-1}$ at 150 K to $1.1 \times 10^{-5} \text{ K}^{-1}$ at room temperature.

6.2.3 Symmetry and Spontaneous Strain The components of the spontaneous strain are constrained by the symmetry properties of the order parameter and can be determined from appropriate unit cell data. It is important to note that unit cell changes associated with normal thermal expansion are not included in the

spontaneous strain, since they are not related to the transition. Therefore, the strain is measured relative to a reference state: the high-temperature behaviour extrapolated below the transition point.

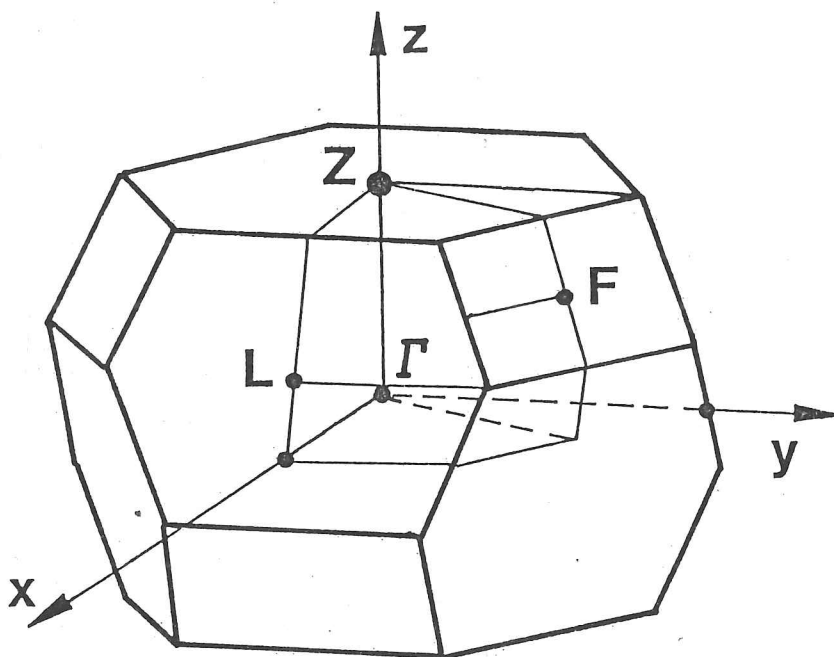


Figure 6.4 The Brillouin zone of NaNO_3 (and CaCO_3). The orientational order/disorder transition is associated with the Z-point.

The orientational ordering transition in NaNO_3 corresponds to a change from space group $R\bar{3}m$ to $R\bar{3}c$ with a doubling of the unit cell along the c-axis; this transition does not involve a change in either crystal system or point group and is not, therefore, a proper ferroic transition. Indeed, the critical point is the Z-point on the surface of the Brillouin zone (Figure 6.4), and the order parameter transforms according to the one-

dimensional representation $Z_2 A_{1u}$ (Petzelt and Dvorak, 1976) which need not involve any strain component. The transition, therefore, does not specify a spontaneous strain, and yet we observe a large coupling between the rotational order-disorder transition and the c cell parameter. In this sense the transition is similar to the $I\bar{1}-P\bar{1}$ transition in anorthite and is another example of co-elastic behaviour (section 1.3.3; chapters 3 and 4), where the strain at the transition is not a true spontaneous strain by symmetry, but nonetheless is a structural strain coupled to the critical behaviour of the order parameter. We see empirically that the only relevant strain component is e_3 along the c -axis, which is given at any temperature T simply by:

$$e_3 = (c_0 - c) / c_0 \quad \{6.1\}$$

where c is the cell dimension of the low-temperature phase at T and c_0 is the cell dimension of the high-temperature phase

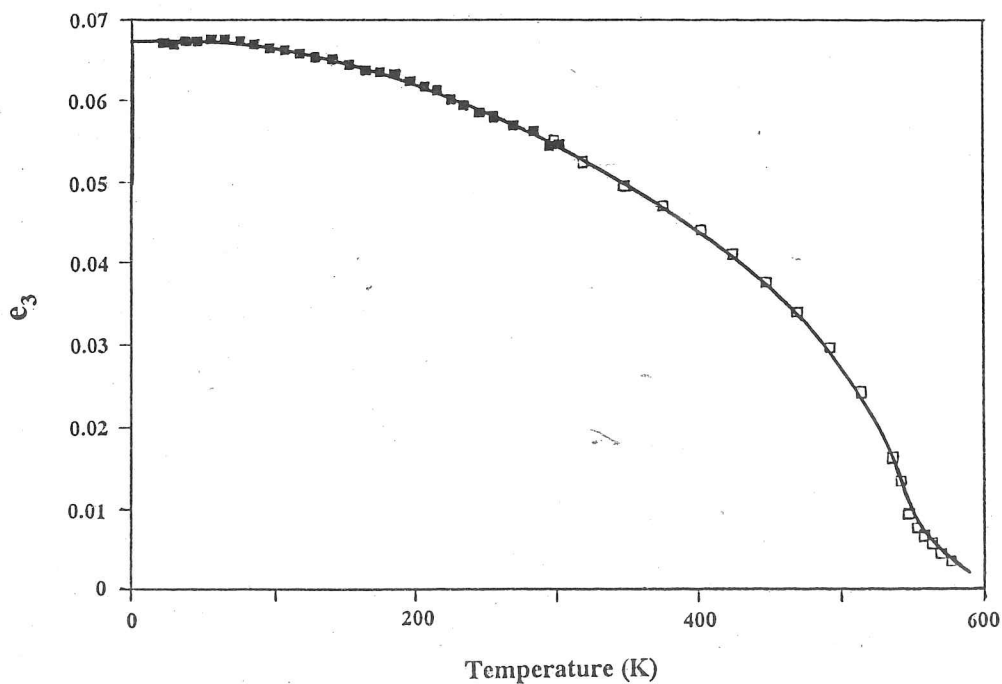


Figure 6.5 Temperature evolution of the spontaneous strain, e_3 , in NaNO_3 . (Filled squares this work, open squares Reeder et al., 1988)

extrapolated to T. Strain components perpendicular to the 3-fold axis are effectively zero, and therefore would not affect the spontaneous strain in any event.

For simplicity, the thermal expansion along the c-axis in the high-temperature phase was assumed to be linear and to follow the behaviour explained in detail by Reeder et al. (1988). Extrapolating the high-temperature lattice parameters to low temperature we arrive at the strain behaviour shown in Figure 6.5 where the high-temperature data collected by R.J. Reeder are incorporated.

6.2.4 Order Parameter Coupling For a zone boundary co-elastic instability, the spontaneous strain cannot be the primary order parameter, although may couple with it. The Landau potential for the excess free energy involving a single order parameter, Q, is of the form given in equation 1.5, and the excess entropy behaves as the square as the order parameter, as demonstrated in equation 1.10.

In a related study, Wruck and Salje (1987) have measured excess entropies for the same NaNO_3 as used in the present investigation, and they find a temperature dependence of the same form as that of the spontaneous strain. Indeed, Reeder et al. (1988) plotted the strain as a function of excess entropy above room temperature and found a linear relationship. Thus, the spontaneous strain couples biquadratically with the order parameter such that:

$$e_s \propto Q^2 \propto t^{2\beta} \quad \{6.2\}$$

where t is the reduced temperature $(1 - T/T_c)$ and β is the critical exponent giving the temperature dependence of the

macroscopic order parameter Q .

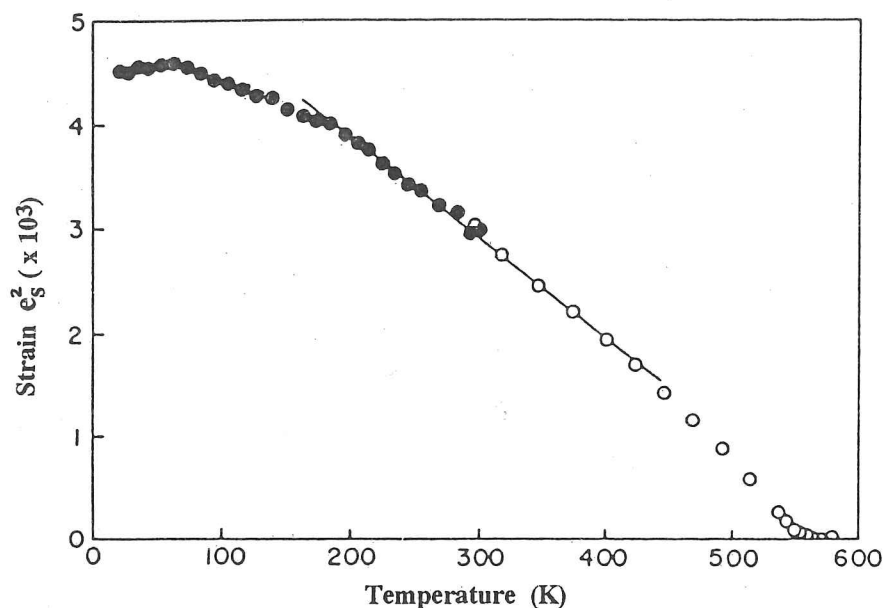


Figure 6.6 Temperature dependence of the square of the spontaneous strain (filled circles, this work; open circles, Reeder et al., 1988). The linear region between 185 K and 430 K corresponds to tricritical behaviour ($\beta = \frac{1}{4}$).

The critical temperature obtained from extrapolation of both the high- and low-temperature e_3^2 data to zero is 553 K (Figure 6.6), in good agreement with values obtained from optical birefringence measurements (553 K) (Poon and Salje, 1988) and from specific heat measurements (551.9 K) (Wruck and Salje, 1987). Examination of the plot of e_3^2 versus T (Figure 6.6) shows a broad linear region from around 185 to 430 K, with an extrapolated T_c of 579 K. By squaring both sides of equation 6.2, it follows that a linear relation between e_3^2 and T (or t) implies $\beta = 0.25$, which corresponds to tricritical behaviour. The data thus support the interpretation of tricritical behaviour below around 430 K, above which temperature a crossover to another type of critical behaviour occurs. The analysis by Reeder et al. (1988) of the region above 430 K suggests that at these temperatures until T_c the critical exponent β takes the value 0.22. The critical exponents for NaNO_3 above the

tricritical regime are very similar to the values obtained from renormalization-group results for the three-states Potts model in three dimensions. This model can be regarded as an Ising-type model generalized to more than two spins (see Wu, 1982 for a review). Shen et al. (1975) suggested that the Bragg-Williams model may be applied to the ordering transition in NaNO_3 , in which event the critical exponent β should assume the classical value 0.5. Given the present observation that $\beta = 0.25$ at room temperature with a crossover to 0.22 above 435 K, this is clearly not the case. The related studies of Poon and Salje (1988) in which β was determined from optical birefringence and of Schmahl (1988) in which β was determined from X-ray superlattice intensity yield values of β identical with the present study.

6.2.5 Scalar Strain and Strain Energy The magnitude of the spontaneous strain is given by (Aizu, 1970):

$$e_s = [\sum_i e_i^2]^{1/2} \quad \{6.3\}$$

and in the present case is identical to the strain component e_3 . At 295 K, the spontaneous strain in NaNO_3 is approximately 55×10^{-3} . This value is large, considering it pertains to a zone boundary instability, and is comparable with examples of zone centre instabilities such as in albite (see Table 6.2).

Material	Critical Point	Strain (295 K)	Reference
$\text{NaAlSi}_3\text{O}_8$	zone centre	53×10^{-3}	Salje et al. (1985a)
As_2O_5	zone centre	16×10^{-3}	Redfern and Salje (1988)
$\text{CaAl}_2\text{Si}_2\text{O}_8$	zone boundary	5×10^{-3}	Redfern and Salje (1987)
$\text{Pb}_3(\text{PO}_4)_2$	zone boundary	33×10^{-3}	Guimaraes (1979)
NaNO_3	zone boundary	55×10^{-3}	This study

Table 6.2 Magnitude of the spontaneous strain at various phase transitions.

It is interesting to note that the symmetry constraints for the transition present no constraint on volume change. Commonly in ferroelastic transitions the strain components are coupled by symmetry so that an increase in one is balanced by a decrease in others, thus leading to little or no change in volume (Redfern and Salje, 1988; see also chapter 2). However, in NaNO_3 and CaCO_3 volume can change as rapidly as c changes. We shall see in section 6.3 that this freedom is significant in the discussion of the calcite/aragonite equilibrium.

Reeder et al. (1988) found that at 295 K, the contribution to the excess internal energy due to the elastic deformation of the structure is nearly 20% which is an outstandingly large value. The excess free energy of NaNO_3 can, therefore, appropriately be decomposed into one part describing local variations, including "molecular" orientations, and a second part describing the strain energy.

6.3 Orientational Ordering and the Calcite/Aragonite Equilibrium

6.3.1 Comparison with Sodium Nitrate The identical symmetry reduction observed in sodium nitrate, NaNO_3 , (Kracek, 1931) has been suggested as a model for the orientational transition in calcite which we consider here. Studies of the critical behaviour at the $R\bar{3}m-R\bar{3}c$ transition in NaNO_3 are more extensive than the current research on calcite because of their relative experimental ease. The studies presented in section 6.2 as well as those of Schmahl (1988), Reeder et al. (1988) and Reeder et

al. (1987) have revealed behaviour broadly similar to that described by Dove and Powell (1989) in the case of calcite. The macroscopic order parameter describing the degree of orientational disorder in sodium nitrate follows essentially tricritical Landau behaviour below T_c with small deviations from tricritical behaviour very close to T_c . We shall see that our results on calcite confirm the tricritical model (Dove and Powell, 1989) for the phase transition in calcite and there is every reason to believe that the temperature dependent behaviour of the structure of sodium nitrate corresponds to similar behaviour in calcite. So far, however, no departures from classical Landau behaviour have been observed in calcite near T_c although such departures have been reported in the order parameter behaviour of sodium nitrate (Poon and Salje, 1988; Reeder et al., 1988). Aside from this sodium nitrate may be studied as an analogue material to calcite since the phase transitions in both materials belong to the same universality class (they share similar critical exponents). In addition the results of Dove and Powell (1989) indicate that we are justified in applying a simple Landau expansion to model the excess thermodynamic quantities associated with the orientational ordering transition. In this section we shall see the predictive power of such a simple free energy expansion for the solution of inter-mineral phase stabilities.

The excess entropy below the orientational ordering transition in calcite represents a direct measure of the thermodynamic influence of the order parameter, Q , associated with orientational ordering. Ideally, the transition in calcite should be studied by differential scanning calorimetry, as has

been carried out for NaNO_3 (Wruck and Salje, 1987; Reeder et al., 1987), but the transition temperature of 1260 K is far above the maximum operating temperature of conventional DSC instruments. In addition, the complication of decarbonation of calcite must be overcome and the high CO_2 pressures needed to prevent decarbonation cannot be maintained in the standard DSC experimental configuration. For this reason it was decided to attempt the measurement of excess enthalpy rather than excess heat capacity. This enthalpy can then be used to derive the expected entropy excess, through the solution of the Landau expansion in which entropy and enthalpy have a common origin.

6.3.2 Measurement of Enthalpy High-temperature enthalpy measurements were carried out on pure calcite using a Setaram HT1500 calorimeter at Princeton University by kind permission of Professor A Navrotsky. Natural calcite was ground by hand in an agate mortar to a fine powder and a measured mass was loaded into platinum capsules of known weights. The capsules were welded closed to contain maximum amounts of the calcite powder, and then weighed again. The average mass of a capsule was around 400 mg, around 20 mg of which was calcite. There was no indication of a transformation from calcite to aragonite during the preparation of the samples, which were subsequently analysed by X-ray diffraction revealing no change from the starting material.

The Setaram HT1500 calorimeter used to make calorimetric measurements is described by Ziegler and Navrotsky (1986). The sample falls from the top of the instrument, at room temperature, into an upper calorimeter crucible surrounded by a thermopile and held at the temperature of interest. Heat flow into this crucible is measured with respect to a similar reference

crucible, positioned directly below the first in the instrument. The calorimeter is suspended within an alumina tube and is separate from the graphite heater. The apparatus allows drops to be made under a vacuum, minimizing convection effects; this procedure increases baseline stability and was adopted for the measurements on calcite.

The advantage of this form of calorimeter over other designs is that the operational temperature of the instrument can be easily changed from day to day. In addition the absorption of heat by the sample is rapid and the response time of the Setaram calorimeter is very short; the measurement of each drop described here was over within nine minutes. The instrument is sensitive to sample geometry, however, and all the samples were (as far as is possible) standardized in weight and shape. It is found that the sensitivity of the calorimeter depends on the operating temperature and the number of samples already dropped into the calorimeter (Ziegler and Navrotsky, 1986). For this reason the calibration factor must be calculated for each drop by alternating sample drops with drops of a standard material of similar mass and dimensions. In these experiments corundum capsules, prepared in an identical manner to the calcite, were used as a standard. A platinum liner was placed inside the alumina calorimeter crucible to increase the thermal conduction between the sample and calorimeter on dropping and to provide a significant thermal mass within the calorimeter.

The temperature of each experiment was regulated and measured by a platinum/rhodium thermocouple placed next to the sample crucible. The thermocouple was calibrated against the melting point of gold. Data were collected using an interfaced

Hewlett-Packard 86B computer. All samples were weighed upon recovery from the instrument to ensure that no loss of material had occurred. At the highest temperatures of measurement, where decarbonation is significant, whenever the pressure of CO₂ burst the platinum capsules a substantial mass reduction was detected. In addition, on these occasions the endothermic nature of the decarbonation reaction increased the calorimeter signal and lead to an unstable baseline. This occurred in three cases and the data from the related sets of runs were discounted. In addition all calcite samples were pre-heated to 850°C for 2 hours before their use for calorimetry to check the welds. Any which were not gas-tight underwent decarbonation with related detectable mass loss.

T/K	H _T -H ₂₉₈ (kJ/mol)	T/K	H _T -H ₂₉₈ (kJ/mol)
973	75.36±0.76(5)*	1200	110.47±1.07(4)
977	76.24±1.10(4)	1212	110.62±1.02(4)
998	77.48±1.45(4)	1225	116.52±1.66(4)
1023	82.60±0.76(4)	1236	117.12±1.93(6)
1049	86.36±0.97(4)	1248	115.13±1.14(6)
1076	89.70±1.29(5)	1254	117.21±1.14(2)
1100	93.09±1.40(2)	1261	117.90±2.35(6)
1130	97.53±1.21(2)	1277	121.96±1.37(5)
1150	103.21±1.24(6)	1301	124.45±1.83(3)
1175	104.80±0.69(5)	1325	125.32±1.69(4)

* Data from drops into Calvet calorimeter.

Table 6.3 Enthalpies of calcite from 973 K to 1325 K. Errors are the standard deviation of the mean. Figures in parenthesis are the number of data points.

6.3.3 Results from Calorimetry The results of the drop experiments are shown in Table 6.3. The enthalpies shown are derived from around five sample drops at each temperature dropped alternately with an equal number of capsules of corundum. A calibration factor for each drop relating the area under the calorimetric peak to the heat content was obtained by referring to the known heat contents of platinum and corundum at each temperature (from the tables of Robie et al., 1979). The total heat content for each capsule was calculated and the contribution from the platinum subtracted to obtain the enthalpies of calcite.

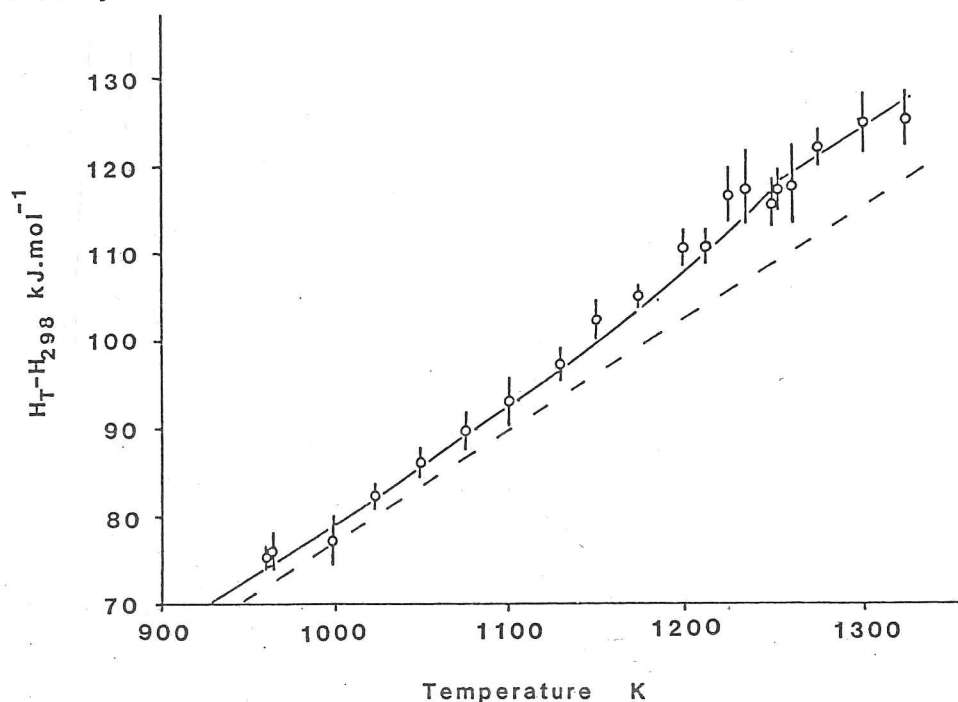


Figure 6.7 Enthalpy of calcite between 900 K and 1350 K. The extrapolation of the low-temperature heat capacity data of Jacobs et al. (1981) is shown by the dashed line. Error bars show $\pm 2\sigma$.

Figure 6.7 shows the data for the enthalpy, H , of calcite above 900 K relative to that at 298.15 K. The dotted line is the extrapolation of the low temperature calorimetric data of Jacobs et al. (1981) whose heat capacity measurements give:

$$H_T - H_{298.15} = -184.79.T + 0.16161.T^2 - 4.3247 \times 10^{-5}.T^3 + 3.6882 \times 10^6.T^{-1} + 7767.T^{\frac{1}{2}} - 104608 \text{ J.mol}^{-1} \quad \{6.5\}.$$

All measurements lie above the extrapolation of the low temperature data. To check if there was a systematic error in the Setaram calorimeter a set of five calcite sample drops together with corundum calibration drops were made using a previously calibrated twin Calvet microcalorimeter at 973 K, as described by Navrotsky (1977). The results from this set of transpose-temperature drops are included in Table 6.3 and Figure 6.7 and are seen to agree with the data obtained from the Setaram instrument. The trend towards higher than expected enthalpies at higher temperatures is thus a real effect. The enthalpies increase markedly just below 1260 K. This enthalpy increase appears to be associated with the previously reported orientational order-disorder transition. We see an enthalpy difference between the extrapolated low temperature calcite ($R\bar{3}c$) enthalpies (which must already include some contribution from the excess enthalpy of orientational disorder) and the high-temperature $R\bar{3}m$ phase of $6.9 \pm 1.1 \text{ kJ.mol}^{-1}$. This is more than five times the average standard error of the data and must be regarded as a significant enthalpy increase. Rather than being an abrupt step in enthalpy the increase takes place gradually below T_c ($1260 \pm 5 \text{ K}$). This is consistent with a continuous tricritical model for the phase transition rather than a first-order phase transition.

6.3.4 Landau Theory of Calcite The theoretical background to the behaviour of thermodynamic parameters at a tricritical phase transition is expounded by Landau and Lifshitz (1954), and more recently by Aleksandrov and Flerov (1979). The thermodynamic implications for the specific heat, enthalpy, and entropy are

discussed in detail by Salje (1988). We start from the conventional expansion of free energy, G , associated with the transition in terms of a one dimensional order parameter, Q , defined as zero above T_c and increasing proportional to $(T_c - T)^\beta$ below T_c to 1 at absolute zero:

$$\Delta G = G - G_0 = \frac{1}{2}a(T-T_c)Q^2 + \frac{1}{4}BQ^4 + \frac{1}{6}CQ^6 \quad \{6.6\}$$

where $C > 0$ and $B \geq 0$. The excess entropy, ΔS_{od} , and enthalpy, ΔH_{od} , associated with the process of disorder and additional to that expected should no transition occur may be obtained. The entropy associated with the transition is easily derived (Carpenter, 1988):

$$\Delta S_{od} = \frac{\partial \Delta G}{\partial T} = \frac{1}{2}aQ^2 \quad \{6.7\}.$$

At a tricritical phase transition $B=0$, $\beta = \frac{1}{4}$ (see section 1.2.5).

This leads to:

$$\Delta H_{od} = -\frac{1}{2}aT_c Q^2 + \frac{1}{6}CQ^6 \quad \{6.8\}$$

where

$$T_c = \frac{C}{a} \quad \{6.9\}$$

and hence

$$\Delta H_{od} = -\frac{a}{3} T_c \quad \{6.10\}$$

at absolute zero (ignoring low-temperature saturation effects).

The enthalpies given in Table 6.3 have been plotted as a negative excess with respect to the high temperature $R\bar{3}m$ phase and are shown in Figure 6.8. The form of enthalpy expected from equation 6.8 has been fitted to these data and is shown by the solid curve. The total excess enthalpy expected at absolute zero

is around $-10 \pm 1.1 \text{ kJ.mol}^{-1}$. This is the total increase in enthalpy due to orientational disorder in the high temperature $R\bar{3}m$ structure. Combining this value of $\Delta H_{od}(T=0)$ with the value

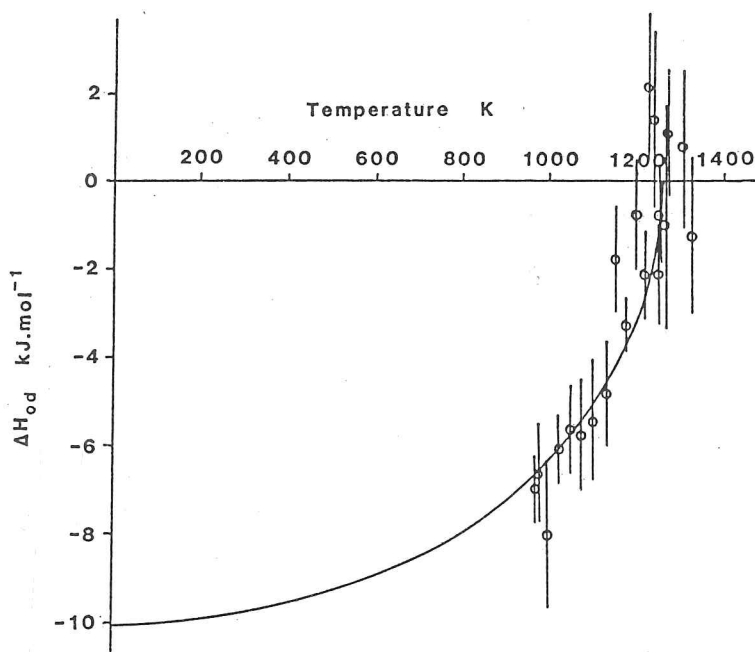


Figure 6.8 Excess enthalpy due to rotational disordering of the CO_3 groups below T_c in calcite. The solid line shows the fitted theoretical excess enthalpy assuming a tricritical model for the phase transition. Error bars show $\pm 2\sigma$.

of T_c determined by Dove and Powell (1989) enables us to evaluate the constants a and C in expression 6.6 above:

$$\begin{aligned} \Delta H_{od}(T=0) &= -10 \pm 1.1 \text{ kJ.mol}^{-1} \\ &= -\frac{a}{3} T_c \quad (T_c = 1260 \pm \text{K}) \\ \Rightarrow a &= 24 \text{ J.mol}^{-1} \cdot \text{K}^{-1} \\ C &= 30 \text{ kJ.mol}^{-1} \end{aligned}$$

From equation 6.7 we see that the zero point entropy is simply $\frac{1}{2}a$ and hence we obtain from the enthalpy measurements presented here:

$$\Delta S_{od}(T=0) = 11.9 \pm 1.3 \text{ J.mol}^{-1} \cdot \text{K}^{-1}$$

which may be compared with the well-known relationship between

excess entropy and thermodynamic probability of disorder, Ω :

$$\Delta S_{\text{od}}(T=0) = R \cdot \ln \Omega \quad \{6.11\}$$

giving $\Omega \approx 4$

We would expect $\Omega = 2$ for the residual zero-point entropy of a two state Ising spin system in an isotropic crystal. The larger value obtained here may arise from phonon contributions, lattice relaxation, calcium mobility or point defects. It is worth mentioning that a similar analysis of the orientational ordering transition in NaNO_3 yielded a much higher value of $\Omega \approx 20$ (Wruck and Salje, 1987). Thus the real physical meaning of Ω is not clear.

In summary the thermodynamic data relating to the excess quantities arising from the phase transition in calcite show the following temperature dependence:

$$\Delta H_{\text{od}} = -424(1260-T)^{\frac{1}{2}} + 0.113(1260-T)^{\frac{3}{2}} \quad \text{J.mol}^{-1} \quad \{6.12\}$$

$$\Delta S_{\text{od}} = 0.383(1260-T)^{\frac{1}{2}} \quad \text{J.mol}^{-1} \cdot \text{K}^{-1} \quad \{6.13\}$$

6.3.5 Implications on the Calcite/Aragonite phase equilibrium

boundary If we now consider the excess thermodynamic quantities defined above with respect to the low temperature $R\bar{3}c$ phase, we can investigate their significance with respect to the calcite/aragonite phase boundary. What is the effect of the extra ΔS_{od} below the $R\bar{3}c$ - $R\bar{3}m$ transition in calcite? In the simplest analysis, ignoring any phase transitions in aragonite (which have not been observed in any case), the Clapeyron equation gives:

$$\frac{dP}{dT} = \frac{\Delta S}{\Delta V} = \frac{S_c + \Delta S_{od} - S_a}{V_c + \Delta V_{od} - V_a}$$

$$= \left(\frac{\Delta S_{c-a}}{\Delta V_{c-a}} + \frac{\Delta S_{od}}{\Delta V_{c-a}} \right) / \left(1 + \frac{\Delta V_{od}}{\Delta V_{c-a}} \right) \quad \{6.14\}$$

where subscript c refers to calcite and a refers to aragonite.

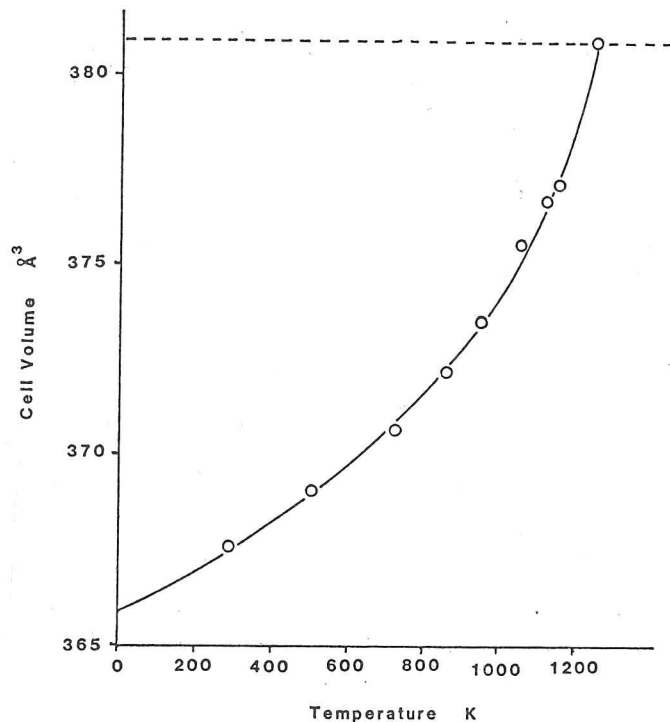


Figure 6.9 Temperature dependence of the unit cell volume of calcite taken from the data of Dove and Powell (1989).

It is now straightforward to calculate the path in P/T space of the equilibrium phase diagram taking orientational disordering into account. ΔV_{od} is the excess molar volume due to the disorder in calcite. The cell volume of calcite as a function of temperature is shown in Figure 6.9, where the dashed line represents the baseline of the totally disordered phase. The strong translation-rotation coupling in calcite results in a significant extension of the c lattice parameter, with the a cell parameter only weakly coupled to the disordering. This thermal expansion is as large as is observed in many ferroelastics (cf. Reeder et al., 1988; Redfern and Salje, 1988; Redfern et

al., 1988) and it appears that a significant proportion of ΔH_{od} is actually due to elastic energy contributions, as we found for NaNO_3 . The excess molar volume can be formulated from the data of Dove and Powell (1989); there are six formula units in the hexagonal cell of calcite and we assume that there is no significant order parameter saturation. In this case, the excess volume above that expected for the totally ordered form is dependent only on Q^2 to a good first approximation:

$$\begin{aligned}\Delta V_{od} &= 1.51 \times 10^{-6} \cdot (1 - Q^2) \\ &= 1.51 \times 10^{-6} \cdot (1 - \sqrt{1 - T/1260}) \quad \text{m}^3 \cdot \text{mol}^{-1} \quad \{6.15\}.\end{aligned}$$

The excess entropy due to disordering (with respect to the totally ordered structure and ignoring order parameter saturation) is simply:

$$\begin{aligned}\Delta S_{od} &= 11.9 \cdot (1 - Q^2) \\ &= 11.9 \cdot (1 - \sqrt{1 - T/1260}) \quad \text{J} \cdot \text{mol}^{-1} \cdot \text{K}^{-1} \quad \{6.16\}.\end{aligned}$$

Other terms in equation 6.14 are $\Delta S_{c-a}/\Delta V_{c-a}$ and ΔV_{c-a} . $\Delta S_{c-a}/\Delta V_{c-a}$ is the slope of the equilibrium phase boundary at low temperatures and pressures which has been taken as 12 kbar/K. This is slightly less than the value Staveley and Linford (1969) quote for the slope at room temperature, but their value must include at least some effect of orientational disorder. The value of ΔV_{c-a} employed is $2.73 \times 10^{-6} \text{ m}^3 \cdot \text{mol}^{-1}$ calculated from the difference in unit cell size at room temperature and pressure, and this is assumed to remain constant. In addition, we assume that T_c for the phase transition is independent of pressure to a first approximation, as indicated by the results of Cohen and Klement (1973). Finally, the static lattice energies

of calcite and aragonite are known to be identical at zero pressure and temperature, hence the phase boundary must pass through the origin. We may now calculate the calcite-aragonite phase boundary by setting the slope at 0 K, incrementing temperature and then determining the slope at 1 K, and so on in steps of temperature, each time adding the appropriate step in pressure. This calculation was carried out using the following approximation of equation 6.14 to determine the slope as a function of temperature:

$$dP/dT = (12 + \Delta S_{od} \times 3.663) / (1 + \Delta V_{od} \times 366300) \text{ kbar/K} \quad \{6.17\}.$$

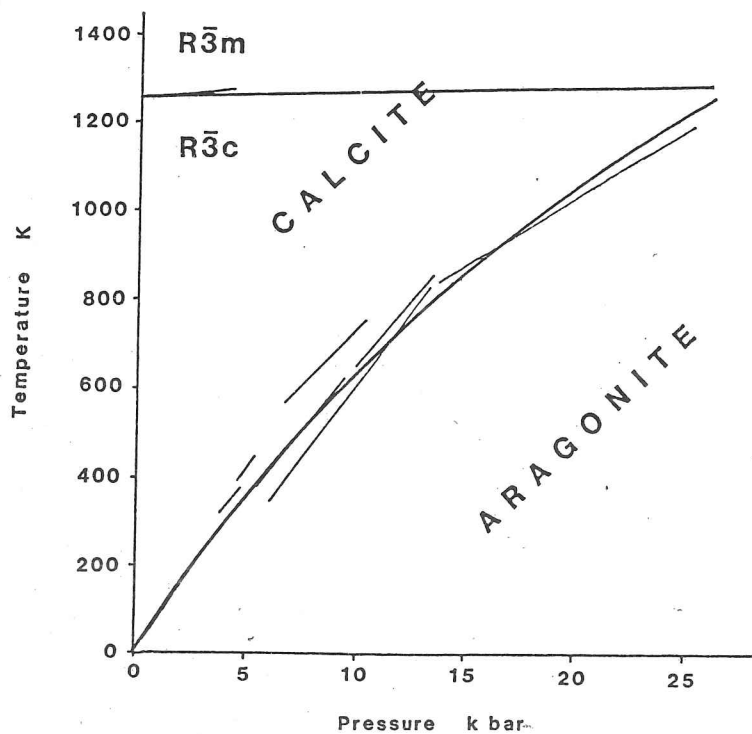


Figure 6.10 The calcite/aragonite phase diagram. Thick lines show the phase boundary calculated from consideration of the R3c-R3m disorder. Thin lines show the experimental delineation of Jamieson (1953), Simmons and Bell (1963), Crawford and Fyfe (1964), Irwing and Wyllie (1973), and Cohen and Klement (1973).

The calculated calcite-aragonite phase diagram is compared with experiment in Figure 6.10. The agreement is excellent. The curving in P/T space is thus fully explained by the influence of the orientational disordering transition on the enthalpy, entropy, and volume of calcite, and we need not infer any other phase transition or the existence of a triple point on the phase boundary.

6.3.6 Consequences of Order-Parameter Saturation In the above discussion we have ignored the possible influence of order-parameter saturation. In the analysis of the calcite-aragonite phase equilibrium order-parameter saturation does not seem to play a significant part. However it should be noted that the values of excess thermodynamic quantities given in equations 6.13 and 6.16 assume that the entropy due to disordering exists all the way down to 0 K. It was seen that in the analagous material NaNO_3 order-parameter saturation does in fact take place below around 70 K (section 6.2.2). Should the same effect occur in calcite at, say, 298 K then the order parameter would saturate to its equilibrium value at this temperature, 0.93, and the excess entropy due to disordering would only ever reach a maximum value of 87% of that given in equations 6.13 and 6.16. It is feasible that saturation could occur at even higher temperatures and the excess entropy could be reduced to as little as 80% of the unsaturated maximum. This would have the effect of lessening the stability of calcite with respect to other minerals in calculations of inter-mineral reactions.

6.4 Summary

The process of orientational disorder of the nitrate or carbonate molecules in the calcite structure is seen to have a very significant influence on the stability and thermodynamic properties of this structure. The c cell parameter of sodium nitrate changes by over 1 \AA between 0 K and T_c , and calcite similarly shows a large cell distortion due to translation-rotation coupling. The co-elastic nature of the transition, therefore, provides a very great negative excess molar volume below the phase transition. Not only does this correspond to a large strain energy, representing a significant proportion of the excess free energy stabilising the low-temperature form with respect to the high-temperature structure, it also explains the increased stabilisation of calcite with respect to aragonite with increasing temperature when considered in the light of the modified Clapeyron equation.

Measurement of the excess enthalpy due to ordering below the orientational order/disorder transition in calcite can be fitted to the known tricritical behaviour of calcite below this transition. The excess entropy so derived, when combined with the data for the excess volume of ordering, is used to determine the calcite/aragonite phase boundary. The $R\bar{3}c$ - $R\bar{3}m$ transition fully accounts for the previously-observed curving of this boundary at high temperatures and pressures. Thus the Landau free energy is seen as a good model not only for the description of the phase transition, but also for the subsequent implications of that intra-mineral process on inter-mineral relations.

The danger of over-estimating excess thermodynamic properties when applying the ^P approach of this chapter should be

noted. It is observed that at low temperatures the order-parameter deviates from the behaviour predicted by Landau, and this order-parameter saturation means that the full potential excess energy of the high-temperature phase with respect to the low-temperature phase which Landau predicts is not attained. Low-temperature data as well as data near and above the phase transition are necessary for the study of these important saturation effects.

CHAPTER 7

GENERAL OVERVIEW AND CONCLUSIONS

We have seen that the behaviour and physical properties of minerals near and below phase transitions is often very different from that expected in the absence of a transition. Anomalous behaviour can be observed in lattice parameters, vibrational mode frequencies, and in fact virtually every structurally sensitive parameter which characterises the mineral. Not only the physical properties of minerals are liable to change; the thermodynamic properties can also show distinct and anomalous behaviour as a result of structural phase transitions.

Spontaneous strain, in particular, has been found to serve as a useful measure of the transition behaviour in minerals, and often couples to the driving mechanism of the transformation. Knowledge of the symmetry relations of the high and low temperature forms may enable the prediction of the deformation pattern expected from the transition, and the form of the strain elements involved. Even when symmetry does not predict a distortive strain, order parameters can always couple to a strain through quadratic or higher-order terms (if not linearly) and it is always possible for a co-elastic strain to arise at a phase transition. This is important, because these co-elastic strains provide a ready experimental method of quantifying a wide range of ordering processes by the careful measurement of lattice parameters. In the course of this thesis we have seen that co-elastic strains couple (via second- and higher-order terms) to Al/Si ordering (as in plagioclases) as well as rotational molecular ordering (as in calcite) in minerals. Care must always

be taken in using strain as a secondary measure of ordering processes, however. The case of cordierite, where the Δ index is not simply coupled to the degree of Al/Si order, demonstrates that spontaneous strain does not always faithfully reflect Al/Si ordering processes in minerals. In such cases therefore, strain measurements should be made in conjunction with other experimental techniques such as hard-mode vibrational spectroscopy, NMR spectroscopy, or structure determination, which can give further information on cationic ordering.

The measurement of lattice parameters must be made not only in the immediate vicinity of the phase transition, but also well above and below it. The high-temperature paraphase behaviour must be well understood before extrapolation to lower temperatures can be performed, and the strain calculated. We have seen that this can be difficult, particularly if the transition of interest is close to the melting point of the crystal. Measurements a long way below the transition give further information regarding the order parameter behaviour, enabling the determination of the critical exponent of the order parameter and detection of crossover phenomena. In addition, very low-temperature lattice parameter measurements yield information on order parameter saturation effects.

Natural specimens and synthesised samples are often unavailable as good single crystals and full structural crystallography is impractical. The technique of X-ray powder diffraction is applicable in these cases, however, and provides just ^{those} structural data needed for strain measurements.

The Landau theory applied to the problems presented in this thesis has been tested most rigorously as a function of

temperature, but it applies just as well with pressure or chemical potential as the extensive variable (as seen in the lattice parameter measurements of plagioclase at high pressure, chapter 4). Landau theory has been seen to apply particularly successfully to the description of displacive phase transitions in framework silicates since the long length scale of correlated ordering limits the regime of order parameter fluctuations. Correlation length and order parameter susceptibility can be investigated by X-ray diffraction, in addition to the measurements of order parameter via strain. High-resolution powder diffraction has proved useful for the measurements of correlated order and incommensurate modulations in cordierite.

The influence of additional solute cations incorporated by interstitial or substitutional solid solution has been investigated in K-bearing cordierite and Ca-rich plagioclases respectively. Solute cations can be dealt with in the framework of Landau theory, since they effectively act as defects applying a local stress perturbation or a homogeneous conjugate field to the order parameter. The concentration of these solute 'defects' is, therefore, a determining factor in their influence on the order parameter. In cordierite K cations in sufficient concentration appear simply to act against the spontaneous strain whilst simultaneously increasing Al/Si disorder. The effect of albite in solid solution with anorthite appears rather similar, altering T_c for the displacive transition and increasing the Al/Si disorder by the coupled substitution process, but in addition Na defect concentrations alter the thermodynamic nature of the transition by interplay via strain.

We have demonstrated, for the case of orientational

disordering in calcite, that as well as shedding new light on mineral processes the additional thermodynamic data which Landau theory successfully predicts may be incorporated into datasets for the calculation of inter-mineral phase equilibria. The stabilising influence of phase transitions on low-temperature polymorphs has significant implications in the realm of geothermometry and geobarometry. It is clear that an accurate predictive description of the thermodynamic properties of minerals, as is provided by Landau theory in many cases, is essential for the deeper understanding of the properties and dynamics of the Earth's crust. Elastic transitions in framework silicates may have further significant implications for the physical properties of the crust. As has been touched upon in this thesis, the onset of an elastic transition is triggered, or accompanied, by marked changes in the elastic properties of minerals. Certain elastic constants (which behave as the ^{inverse} order parameter susceptibility, χ^{-1}) will vanish at a proper ferroelastic transition, and will decrease rapidly above and below T_c to provide the structural instability which drives the transition. We can speculate on the geophysical importance of these features of phase transitions in minerals: crustal rocks containing minerals which undergo these transition should themselves, therefore, show anomalies in sound velocity at the depth corresponding to a temperature T_c . At this depth the increased heat capacity due to the transition will also serve to stabilise the temperature near T_c , should there be heat flow through the rock (a reasonable assumption). Simple measurements of the temperature dependence of sound velocity in aggregates of framework silicates could, perhaps, further test such possible

implications.

For the main part, this thesis has been concerned with the macroscopic measurement of ordering phenomena at displacive transitions. The link between local processes and long-range processes was touched upon in the infrared study of K-bearing cordierite. Deeper insight into phase transition phenomena in minerals is undoubtedly gained when a variety of techniques, each probing properties in a specific way, are applied to the study of that transition. For example, spectroscopic methods are able to yield information on the short-range strains associated with distortive transitions. Nonetheless, the essential features of elastic transitions are revealed by the strain, and by the properties which couple to the strain. The use of spontaneous strain and complementary experimental techniques, coupled with predictive models such as Landau theory, form the tools which enable us to understand the dynamic response of minerals to those environments and forces encountered in the Earth.

APPENDIX 1

HIGH-TEMPERATURE GUINIER X-RAY POWDER DIFFRACTION

A1.1 The Huber Guinier System

The small ferroelastic and co-elastic strains measured in framework structures in the course of this work required the accurate determination of line positions of powder diffraction patterns over a wide range of temperature. The instrumental requirements of the problems and approach described in this thesis are not met by standard laboratory Debye-Scherrer cameras and diffractometers. High-precision lattice parameters, and linewidth measurements, require a high-resolution instrument. Guinier geometry provides better resolution, greater line intensity, and reduced background compared to the non-focussing Debye-Scherrer method. Accurate cell parameters of As_2O_5 , anorthite, and NaNO_3 were obtained on Huber Guinier powder diffraction apparatus.

The Guinier high-temperature powder chamber employs a precision asymmetrically ground curved quartz Johansson monochromator crystal. A fine line focus X-ray tube serves as source, and the diverging beam is monochromated and focused onto the camera cylinder by the quartz crystal. This geometry has the advantage over others which focus on a flat sample, since the quality of the diffraction pattern is not as sensitive to sample position, and it also allows transmission diffraction patterns to be made. The resolution of the Guinier system depends upon the focal width of the X-ray tube, the quality of the monochromator crystal, the thickness and particle size of the specimen, and the alignment of the instrument.

A1.1.1 Instrumental Configuration The 0.4 mm fine focus Cu X-ray tube provided a source small enough that the $K\alpha_1$ and $K\alpha_2$ lines could be separated by the monochromator. Chromatic dispersion from the monochromator is unavoidable, and also occurs on diffraction at the specimen. Selection of a suitable geometric arrangement of sample with respect to monochromator can either add or subtract the dispersion of one from the other. The asymmetric transmission geometry employed in this work minimized the line-broadening effects of dispersion and allowed diffraction patterns to be recorded between 2° and $106^\circ 2\theta$.

The correct adjustment of monochromator position with respect to the source and the camera chamber is essential for satisfactory results. Once alignment had been carried out it was found that any small shock to the surface upon which the camera rested could misalign the system. For this reason the apparatus was mounted on a slate slab; this provided the necessary mechanical stability.

A1.1.2 Sample Preparation and Mount In each case the sample was mounted as a powder for transmission photographs on an oscillating goniometer at the hot spot of a U-form furnace.

A portion of crystal was ground under acetone in a pestle and mortar by hand and dried at 50°C . High-purity internal standard (Si of comparable size fraction was usually employed) was mixed with the specimen. The material was then mixed with glycerol to form a paste which could be gently spread into the opening of a Pt wire loop with dimensions $3\text{ mm} \times 1\text{ mm}$ and a thickness of 0.1 mm to form a thin film. The thin film paste was then briefly heated at around 100°C , at which temperature the glycerol burnt off to leave a thin (0.1 mm or less) smooth powder

specimen in the loop together with amorphous carbon. The Pt loop was held in an insulating ceramic rod which was mounted directly into the standard goniometer sample holder.

It was found that sample thickness and flatness both affect the linewidths of the diffraction patterns, so great care was taken at this stage of sample preparation.

The Pt loop sample holder was aligned by optical telescope at the centre of oscillation of the camera and perpendicular to the incident beam. The sample and camera chamber were oscillated through around 5° throughout all exposures to improve line uniformity and intensity.

A1.1.3 Modification of Oscillation Mechanism The oscillation mechanism of the 632 high-temperature powder camera manufactured by Huber contains some design errors, which lead to rapid wear of the oscillation mechanism and uneven movement. Eventually (after several hundred hours use) the oscillation mechanism fails. The flaw in design lies in the microswitch mechanism which controls the range of oscillation. The instrument as supplied uses a single microswitch oscillating between two movable stops. The polythene bearing of the microswitch quickly wears and the increased friction prohibits free movement and switching. To overcome this problem the mechanism was modified to incorporate a second microswitch and relay mechanism to operate the oscillating motor. Details of these modifications are given in a technical note by Papendick (1986).

A1.2 Furnace and Temperature Calibration

Sample heating was accomplished with a heater similar to the design described by Brown et al. (1973). This simple design

has a wide aperture and allows a large range of diffraction angles to be sampled. The thermocouple element is placed between the alumina-covered platinum-wound heater rods, immediately above the specimen. The sample is heated principally by radiant heat transfer, but air heating also contributes. Draughts obviously cause temperature fluctuations in this set-up, and for this reason the heater is surrounded by a lightly absorbing Kapton foil to keep the temperature constant.

Thermal gradients within the heater are quite large, and the sample position must remain constant with respect to heater and thermocouple. The true temperature of the sample can differ from the temperature registered by the thermocouple by over 100°C. An uneven temperature distribution in the sample is revealed in the diffraction pattern, when lines are not vertical or constant width along their length. To minimise these errors the position of the Pt sample loop within the furnace was set very carefully. As far as is possible the specimen was set at an identical position within the furnace for every experiment. In particular the top of the Pt loop was always set to lie within 1 mm of the thermocouple bead. The temperature controller maintained the temperature stability of the furnace to within 1 K of the set temperature.

Absolute calibration of the heater was carried out by measuring transition temperatures of various structural phase transitions and melting and sublimation reactions. High-purity reagent grade chemicals were placed in the Pt sample loop for calibration purposes, and the beginning of melting was observed using the standard telescope supplied. The melting of these standards was performed several times and found to be reproducible. At very

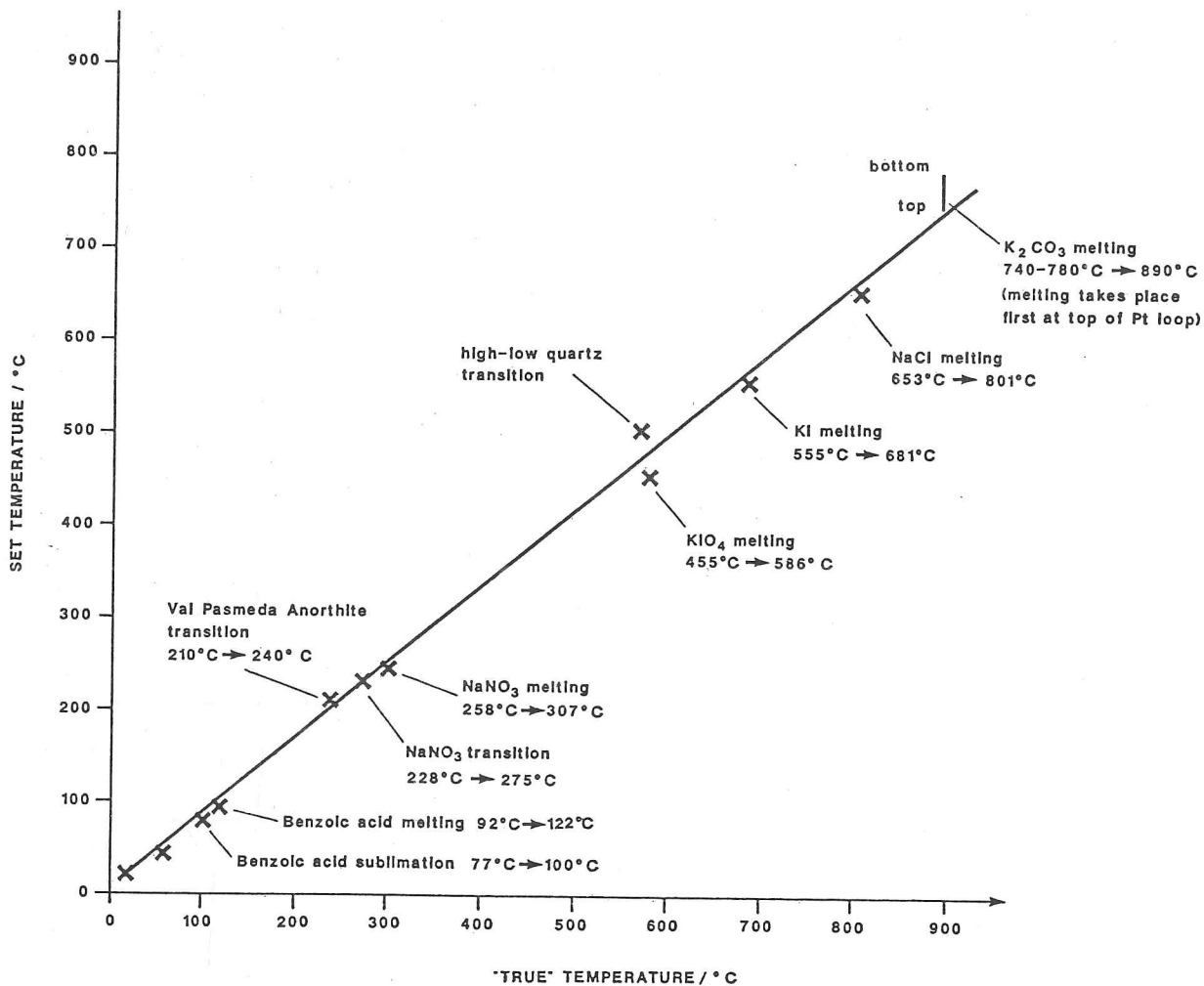


Figure A1.1 Calibration curve for the Huber U-form heater.

high temperatures the temperature gradient along the height of the loop was detected, since melting of K_2CO_3 took place first at the top of the loop (near the thermocouple) and proceeded down the sample. The calibration curve for the heater is shown in Figure A1.1, and the best fit straight line used throughout this thesis was:

$$T_{\text{true}} = (T_{\text{set}} \times 1.21) - 4.2 \quad (^\circ\text{C}) \quad \{A1.1\}$$

It is reassuring that this calibration agrees with that of DeDombal on a similar furnace using an independent thermocouple placed in the same position as is usually occupied by the Pt sample loop (R.F. DeDombal, pers. comm.).

APPENDIX 2

PROGRAMS FOR SPONTANEOUS STRAIN CALCULATION

A2.1 'STRAINS'

The listing of the pascal program 'STRAINS', developed for the calculation of spontaneous strain in triclinic feldspars, follows:

```
PROGRAM strains(input,infile,output,outfile);

CONST   pi=3.1415927;

VAR     l11,l22,l33,l12,l13,l23,a,b,c,a0,b0,c0      : real;
        alpha,betastar,gamma,alpha0,beta0star,gamma0 : real;
        inname,outname                               : string[14];
        infile,outfile                               : text;
        i                                             : integer;
        title                                         : string[30];

BEGIN
  writeln(clrhom);
  FOR i:=1 TO 5 DO writeln;
  write('input name of file containing cell parameters: ');
  readln(inname); writeln;
  write('output file name (LST: for printer, CON: for screen): ');
  readln(outname);

  assign (infile,inname); reset(infile);
  assign (outfile,outname); rewrite(outfile);
  FOR i:=1 TO 3 DO writeln;

  readln(infile,title);
  readln(infile,a,b,c,a0,b0,c0);
  readln(infile,alpha,betastar,gamma,alpha0,beta0star,gamma0);

  alpha:=alpha*pi/180;betastar:=betastar*pi/180;gamma:=gamma*pi/180;
  alpha0:=alpha0*pi/180;beta0star:=beta0star*pi/180;gamma0:=gamma0*pi/180;

  l11 := (a*sin(gamma)/(a0*sin(gamma0)))-1;
  l22 := (b/b0)-1;
  l33 := (c*sin(alpha)*sin(betastar)/(c0*sin(alpha0)*sin(beta0star)))-1;
  l12 := ((a*cos(gamma)/(a0*sin(gamma0)))-(b*cos(gamma0)/(b0*sin(gamma0)))/2;
  l13 := ((a*sin(gamma)*cos(beta0star)/(a0*sin(gamma0)*sin(beta0star))
           -(c*sin(alpha)*cos(betastar)/(c0*sin(alpha0)*sin(beta0star)))/2;
  l23 := ((c*cos(alpha)/(c0*sin(alpha0)*sin(beta0star)))+(cos(beta0star)*
           ((a*cos(gamma)/a0)-(b*cos(gamma0)/b0))/sin(beta0star))-(b*cos(alpha0)/
           (b0*sin(alpha0)*sin(beta0star)))/2;
```

```

writeln(outfile,'data generated for ',title);writeln(outfile);
writeln(outfile,'strain tensor : ');
FOR i:=1 TO 3 DO writeln(outfile);
writeln(outfile,l11:11:6,l12:11:6,l13:11:6);
writeln(outfile,'    ':11,l22:11:6,l23:11:6);
writeln(outfile,'    ':11,'    ':11,l33:11:6);

close (infile);
close (outfile);

```

END.

A2.2 'DIAGNL'

The pascal program 'DIAGNL', developed for the calculation of Eigenvalues and Eigenvectors of a general spontaneous strain tensor is listed below:

```

PROGRAM diagnl(input,infile,output,outfile);

CONST  matmax=30;
       g      =11;
       d      = 6;

TYPE   matdim = 1..matmax;
       xary   = array[matdim,matdim] of real;

VAR    h,u           : xary;
       i,j,size      : matdim;
       inname,outname : string[14];
       infile,outfile : text;

PROCEDURE MatrixDump(var x:xary);

VAR i,j:matdim;

BEGIN
writeln(outfile);
  FOR i:=1 TO size DO
    BEGIN
  FOR j:=1 TO size DO
    write(outfile,x[i,j]:g:d);
    writeln(outfile);
    END;
  FOR i:=1 TO 3 DO
    writeln(outfile);

```

END;

PROCEDURE MatrixDiagonalization(VAR a,s:xary; n:matdim);

VAR i,j,p,q : matdim;
nu,nufinal,rho,lambda,mu,omega,sine,cosine : real;
temp,temp2,co2,si2,sico,sico2,app,aqq,apq : real;
offdiagfound : boolean;

BEGIN

rho := 1.0E-8;

FOR i:=1 TO n DO

FOR j:=1 TO n DO

IF i<>j THEN s[i,j]:=0.0

ELSE s[i,j]:=1.0;

nu:=0.0;

FOR i:=1 TO n DO

FOR j:=1 TO n DO

IF i<>j THEN nu:=nu+sqr(a[i,j]);

nu:=sqrt(nu);

nufinal:=nu*rho/nu;

REPEAT

nu:=nu/n;

FOR q:=2 TO n DO

BEGIN

p:=1;

REPEAT

offdiagfound:=false;

IF abs(a[p,q])>nu THEN

BEGIN

offdiagfound:=true;

app:=a[p,p];

aqq:=a[q,q];

apq:=a[p,q];

lambda:=-apq;

mu:=(app-aqq)/2;

IF (mu=0) OR (mu<rho) THEN omega:=-1

ELSE

BEGIN

omega:=lambda/sqrt(sqr(lambda)+sqr(mu));

IF mu<0 THEN omega:=-omega;

END;

sine:=omega/sqrt(2*(1+sqrt(1-sqr(omega))));

cosine:=sqrt(1-sqr(sine));

FOR i:=1 TO n DO

BEGIN

temp:=a[i,p]*cosine-a[i,q]*sine;

a[i,q]:=a[i,p]*sine+a[i,q]*cosine;

a[i,p]:=temp;

temp:=s[i,p]*cosine-s[i,q]*sine;

s[i,q]:=s[i,p]*sine+s[i,q]*cosine;

s[i,p]:=temp;

END;

co2:=sqr(cosine);

si2:=sqr(sine);

```

        sico:=sine*cosine;
        sico2:=2*sico*apq;
        a[p,p]:=app*co2+aqq*si2-sico2;
        a[q,q]:=app*si2+aqq*co2+sico2;
        a[q,p]:=(app-aqq)*sico+apq*(co2-si2);
        a[p,q]:=a[q,p];
        FOR i:=1 TO n DO
            BEGIN
                a[p,i]:=a[i,p];
                a[q,i]:=a[i,q];
            END;
        END;
        p:=p+1;
        UNTIL p>(q-1);
    END;
UNTIL (nu<=nufinal) AND (NOT offdiagfound);
END;
BEGIN
    writeln(clrhom);
    write('input data file name? ');
    readln(inname);
    write('output file?(LST: for printer, CON: for screen) ');
    readln(outname);
    assign(infile,inname);reset(infile);
    assign(outfile,outname);reset(outfile);
    readln(infile,size);
    FOR i:=1 TO size DO
        BEGIN
            FOR j:=1 TO size DO
                read(infile,h[i,j]);
                readln(infile);
            END;
        MatrixDiagonalization(h,u,size);
        writeln(outfile);
        writeln(outfile,'Matrix of eigenvalues: ');
        MatrixDump(h);
        writeln(outfile,'Matrix of eigenvectors: ');
        MatrixDump(u);
    END.

```

REFERENCES CITED

- Adlhart W, Frey F, Jagodzinski H (1980a) X-ray and neutron investigations of the $P\bar{1}-I\bar{1}$ transition in pure anorthite. Acta Crystallogr. A36: 450-460.
- Adlhart W, Frey F, Jagodzinski H (1980b) X-ray and neutron investigations of the $P\bar{1}-I\bar{1}$ transition in anorthite with low albite content. Acta Crystallogr. A36: 461-470.
- Aizu K (1969) Possible species of "ferroelastic" crystals and of simultaneously ferroelectric and ferroelastic crystals. J. Phys. Soc. Japan 27: 387-396.
- Aizu K (1970) Determination of state parameters and formulation of spontaneous strain for ferroelastics. J. Phys. Soc. Japan 28: 706-716.
- Aleksandrov KS, Flerov IN (1979) Ranges of applicability of thermodynamic theory of structural phase transitions near the tricritical point. Sov. Phys. Solid State 21: 195-200.
- Als-Nielsen J, Birgeneau RJ (1977) Mean field theory, the Ginzburg critereon, and marginal dimensionality of phase transitions. Am. J. Phys. 45: 554-560.
- Angel RJ (1988) High pressure structure of anorthite. Am. Mineral. 73: 1114-1119.
- Angel RJ, Ross NL (1988) The $I\bar{1}-P\bar{1}$ transition in anorthite-rich feldspars. CIW (Geophysical Laboratory) Yearbook, 1988.
- Angel RJ, Hazen RM, McCormick TC, Prewitt CT, Smyth JA (1988) Compressibility of end-member feldspars. Phys. Chem. Minerals 15: 313-318.
- Angel RJ, Carpenter MA, Finger LW (1989a) Structural variation of order-disorder behaviour in anorthite-rich crystals. In

- preparation.
- Angel RJ, Redfern SAT, Ross NL (1989b) Spontaneous strain below the $I\bar{1}-P\bar{1}$ transition in anorthite at pressure. *Phys. Chem. Minerals* 16: 539-544.
- Arora AK, Umadevi V (1982) Instrumental distortions of Raman lines. *Appl. Spectroscopy* 36: 242-427.
- Barsch GR, Krumhansl JA (1984) Twin boundaries in ferroelastic media without interface dislocations. *Phys. Rev. Lett.* 53: 1069-1072.
- Bhagavantam S (1966) Crystal symmetry and physical properties. Academic Press, London.
- Bismayer U, Salje E (1981) Ferroelastic phases in $Pb_3(PO_4)_2 - Pb_3(AsO_4)_2$; X-ray and optical experiments. *Acta Crystallogr.* A37: 145-153.
- Bismayer U, Salje E, Jansen M, Dreher S (1986) Raman scattering near the structural phase transition of As_2O_5 : order parameter treatment. *J. Phys. C: Solid State Phys.* 19: 4537-4545.
- Boccara N (1968) Second-order phase transitions characterized by a deformation of the unit cell. *Annals Phys.* 47: 40-64.
- Boeke HE (1912) Die Schmelzerscheinungen und die Umkehrbare Umwandlung des Calcium Carbonates. *N. Jahrb. Mineral. Geol.* 1: 91-121.
- Borg IY, Heard HC (1969) Mechanical twinning and slip in experimentally deformed plagioclase. *Contrib. Mineral. Petrol.* 23: 128-135.
- Borg IY, Smith DK (1969) Calculated X-ray powder patterns for silicate minerals. *Geol. Soc. Amer. Mem.* 122: 896 pp.
- Bown MG, Gay P (1958) The reciprocal lattice geometry of the

- plagioclase feldspar structures. Z. Kristallogr. 111: 1-14.
- Brehat F, Wyncke B (1985) Analysis of the temperature-dependent infrared active lattice modes in the ordered phase of sodium nitrate. J. Phys. C: Solid State Phys. 18: 4247-4259.
- Brown GE, Sueno S, Prewitt CT (1973) A new single-crystal heater for the precession camera and four-circle diffractometer. Am. Mineral. 58: 698-704.
- Brown WL, Hoffman W, Laves F (1969) Uber kontinuierliche und reversible Transformation des Anorthits ($\text{CaAl}_2\text{Si}_2\text{O}_8$) zwischen 25 und 350°C. Naturwissenschaften 50: 221.
- Bruce AD, Cowley RA (1981) Structural Phase Transitions. Taylor & Francis, London.
- Carpenter MA (1988) Thermochemistry of aluminum/silicon ordering in feldspar minerals. In E Salje (ed.) Physical Properties and Thermodynamic Behaviour of Minerals. NATO ASI C225, Reidel, Boston: 265-323.
- Carpenter MA, Ferry JM (1984) Constraints on the thermodynamic mixing properties of plagioclase feldspars. Contrib. Mineral. Petrol. 87: 138-148.
- Carpenter MA, McConnell JDC (1984) Experimental delineation of the $\text{C}\bar{1}$ - $\text{I}\bar{1}$ transformation in intermediate plagioclase feldspars. Am. Mineral. 69: 112-121.
- Carpenter MA, Putnis A, Navrotsky A, McConnell JDC (1983) Enthalpy effects associated with Al,Si ordering in anhydrous Mg cordierite. Geochim. Cosmochim. Acta 47: 899-906.
- Carpenter MA, McConnell JDC, Navrotsky A (1985) Enthalpies of ordering in the plagioclase feldspar solid solution. Geochim. Cosmochim. Acta 49: 947-966.
- Chang LLY (1965) Subsolidus phase relations in the systems BaCO_3 -

- SrCo_3 , $\text{SrCO}_3\text{-CaCO}_3$, and $\text{BaCO}_3\text{-CaCO}_3$. J. Geol. 73: 346-368.
- Cohen JP, Ross FK, Gibbs GV (1977) An X-ray and neutron diffraction study of hydrous low cordierite. Am. Mineral. 62: 67-78.
- Cohen LH, Klement W (1973) Determination of high-temperature transition in calcite to 5 kbar by differential thermal analysis in hydrostatic apparatus. J. Geol. 81: 724-727.
- Cowley RA (1976) Acoustic phonon instabilities and structural phase transitions. Phys. Rev. B 13: 4877-4885.
- Crawford WA, Fyfe WS (1964) Calcite-aragonite equilibrium at 100°C. Science 144: 1569-1570.
- Czank M (1973) Strukturuntersuchungen von Anorthit im Temperaturbereich von 20°C bis 1430°C. Dissertation, ETH Zurich.
- Czank M, Van Landuyt J, Schulz H, Laves F, Amelinckx S (1973) Electron microscopic study of the structural changes as a function of temperature in anorthite. Z. Kristallogr. 138: 403-418.
- David WIF (1983) Structural relationships between spontaneous strain and acoustic properties in ferroelastics. J. Phys. C: Solid State Phys. 16: 2455-2470.
- Dove MT, Powell BM (1989) Neutron diffraction study of the tricritical orientational order/disorder phase transition in calcite at 1260 K. Phys. Chem. Minerals 16: 503-507.
- Dove MT, Heilmann IU, Kjems JK, Kurittu J, Pawley GS (1983) A neutron study of phonons in per-deuterated S-triazine. Phys. Stat. Sol. b 120: 173-181
- Dove MT, Putnis A, David WIF, Harrison WTA (1989) Neutron diffraction study of the structural states of synthetic

- magnesium cordierite. Am. Mineral. in press.
- Eitel W (1923) Über das binäre System CaCO_3 - Ca_2SiO_4 und den Spurrit. N. Jahrb. Mineral. Beil. 48: 63-74.
- Foit FF, Peacor DR (1973) The anorthite crystal structure at 410 and 830°C. Am Mineral. 58: 665-675.
- Folk R, Iro H, Schwabl F (1976) Critical statics of elastic phase transitions. Z. Phys. B 25: 69-81.
- Fousek J, Janovec V (1969) The orientation of domain walls in twinned ferroelectric crystals. J. Appl. Phys. 40: 135-142.
- Frey F, Jagodzinski H, Prandl W, Yelon WB (1977) Dynamical character of the primitive to body-centred phase transition in anorthite. Phys. Chem. Minerals 1: 227-231.
- Gay P (1953) The structures of plagioclase feldspars: III An X-ray study of anorthites and bytownites. Mineral. Mag. 30: 169-177.
- Gibbs GV (1966) The polymorphism of cordierite I: the crystal structure of low cordierite. Am. Mineral. 51: 1068-1087.
- Ginzburg VL (1960) Some remarks on phase transitions of the second kind and the macroscopic theory of ferroelectric materials. Sov. Phys. Solid State 2: 1824-1834.
- Ginzburg VL, Levanyuk AP, Sobyenin AA (1987) Comments on the applicability of the Landau theory for structural phase transitions. Ferroelectrics 73: 171-182.
- Glazer AM (1988) Linear and circular birefringence and crystal structures. In E Salje (ed.) Physical Properties and Thermodynamic Behaviour of Minerals. NATO ASI C225, Reidel, Boston: 185-212.
- Gufan YM, Larin ES (1980) Theory of phase transitions described

- by two order parameters. Sov. Phys. Solid State 22: 270-275.
- Guimaraes DMC (1979) Temperature dependence of lattice parameters and spontaneous strain in $\text{Pb}_3(\text{PO}_4)_2$. Phase Transitions 1: 143-154.
- Güttler B, Salje E, Putnis A (1989) Structural states of Mg-cordierite III: Infrared spectroscopy and the nature of the hexagonal-modulated transition. Phys. Chem. Minerals 16: 365-373.
- Ibrahim MM, Ramachandran V, Sarangapani K, Srinivasan R (1986) Thermal expansion of sodium nitrate I. J. Phys. Chem. Solids 47: 517-520.
- Idenbom VL (1960) Phase transitions without a change in the number of atoms in the unit cell of the crystal. Sov. Phys. Crystallogr. 5: 106-115.
- Ihringer J (1982) An automated low-temperature Guinier X-ray diffractometer and camera. J. Appl. Crystallogr. 15: 1-4.
- Irwing AJ, Wyllie PJ (1973) Melting relationships in $\text{CaCO}_3\text{-CO}_2$ and MgO-CO_2 to 36 kilobars with comments on CO_2 in the mantle. Earth Planet. Sci. Lett. 20: 220-225.
- Imry Y (1975) On the statistical mechanics of coupled order parameters. J. Phys. C: Solid State Physics 8: 567-577.
- Jacobs GK, Kerrick DM, Krupka KM (1981) The high-temperature heat capacity of natural calcite (CaCO_3). Phys. Chem. Minerals 7: 55-59.
- Jamieson JC (1953) Phase equilibrium in the system calcite-aragonite. J. Chem. Phys. 21: 1385-1390.
- Janovec V, Dvorak V, Petzelt J (1975) Symmetry classification and properties of equi-translation structural phase transitions.

- Czech. J. Phys. B22: 974-994.
- Jansen M (1978) Die Kristallstruktur von As_2O_5 , eine neue Raumnetzstruktur. Z. Anorg. Allg. Chem. 441: 5-12.
- Jansen M (1979) Über eine neue Modifikation von As_2O_5 . Z. Naturforsch. 34b: 10-13.
- Johannes W, Puhán D (1971) The calcite-aragonite transition, reinvestigated. Contrib. Mineral. Petrol. 31: 28-38.
- Kalus C (1978) Neue Strukturbestimmung des Anorthits unter Berücksichtigung möglicher Alternativen. Dissertation, Univ. München.
- Kawamata Y, Nissen H-U, Beeli C, Hulliger F, Ott HR (1988) Strained orthogonal twinning in the high- T_c superconductor $\text{Ba}_2\text{HoCu}_3\text{O}_{7-x}$. Z. Phys. B 72: 345-352.
- Kempster CJE, Megaw HD, Radoslovich EW (1962) The structure of anorthite, $\text{CaAl}_2\text{Si}_2\text{O}_8$. I: structure analysis. Acta Crystallogr. 15: 1005-1017.
- Kirkpatrick RJ, Carpenter MA, Yang W-H, Montez B (1987) ^{29}Si magic-angle NMR spectroscopy of low-temperature ordered plagioclase feldspars. Nature 325: 236-238.
- Kociński J (1983) Theory of Symmetry Changes at Continuous Phase Transitions. Elsevier, Amsterdam.
- Kracek FC (1931) Gradual transition in sodium nitrate. I: Physico-chemical criteria of the transition. J. Am. Chem. Soc. 53: 2609-2624.
- Kracek FC, Posnjak E, Hendricks SB (1931) Gradual transition in sodium nitrate. II: The structure at various temperatures and its bearing on molecular rotation. J. Am. Chem. Soc. 53: 3339-3348.
- Krishna Rao KV, Satyanarayan Murthy K (1970) Precision lattice

- parameters and thermal expansion of sodium nitrate. J. Phys. Chem. Solids 31: 887-890.
- Kroll H (1983) Lattice parameters and determinative methods for plagioclase and ternary feldspars. In PH Ribbe (ed.) Feldspar Mineralogy. Mineral. Soc. Am. Reviews in Mineralogy 2 (2nd edn.): 101-119.
- Landau LD (1937) K teorii fazovykh perekhodov. Zh. Eksperi. Teoretich. Fiziki 7: 19, 627. Translated in D Ter Haar (ed.) (1965) Collected Papers of L.D.Landau. Pergamon, Oxford: 193-216.
- Landau LD, Lifshitz EM (1954) Statistical Physics. Addison Wesley, Reading.
- Langer K, Schreyer W (1969) Infrared and powder X-ray diffraction studies on the polymorphism of cordierite $Mg_2(Al_4Si_5O_{18})$. Am. Mineral. 54: 1442-1459.
- Laves F, Goldsmith JR (1954) Long-range-short-range order in calcic plagioclases as a continuous and reversible function of temperature. Acta Crystallogr. 7: 465-472.
- Laves F, Czank M, Schulz H (1970) The temperature dependence of reflection intensities of anorthite ($CaAl_2Si_2O_8$) and the corresponding formation of domains. Schweiz Mineral. Petrogr. Mitt. 50: 519-525.
- Levanyuk AP, Osipov VV, Sigov AS, Sobyenin AA (1979) Change of defect structure and the resultant anomalies in the properties of substance near phase transition points. Sov. Phys. JETP 49: 176-188.
- MacKenzie GA, Pawley GS (1979) A neutron diffraction study of DCN. J. Phys. C: Solid State Phys. 12: 2717-2735.
- Markgraf SA, Reeder RJ (1985) High-temperature structure

- refinements of calcite and magnesite. *Am. Mineral.* 70: 590-600.
- McConnell JDC (1975) Microstructures of minerals as petrogenetic indicators. *Ann. Rev. Earth Planet. Sci.* 3: 129-155.
- McConnell JDC (1985) Symmetry aspects of order-disorder and the application of Landau theory. In SW Keiffer & A Navrotsky (eds.) Microscopic to Macroscopic. *Mineral. Soc. Am. Reviews in Mineralogy* 14: 165-186.
- Meagher EP, Gibbs GV (1977) The polymorphism of cordierite II: the crystal structure of indialite. *Can. Mineral.* 15: 43-49.
- Michel KH (1984) Phase transitions in strongly anharmonic and orientational disordered crystals. *Z. Phys. B* 54: 129-137.
- Mirwald PW (1976) A differential thermal analysis study of the high-temperature polymorphism of calcite at high pressure. *Contrib. Mineral. Petrol.* 59: 33-40.
- Mirwald PW (1979) Determination of a high-temperature transition of calcite at 800°C and one bar CO₂ pressure. *N. Jb. Mineral. Mh.* 7: 309-315.
- Miyashiro A (1957) Cordierite-indialite relations. *Am. J. Sci.* 255: 43-62.
- Mügge O, Heide F (1931) Einfache Schiebungen am Anorthit. *Neues Jb. Mineral. Abt. A* 64: 163-169.
- Müller WF, Wenk H-R, Bell WL, Thomas G (1973) Analysis of the displacement vectors of antiphase domain boundaries in anorthites, (CaAl₂Si₂O₈). *Contrib. Mineral. Petrol.* 40: 63-74.
- Navrotsky A (1977) Progress and new directions in high temperature calorimetry. *Phys. Chem. Minerals* 2: 89-104.
- Newnham RE (1974) Domains in minerals. *Am. Mineral.* 59: 906-918.

- Nye JF (1957) Physical properties of crystals. Oxford University Press, London.
- Oleksy C, Przystawa J (1983) On phase transitions with bilinearly coupled order parameters. *Physica* 121A: 145-149.
- Palmer DC, Putnis A, Salje E (1988) Twinning in tetragonal leucite. *Phys. Chem. Minerals* 16: 298-303.
- Palmer DC, Salje E, Schmahl WW (1989) Phase transitions in leucite I: X-ray diffraction studies. *Phys. Chem. Minerals* submitted.
- Papendick M (1986) Technische Modifizierung der Huber Hochtemperaturkamera 631/632 und Optimierung des Aufnahmeverfahrens. Technical Note. Inst. Kristallogr. Petrogr., Univ. Hannover.
- Paul GL, Pryor AW (1972) The study of sodium nitrate by neutron diffraction. *Acta Crystallogr.* B28: 2700-2702.
- Peercy PS, Fritz IJ (1974) Pressure-induced phase transition in paratellurite (TeO_2). *Phys. Rev. Lett.* 32: 466-469.
- Petzelt J, Dvorak V (1976) Changes of infrared and Raman spectra induced by structural phase transitions: II. Examples. *J. Phys. C: Solid State Phys.* 9: 1587-1601.
- Poon WCK (1988) Raman and birefringence studies of phase transitions. Dissertation, University of Cambridge.
- Poon WCK, Salje E (1988) The excess optical birefringence and phase transition in sodium nitrate. *J. Phys. C: Solid State Phys.* 21: 715-729.
- Putnis A (1980) The distortion index in anhydrous Mg-cordierite. *Contrib. Mineral. Petrol.* 74: 135-141.
- Putnis A, Angel RJ (1985) Al, Si ordering in cordierite using magic angle spinning NMR II: Models of Al, Si order from NMR

- data. Phys. Chem. Minerals 12: 217-222.
- Putnis A, Bish DL (1983) The mechanism and kinetics of Al,Si ordering in Mg-cordierite. Am. Mineral. 68: 60-65.
- Putnis A, Fyfe CA, Gobbi GC (1985) Al,Si ordering in cordierite using magic angle spinning NMR. I: Si-29 spectra of synthetic cordierites. Phys. Chem. Minerals 12: 211-216.
- Putnis A, Salje E, Redfern SAT, Fyfe CA, Strobl H (1987) Structural states of Mg-cordierite I: order parameters from synchrotron X-ray and NMR data. Phys. Chem. Minerals 14: 446-454.
- Rae AIM (1982) The structural phase change in s-triazine: the quasi-harmonic approximation. J. Phys. C: Solid State Phys. 15: 1883-1898.
- Ralston A, Wilf HS (1960) Mathematical methods for digital computers vol 1. Wiley, New York.
- Rao CNR, Rao KJ (1978) Phase Transitions in Solids. McGraw Hill, New York.
- Redfern SAT, Salje E (1987) Thermodynamics of plagioclase II: temperature evolution of the spontaneous strain at the $I\bar{1}-P\bar{1}$ phase transition in anorthite. Phys. Chem. Minerals 14: 189-195.
- Redfern SAT, Salje E (1988) Spontaneous strain and the ferroelastic phase transition in As_2O_5 . J. Phys. C: Solid State Phys. 21: 277-285.
- Redfern SAT, Graeme-Barber A, Salje E (1988) Thermodynamics of plagioclase III: Spontaneous strain at the $I\bar{1}-P\bar{1}$ phase transition in Ca-rich plagioclase. Phys. Chem. Minerals 16: 157-163.
- Redfern SAT, Salje E, Maresch W, Schreyer W (1989a) Powder X-ray

- diffraction and infrared study of the hexagonal to orthorhombic phase transition in K-bearing cordierite. Am. Mineral. in press.
- Redfern SAT, Salje E, Navrotsky A (1989b) High-temperature enthalpy at the orientational order-disorder transition in calcite: implications for the calcite/aragonite phase equilibrium. Contrib. Mineral. Petrol. 101: 479-484.
- Reeder RJ, Wruck B, Schmahl WW, Poon W, Salje E (1987) Spontaneous strain and excess specific heat of the orientational ordering transition in NaNO_3 . Terra Cognita 7: 264.
- Reeder RJ, Redfern SAT, Salje E (1988) Spontaneous strain at the structural phase transition in NaNO_3 . Phys. Chem. Minerals 15: 605-611.
- Reinsborough VC, Wetmore FEW (1967) Specific heat of sodium nitrate and silver nitrate by medium high temperature adiabatic calorimetry. Aust. J. Chem. 20: 1-8.
- Robie RA, Hemingway BS, Fisher JR (1979) Thermodynamic properties of minerals and related substances at 298.15 K and 1 bar (10^5 Pascals) pressure and at higher temperatures. U.S. Geol. Surv. Bull. 1452: 456pp.
- Ryzhova TV (1964) Elastic properties of plagioclase. Izv. Geophys. Ser. 7: 1049-1051.
- Salje E (1985) Thermodynamics of sodium feldspar I: Order parameter treatment and strain induced coupling effects. Phys. Chem. Minerals 12: 93-98.
- Salje E (1987a) Structural states of Mg-cordierite II: Landau theory. Phys. Chem. Minerals 14: 455-460.
- Salje E (1987b) Thermodynamics of plagioclases I: Theory of the

- $I\bar{1}-P\bar{1}$ phase transition in anorthite and Ca-rich plagioclases. Phys. Chem. Minerals 14: 181-188
- Salje E (1988) Structural phase transitions and specific heat anomalies. In E Salje (Ed) Physical properties and thermodynamic behaviour of minerals. NATO ASI C255, Reidel, Boston: 75-118.
- Salje (1989) Towards a better understanding of time-dependent geological processes: kinetics of structural phase transitions in minerals. Terra Nova 1: 35-44.
- Salje E, Devarajan V (1986) Phase transitions in systems with strain-induced coupling between two order parameters. Phase Transitions 6: 235-248.
- Salje E, Viswanathan K (1976) The phase diagram calcite-aragonite as derived from the crystallographic properties. Contrib. Mineral. Petrol. 55: 55-67.
- Salje E, Kuscholke B, Wruck B, Kroll H (1985a) Thermodynamics of sodium feldspar II: Experimental results and numerical calculations. Phys. Chem. Minerals 12: 99-107.
- Salje E, Kuscholke B, Wruck B (1985b) Domain wall formation in minerals: I theory of twin domain boundary shapes in Na-feldspar. Phys. Chem. Minerals 12: 132-140.
- Salje E, Bismayer U, Jansen M (1987) Temperature evolution of the ferroelastic order parameter of As_2O_5 as determined from optical birefringence. J. Phys. C: Solid State Phys. 20: 3613-3620.
- Salje E, Güttler B, Redfern SAT (1989) Infrared and X-ray study of the high-low quartz transition. In preparation.
- Sapriel J (1975) Domain-wall orientations in ferroelastics. Phys. Rev. B 12: 5128-5140.

- Schlenker JL, Gibbs GV, Boisen MB (1978) Strain-tensor components expressed in terms of lattice parameters. *Acta Crystallogr.* A34: 52-54.
- Schmahl WW (1988) Diffraction intensities as thermodynamic parameters: Orientational ordering in NaNO_3 . Abstract, 27th meeting A.G.Kr., Konstanz, 1988. *Z. Kristallogr.* 182: 231-233.
- Schmahl WW, Redfern SAT (1988) An X-ray study of coupling between acoustic and optic modes at the ferroelastic phase transition in As_2O_5 . *J. Phys. C: Solid State Phys.* 21: 3719-3725.
- Schmid H, Burkhardt E, Walker E, Brixel W, Clin M, Rivera J-P, Jorda J-L, François M, Yvon K (1988) Polarized light and X-ray precession study of the ferroelastic domains of $\text{YBa}_2\text{Cu}_3\text{O}_{7-\delta}$. *Z. Phys. B* 72: 305-322.
- Schreyer W (1985) Experimental studies on cation substitutions and fluid incorporation in cordierite. *Bull. Minéral.* 108: 273-279.
- Schreyer W, Schairer JF (1961) Compositions and structural states of anhydrous Mg-cordierites: a reinvestigation of the central part of the system $\text{MgO}-\text{Al}_2\text{O}_3-\text{SiO}_2$. *J. Petrol.* 2: 324-406.
- Shen TY, Mitra SS, Prask H, Trevino SF (1975) Order-disorder phenomenon in sodium nitrate studied by low frequency Raman-scattering. *Phys. Rev. B* 12: 4530-4533.
- Simmons G, Bell P (1963) Calcite-aragonite equilibrium. *Science* 139: 1197-1198.
- Smart RM, Glasser FP (1977) Stable cordierite solid solutions in the $\text{MgO}-\text{Al}_2\text{O}_3-\text{SiO}_2$ system: composition, polymorphism and thermal expansion. *Sci. Ceram.* 9: 256-263.

- Smith JF, Wohlleben D (1988) Twin refinement below room temperature in the 1-2-3 high T_c superconductors. *Z. Phys. B* 72: 323-334.
- Smith JR (1958) The optical properties of heated plagioclases. *Am. Mineral.* 43: 1179-1194.
- Staehli JL, Brinkmann D (1974) A nuclear magnetic resonance study of the phase transition in anorthite, $CaAl_2Si_2O_8$. *Z. Kristallogr.* 140: 360-373.
- Starkey J (1967) On the relationship of pericline and albite twinning to the composition and structural state of plagioclase feldspar. *Schweiz Mineral. Petrogr. Mitt.* 47: 257-268.
- Staveley LAK, Linford RG (1969) The heat capacity and entropy of calcite and aragonite, and their interpretation. *J. Chem. Thermodynamics* 1: 1-11.
- Stewart DB, Ribbe PH (1983) Optical properties of feldspars. In PH Ribbe (ed.) Feldspar Mineralogy. *Min. Soc. Am. Reviews in Mineralogy* 2 (2nd edn.): 121-140.
- Strømme KO (1969) The crystal structure of sodium nitrate in the high-temperature phase. *Acta Chem. Scand.* 23: 1616-1624.
- Strukov BA, Taraskin SA, Minaeva KA, Fedorikhin VA (1980) Critical phenomena in perfect and imperfect TGS crystals. *Ferroelectrics* 25: 399-402.
- Taylor (1933) The structure of sanidine and other feldspars. *Z. Kristallogr.* 85: 425-442.
- Terauchi H, Yamada Y (1972) X-ray study of phase transition in $NaNO_3$. *J. Phys. Soc. Japan* 33: 446-454.
- Tolédano J-C (1979) Symmetry-determined phenomena at crystalline phase transitions. *J. Solid State Chem.* 27: 41-49.

- Tolédano J-C, Tolédano P (1980) Order parameter symmetries and free-energy expansions for purely ferroelastic transitions. Phys. Rev. B 21: 1139-1172.
- Tolédano J-C, Tolédano P (1987) The Landau Theory of Phase Transitions. World Scientific, Singapore.
- Wadhawan VK (1982) Ferroelasticity and related properties of crystals. Phase Transitions 3: 3-103.
- Wadhawan VK (1988) Epitaxy and disorientations in the ferroelastic superconductor $\text{YBa}_2\text{Cu}_3\text{O}_{7-x}$. Phys. Rev. B 38: 8936-8939.
- Wadhawan VK, Glazer AM (1981) Evidence for a tricritical point in the ferroelastic solid-solution series $\text{Pb}_3(\text{P}_{1-x}\text{V}_x\text{O}_4)_2$. Phase Transitions 2: 75-84.
- Wainwright JE, Starkey J (1971) A refinement of the structure of anorthite. Z. Kristallogr. 133: 75-84.
- Wolfsdorff P (1983) Experimentelle Arbeiten zum Alkalieinbau in Corrierit. Diplome Thesis, Rhur-Univ., Bochum.
- Wruck B (1986) Einfluß des Na-Gehaltes und der Al,Si Fehlordnung auf das thermodynamische Verhalten der Phasenumwandlung $\text{P}\bar{1}$ - $\text{I}\bar{1}$ in Anorthit. Dissertation, Univ. Hannover.
- Wruck B, Salje E (1987) Unpublished data.
- Wu FY (1982) The Potts model. Rev. Mod. Phys. 54: 235-268.
- Yelon WB, Cox DE, Kortman PJ, Daniels WB (1974) Neutron diffraction study of Nd_4Cl in the tricritical region. Phys. Rev. B 9: 4943-4856.
- Yoshimitsu K (1986) Structural phase transition to a lower-symmetry phase with increasing temperature. Progress Theor. Phys. 76: 810-819.
- Zeigler D, Navrotsky A (1986) Direct measurement of the enthalpy

of fusion of diopside. Geochim. Cosmochim. Acta 50: 2461-
2466.

